ABSTRACT

Title of Document: VERTICAL DYNAMIC RESPONSE OF MICROPILE GROUPS USING A NON-LINEAR SOIL BEHAVIOR

Directed by: Professor, M. Sherif Aggour,
Department of Civil and Environmental Engineering.

Micropile groups are commonly used as a foundation support in many applications in geotechnical engineering. This study presents a three-dimensional finite element analysis of micropile group model subjected to vertical dynamic loads from a machine foundation. A modified Drucker-Prager constitutive model was used to simulate the nonlinear behavior of the soil as well as the soil-micropile interaction. The soil continuum was modeled using solid continuum elements in the FEM model, while micropiles were represented using beam elements and appropriate interaction properties were assigned to the interface elements. The accuracy of the model developed was verified by its application to the published experimental data.

A series of parametric studies were conducted to examine the effects of different parameters on the behavior of the soil-micropile system, including soil nonlinearity, inclination angle, spacing of the micropiles in the group, soil shear/micropile stiffness ratio, machine foundation mass, and the frequency content of the applied load, etc. The obtained results offered valuable insights into the influence of each parameter on the response of micropile groups. The results of these studies demonstrated the effectiveness of the modified Drucker-Prager constitutive model and the three-dimensional finite element analysis in predicting the behavior of micropile groups under dynamic loading. This study contributes to advancing the understanding of the behavior of micropile groups and their interaction with soil under vertical dynamic loading conditions, and it provides criteria for an improved design of the micropile groups under machine foundation loads.

Keywords: micropile groups, machine foundations, three-dimensional finite element analysis (3D FEA) , modified Drucker-Prager, soil-micropile interaction.

VERTICAL DYNAMIC STUDY OF MICROPILE GROUPS USING A NON-LINEAR SOIL BEHAVIOR

by

Ali-Matthew Sheikhbahaei

Dissertation submitted to the Faculty of the Graduate School of the
University of Maryland, College Park, in partial fulfillment
of the requirements for the degree of
Doctor of Philosophy
2023

Advisory Committee:
Professor M. Sherif Aggour, Chair
Professor Ahmet Aydilek
Professor Chung C. Fu
Professor Peter Chang
Professor Sung Lee

Dedication

To my loving mom and dad, Pari and Reza

Your unwavering love, support, and sacrifice have been the driving force behind my academic journey. I am forever grateful for your belief in me and the countless ways you have shaped my life. This dissertation is dedicated to both of you, with heartfelt appreciation for your guidance, encouragement, and boundless love.

With deepest gratitude

Acknowledgements

I extend my deepest gratitude to my advisor, Professor M. Sherif Aggour, for his unwavering guidance and invaluable support throughout the journey of this thesis. His dedication, expertise, and relentless commitment to my academic growth have been instrumental in shaping the outcome of this research.

I would also like to express my appreciation to the esteemed members of my committee, Professors Ahmet Aydilek, Chung Fu, Peter Chang, Sung Lee, for their insightful feedback and constructive input, which greatly enhanced the quality of this work.

Furthermore, I am very grateful to the team at the Hong Kong Polytechnique University for their invaluable researches on this topic and conducting the shaking table test experiments. Their contribution played a pivotal role in validating and strengthening the findings of this research.

Lastly, I am indebted to my parents, whose unwavering love, encouragement, and sacrifices have been the driving force behind my pursuit of knowledge. This accomplishment would not have been possible without their unwavering support.

To all those who have played a part, whether big or small, in shaping this thesis, I offer my heartfelt thanks.

Table of Contents

LIST OF FIGURES

LIST OF TABLES

Chapter 1 - Introduction

1.1. Background

Micropiles are a type of deep foundation system commonly used in civil engineering to improve and strengthen the ground. They have a wide range of applications, including underpinning, bridge abutments, and slope stabilization projects. Some advantages of using micropiles include their ability to withstand both axial and lateral loads, high flexibility over time under vertical, lateral, and seismic loads, minimal disturbance to surrounding structures during construction, and easy installation at inclined angles. They require minimal excavation due to their small diameter and can be installed with low noise and vibration machines. Micropiles are also effective at reducing foundation settlement and minimizing impacts on surrounding historic structures under repair. They can be installed in construction sites with various execution constraints and in various soil types, and through bond between the grout and soil can resist some negative skin friction under dynamic load although this resistance may be limited due to their smaller circumferential surface.

Once inserted into the ground, micropiles strengthen and stabilize the surrounding soil and are capable of transferring substantial amounts of axial loads. They are a cost-effective and efficient substitute for traditional deep foundation systems, such as driven piles and drilled shafts. These systems are mainly used to increase bearing capacity and reduce settlements, particularly for strengthening existing foundations, including machine foundations. Frictional resistance between the surface of the pile and its surrounding soil, as well as the associated group/network effects of micropiles, are possible mechanisms for ground improvement. Micropile groups can provide support to machine foundations to limit the vibration amplitude caused by machine operations.

The use of these systems overall improves the natural frequency of the soil-micropile system and can mitigate the vibrations caused by the operation of the machine foundation.

1.2. Statement of the Problem

While a series of numerical and experimental studies have been performed to examine the behavior of micropiles and micropile groups, few have modeled the behavior of these structures under dynamic loading conditions, such as machine foundations. Additionally, past studies have shown a lack of advanced modeling for soil-structure interaction. It is essential to model soil and soil-structure interaction behavior properly with reasonable accuracy to capture the behavior of these structures under dynamic loads properly. Generally, soil stress-strain behavior under dynamic loading conditions is more complex than under static loading conditions, and due to their plastic behavior under dynamic loads, linear constitutive modeling cannot accurately capture their behavior. In addition, it should be noted that micropiles have unique characteristics that set them apart from conventional piles. These include their relatively small diameter, high strength, and the presence of a grouted bond zone. This bond zone can have a substantial effect on the overall behavior of a group of micropiles, which is not observed in conventional bored or driven piles.

The purpose of this research is to perform a series of three-dimensional finite element numerical analyses on groups of micropiles inserted into the ground while subjected to vertical dynamic loads of machine foundations. Since soil stress-strain behavior under dynamic loading is accompanied by a great degree of plasticity and deformations, it is critical to incorporate an appropriate soil constitutive behavior to represent soil behavior under these loading conditions. Furthermore, a series of parametric studies are conducted to understand the effects of various important

parameters, such as micropile spacing, micropile inclination angle, frequency of input motion, and stiffness ratio on the performance of the micropile group.

To assure reasonable and accurate results, a verification three-dimensional model is developed in the finite element software ABAQUS, and the results are verified with an experimental study. The verification model simulates the performance of micropile groups in cases of static and dynamic conditions using nonlinear soil behavior for the soil (i.e., Modified Drucker Prager with Cap). After verifying the accuracy of the finite element model through comparison with field and experimental data and ensuring the appropriate selection of three-dimensional FEM[1] model, boundaries, and soil constitutive parameters, the study will proceed to investigate other salient factors that may influence the behavior of the micropile group.

1.3. Structure of the Dissertation

Chapter 2 will provide a comprehensive review of the existing literature on micropiles, with a particular focus on the behavior of micropile groups under dynamic loading conditions. This chapter will explore the findings and observations of past research and identify any knowledge gaps that remain to be addressed.

Chapter 3 will detail the soil constitutive modeling used in the numerical modeling and the selection of soil constitutive parameters. This chapter will also discuss boundary conditions, numerical analysis techniques, and any other relevant aspects of numerical simulations.

[1] Finite Element Method

Chapter 4 will present the results of the verification of the finite element model and the outcomes of the parametric studies on the critical factors influencing the performance of the micropile groups. The findings from this chapter will contribute to understanding the behavior of micropile groups subjected to dynamic loads from machine foundations and provide some insight into the design of these systems.

In the concluding chapter, the key findings and conclusions of the research will be summarized and discussed in detail. This will include a comprehensive review of the main contributions and limitations of the study, an assessment of the significance of the results and design contributions. Additionally, recommendations for future research directions will be provided, highlighting potential areas of further investigation and improvement in the field of micropile behavior under vertical dynamic loading conditions.

Chapter 2 - Literature Review

2.1. Introduction

Piles are generally divided into two categories: driven piles and bored piles (Fleming et al. 1985). Driven piles, also known as displacement piles, are members that are installed into the ground by driving and as a result, they push the surrounding soil laterally during the installation. Bored piles, also known as replacement piles, are built in a borehole that has already been excavated, thus replacing excavated soils. Micropiles, however, are grouted in small diameter piles (normally less than 300 mm or 12") that are inserted and grouted in the ground and can resist axial and lateral loads. In a group, they can be used instead of conventional piles. Micropiles are installed using methods that produce the least disturbance to nearby structures, and the surrounding soils. They can also be installed in situations when there is limited access in various soil conditions and at various inclination angles. Due to their ease of installation, minimal vibration, and noise from the installation process, they are seen as an engineering industry-friendly tool for retrofitting foundation and reinforcing weak grounds.

In conventional piles, most of the applied loads are supported by reinforced concrete, therefore the capacity of the pile or pile group is increased by increasing the cross-sectional area of the piles. However, the capacity of micropile or micropile group is mainly provided by the steel elements that have capacity in both tensile and compression. The methods employed for drilling and insertion of the micropiles into the ground ultimately results in bondage between the micropile element and the surrounding ground by means of grout. The grout transfers the applied forces from the reinforced element to the ground through the friction between the grout and the surrounding ground. Due to the fact that the diameter of micropiles is small and as a result the

surface area of micropiles tip is small, thus contribution of the tip bearing capacity in micropiles is ignored in micropile bearing capacity calculations. The resistance of grout-soil connection is significantly influenced by the type of soil, grout injection method and injection pressure and other factors. Figure 2-1 illustrates micropile construction sequence from the FHWA Micropile Design and Construction (2005).

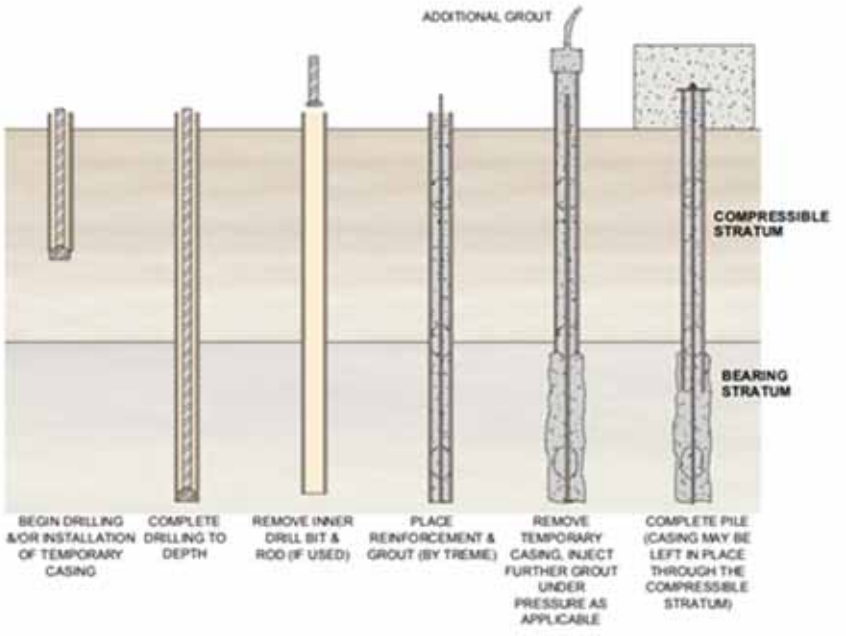

Figure 2-1: Micropile Construction Sequence (FHWA Micropile Design and Construction, 2005)

2.2. History of Micropiles

The idea of using micropile systems was first introduced by Italian engineers in early 1950s for underpinning applications of historic structures in the aftermath of World War II. Italian engineers sought a reliable technology which could withstand large vertical and lateral loads with the minimal displacement, and at the same time least disturbance to existing structures. Fondedile, an Italian contractor, developed micropiles also known as “Root piles” for retrofitting applications due to their speed of execution, their ease of use in damaged buildings and fast performance. Root

piles were piles with a diameter of less than 30 cm, composed of steel reinforcement, and injected with grout. The plate-loading tests performed on the Root piles showed measured capacities of up to 400 *kN*, although the nominal design capacity was calculated to be less based on the design methods for conventional piles. The use of Root piles increased further in Italy and across Europe; In 1962, Fondedile started this technology in United Kingdom in order to strengthen and underpin a number of historical buildings. In 1965, Root piles were used in Germany and Sweden to strengthen and underpin urban transportation facilities. In 1973, Fondedile began introducing micropiles in the United States with engaging in a few projects in New York and Boston, and by mid-70s American specialty contractors started using the technology in by variations in grouts or drilling techniques. Technology developed rapidly, although by the mid-1980s it slowed down due to economic reasons. By the late-80s, due to research efforts by FHWA and trade association promotions by the government, the use of technology took some momentum. FHWA participated in several research and development projects dedicated to specialty geotechnical engineering applications such as micropiles in an effort to encourage the construction industry to use this technology further in the infrastructure projects and published multiple manuals to provide guidelines on design and specification of the micropiles and in mid-90s. By mid-2000s, the International Building Code (IBC) and AASHTO LRFD building design specifications provided special design guidelines in their codes dedicated for design and construction of micropiles and since then the use of micropiles have been widespread in hundreds of engineering and infrastructure projects in North America.

2.3. Applications of Micropiles

With advances in drilling and grouting techniques in the past 20 years, the use of micropiles in engineering applications has significantly increased. Micropiles are currently used as structural support; or as an in-situ reinforcement. Use of micropiles as structural support includes support of new foundations or underpinning of existing ones, seismic retrofitting, and support of embankments, retaining walls and other earth retaining structures. Figure 2-2 schematically illustrates a summary of different micropile applications.

The use of micropiles is almost the best option as a support system, especially in areas with limited access and low headroom where large construction equipment cannot be used. In addition, there's a growing trend in using micropiles due to their cost-effectiveness in applications such as seismic retrofitting, resisting against lateral loading, stability of slopes, and use in places where elements are needed to withstand tension. An example of the use of micropiles to support the foundations of structures is shown in Figure 2-3.

The growth of micropile technology has been accompanied by more publications and design guidelines in this field. This growth in use has been evident in the projects that have used this technology to solve complex engineering problems and the publications that have been developed on how this technology was implemented.

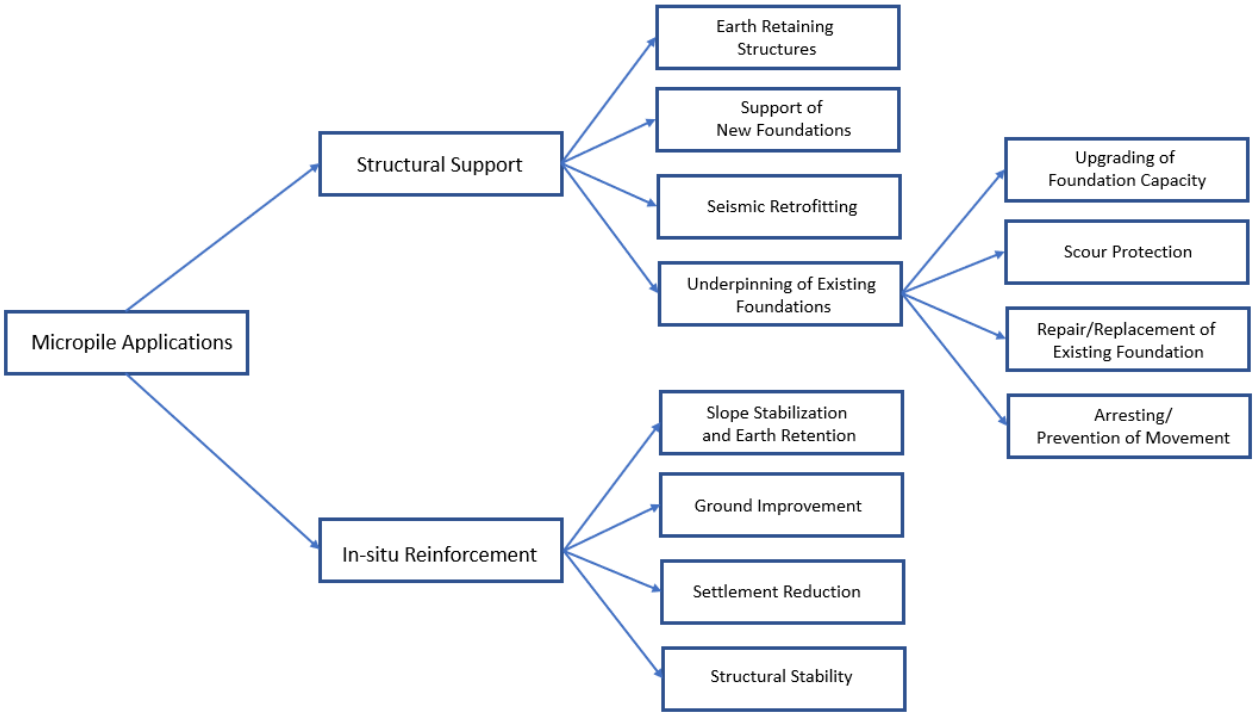

Figure 2-2: Classification of Micropile Applications (FHWA Micropile Design and Construction, 2005)

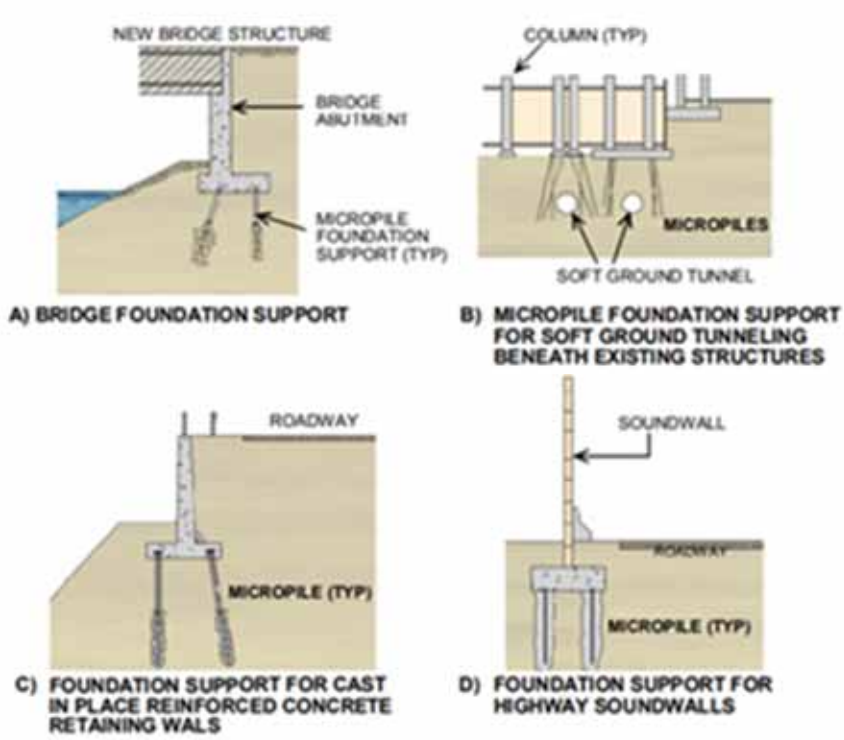

Figure 2-3: Use of Micropile as Foundation Support (FHWA Micropile Design and Construction, 2005)

2.4. Classification of Micropiles

The Federal Highway Administration (FHWA) developed a guideline in 1997 that summarized the state-of-the-practice for micropiles (Drilled and Grouted Micropiles, State-of-Practice Review, 1997). The classification system of micropiles was based on two criteria: design and construction. The design classification approach is based on the behavior of micropile subjected to loadings and the construction classification is based on micropile construction method i.e., method of grouting. The grouting method determines the capacity of the grout-soil bond, which can impact micropile capacity. The classification system consists of two parts: a number that specifies the behavior of the micropile (design), and a letter that indicates the grouting method (construction).

2.4.1 Design Application Classification

The design of an individual micropiles is generally different from the design of network of closely spaced reticulated micropiles and because of this difference micropiles are categorized into two classes: CASE 1 micropile elements and CASE 2 micropile elements. CASE 1 micropiles are loaded directly and the micropile element resists against most of the applied loads. CASE 2 micropiles elements act as composite or network of micropile, and the soil is reinforced and resists the applied loads. The CASE 2 micropile are sometimes referred to a reticulated micropile network.

CASE 1 micropiles can be used instead of most conventional piles and can transfer the load to the competent bedrock. The CASE 1 micropiles can resist axial or lateral loading and these loads are mainly supported by steel rebar reinforcement as well as the ground-grout bond area. Based

on available data, at least 90% of international applications and almost all projects in the United States involve CASE 1 micropiles. CASE 1 micropiles are designed to function individually, although they may be installed in groups. Figure 2-4 illustrates the CASE 1 class of micropiles in different engineering application (FHWA Micropile Design and Construction, (2005))

CASE 2 micropiles include a network of micropiles also known as reticulated micropiles which are used as components of a reinforced soil mass in order to stabilize slopes or foundations. Unlike CASE 1 micropiles, the structural loads are applied to the entire reinforced soil mass. CASE 2 micropiles are reinforced lightly compared to CASE 1 micropiles as they are not directly loaded like CASE 1 elements. The CASE 2 micropiles create a closed environment and then reinforce the reinforced composite soil. An example of CASE 2 micropiles is illustrated in Figure 2-5. (FHWA Micropile Design and Construction, (2005))

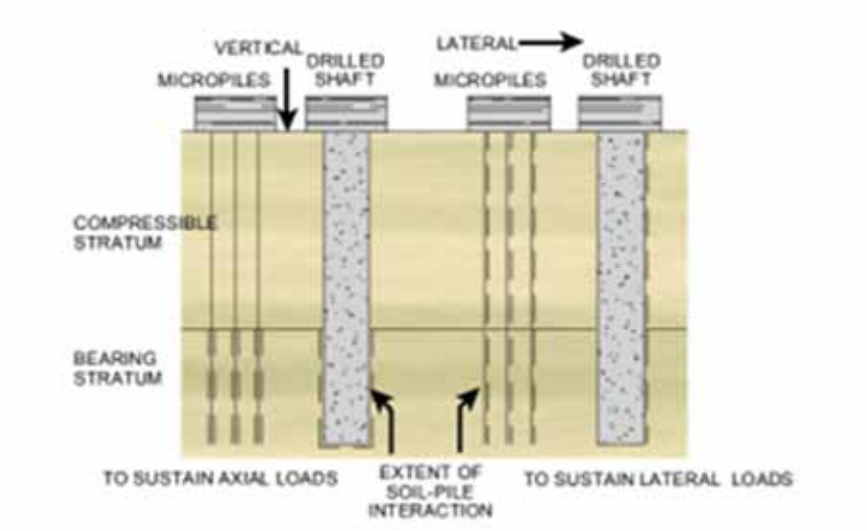

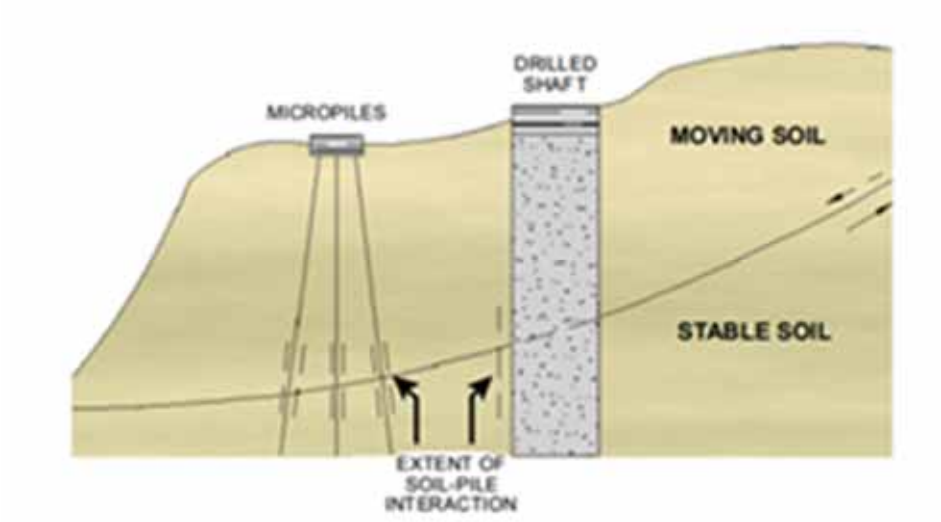

Figure 2-4: CASE 1 Micropiles (FHWA Micropile Design and Construction, 2005)

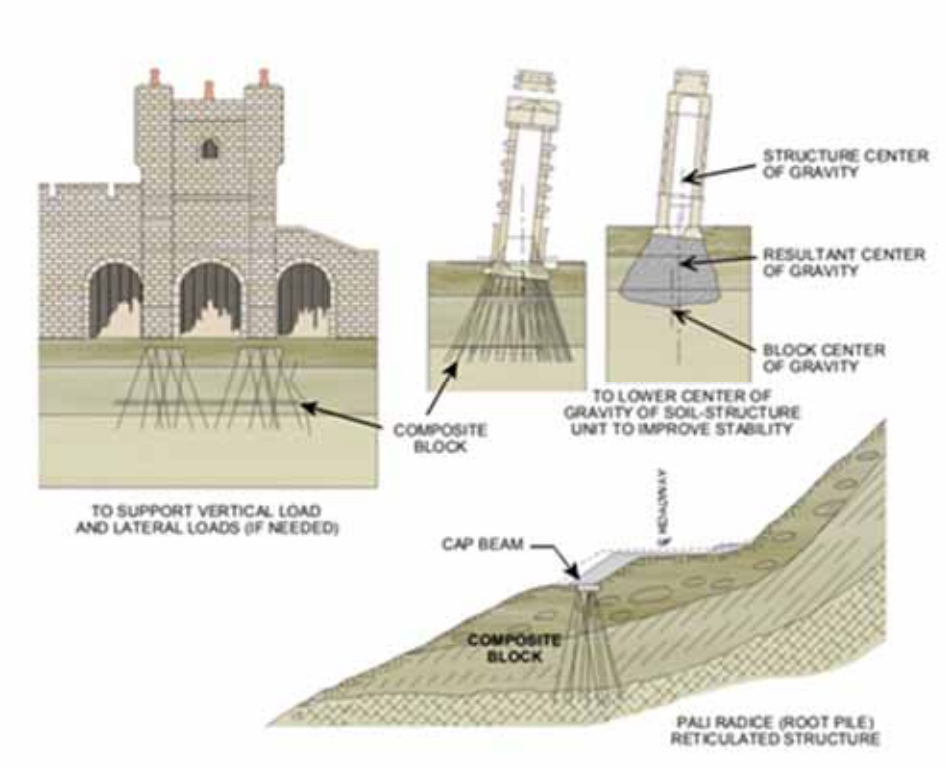

Figure 2-5: CASE 2 Micropiles (FHWA Micropile Design and Construction, 2005)

2.4.2 Construction Type Classification

The grouting method generally determines the ground-grout bond capacity. The capacity of the ground-grout bond area changes directly with the varying the grouting technique. Construction classification categorizes micropiles from A to E and is primarily based on the method of the installation and the grouting pressure used during the construction. Per FHWA design specifications, the use of drilling piping and rebar determines sub-classification. The classification is shown in Figure 2-6 and the details of this classification are provided below.

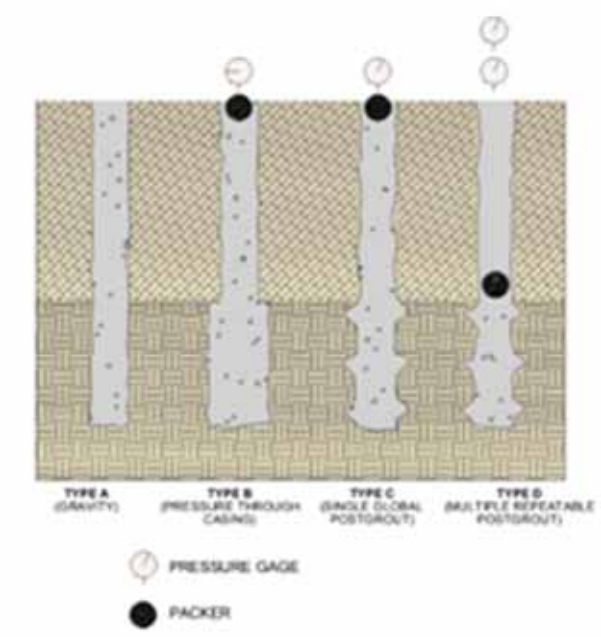

Figure 2-6: Micropile Classification System Based on Type of Grouting (FHWA Micropile Design and Construction, 2005)

Type A: this classification refers to the micropiles in which the grout is only placed under the gravity head in the borehole. Sand-cement mortars or neat cement grout can be used since the grout column is not under pressure. The lower part of the pile bore may be drilled larger in order to

increase the tensile capacity, although this method is not common and is usually used in other cases.

Type B: this classification refers to the micropiles in which neat cement grout is poured into the borehole under pressure as the drill casing is withdrawn. In order to prevent hydraulic failure of the surrounding ground, the grouting pressure is usually limited to between 0.5 MPa and 1 MPa (72 to 145 psi).

Type C: this classification refers to the micropile with two injection stages; first the neat cement grout is placed under the gravity head in the borehole similar to Type A, and then before the initial grout hardens (typically between 15 to 25 minutes), a similar grout is injected via sleeved grout pipe and without the use of the packer under a pressure of 1 MPa (145 psi).

Type D: this classification refers to micropiles injected in a two-stage process similar to Type C, but with some modifications in the second injection stage. The neat cement grout is placed in the borehole under gravity head as in types A and C or under pressure similar to B. After the hardening of the initial injection stage, additional grout is injected into the borehole with a pressure of 2 MPa to 8 MPa (290 to 1,160 psi). In this type, a packer may be used on the lower side, and it is known that the use of this type is very common globally.

Table 2-1 from FHWA Micropile Design and Construction, (2005) describes the classification based on grouting technique (construction) in detail. Some classifications (numbers 1, 2 and 3) are given in the table in order to show the effect of piping and rebars for each injection method. This table is derived from.

Table 2-1: Micropile classification based on grouting technique (construction) - (FHWA Micropile Design and Construction, 2005)

Micropile Type and Grouting Method	Sub-type	Drill Casing	Reinforcement	Grout
Type A Gravity grout only	A1	Temporary or unlined (open hole or auger)	None, single bar, cage, tube or structural section	Sand/cement mortar or neat cement grout tremied to base of hole (or casing), no excess pressure applied
	A2	Permanent, full length	Drill casing itself	
	A3	Permanent, upper shaft only	Drill casing in upper shaft, bar(s) or tube in lower shaft (may extend full length)	
Type B Pressure - grouted through the casing or auger during withdrawal	B1	Temporary or unlined (open hole or auger)	Monobar(s) or tube (cages rare due to lower structural capacity)	Neat cement grout is first tremied into drill casing/auger. Excess pressure (up to 1 MPa (145 psi) typically) is applied to additional grout injected during withdrawal of casing/auger
	B2	Permanent, partial length	Drill casing itself	
	B3	Permanent, upper shaft only	Drill casing in upper shaft, bar(s) or tube in lower shaft (may extend full length)	
Type C Primary grout placed under gravity head, then one phase of secondary "global" pressure grouting	C1	Temporary or unlined (open hole or auger)	Single bars or tube (cages rare due to lower structural capacity)	Neat cement grout is first tremied into hole (or casing/auger). Between 15 to 25 minutes later, similar grout injected through tube (or reinforcing pipe) from head, once pressure is greater than 1 MPa (145 psi)
	C2	Not conducted	–	
	C3	Not conducted	–	
Type D Primary grout placed under gravity head (Type A) or under pressure (Type B). Then one or more phases of secondary "global" pressure grouting	D1	Temporary or unlined (open hole or auger)	Single bars or tube (cages rare due to lower structural capacity)	Neat cement grout is first tremied (Type A) and/or pressurized (Type B) into hole or casing/auger. Several hours later, similar grout injected through sleeved pipe (or sleeved reinforcement) via packers, as many times as necessary to achieve bond
	D2	Possible only if regrout tube placed full-length outside casing	Drill casing itself	
	D3	Permanent, upper shaft only	Drill casing in upper shaft, bar(s) or tube in lower shaft (may extend full length)	

2.5. An Overview of Previous Studies

The response of a structure to the dynamic load is significantly affected by site characteristics, external loading, soil properties, and the structure itself. Therefore, special attention has been paid recently to the publications that evaluate the site response and focus on soil-structure interaction issues for micropile systems:

2.5.1 Experimental Studies on Micropiles

This part of the research looks deeper at the recent experimental studies conducted on micropiles in various soil and loading conditions. The findings from these studies are summarized in the following section The study by Yamane et al. (2000) focused on the vertical behavior of micropiles and included lateral and vertical load tests. The study also included lateral load tests on seven individual micropiles to assess their bending capacity. Five (5) of these micropiles were made up of steel pipes, grout, and thread-lugged bars, while one was similar to these but with additional coupling joints for the steel pipes. The final micropile was simply a plain steel pipe.

Yang et al. (2000) conducted a series of shaking table experiments to evaluate the performance of a single micropile under seismic stress. The test involved a hollow aluminum model micropile placed in a dry sand bed within a laminar container attached to the shake table. The micropile was subjected to sinusoidal horizontal vibrations. The pile's response was calculated using three SSI [2] models, including the standard dynamic beam-on-Winkler-foundation model, the simplified beam-on-Winkler-foundation model, and the 'Pilate' model. The results revealed that when the shaking

[2] Soil-Structure Interaction

table was excited at weak acceleration (below 0.25g), the micropile followed the motion of the soil, and the maximum bending moments occurred near the surface of the sand. This suggests that inertial effects play a significant role in the bending of micropiles during excitations.

Miura et al. (2000) conducted a series of model tests to understand the mechanism behind improving the bearing capacity of footings reinforced with a group of micropiles. The circular footings were reinforced with micropiles arranged in different configurations and were subjected to both vertical and inclined loads. The comparative analysis of the observed load-displacement behavior was used to discuss the factors affecting the bearing capacity improvement. The results showed that the relative density significantly affected the bearing capacity, with dense ground having a notably higher bearing capacity compared to medium and loose ground. In the case of surface footings, shear failure was only observed on the surface in the dense ground due to the dilatant behavior of the ground material, which increased the skin friction on the micropiles and improved the bearing capacity. The interaction between the footing and the group of micropiles was more effective under vertical loading compared to inclined loading.

Juran et al. (2001) conducted a series of tests using a centrifuge on single micropiles, micropile groups, and micropile networks. Different configurations, inclinations, number of micropiles, and loading levels were examined. Finite difference programs, LPILE and GROUP, were utilized to model the centrifuge tests. These tests were aimed at exploring the interaction behavior between the structure, soil, and micropile, as well as evaluating the response of the micropile systems under earthquake loading.

The FOREVER[3] program conducted research on micropiles using centrifuge tests, three-dimensional finite element modeling, and simple models with springs and dashpots. The project led to a better understanding of micropile behavior under seismic loading, with the following main results obtained (FOREVER, 2008, Schlosser et al. 2012 and 2013):

- The results of the FOREVER project on micropiles show that the latest simplified calculation methods based on Winkler's model can be used for the seismic design of foundation micropiles, as they are comparable to the results obtained from both centrifuge tests and three-dimensional finite element modeling;
- Micropile groups exhibit a positive group effect due to a structural effect resulting from connecting the micropiles to the cap. This effect reduces bending moments within the micropiles and top displacements as the spacing between micropiles decreases. Although this effect is not typically quantified, it can be neglected as it is conservative.
- The results of experiments conducted on groups of horizontally loaded micropiles show that these groups exhibit similar effects to regular piles with conventional diameter dimensions. The total resistance of a micropile group is less than the sum of the individual resistances of each micropile due to the shadow effect of piles in front of others in the back. However, this negative effect can be ignored once the spacing between the micropiles reaches 6 to 7 diameters.
- When micropiles are placed in a row perpendicular to the loading direction, the group resistance is weakened due to mechanical interactions within the soil, however this decrease is small and can be neglected once the spacing has exceeded 3 diameters. Additionally, micropiles installed using soil displacement techniques show higher

[3] FOrmation et REcherche en Fondations VErticales Renforcées

stiffness under horizontal loading compared to those installed using non-displacement techniques.

Bruce et al. (1997) proposed a classification system for micropile design, briefly described in a series of papers summarizing the research project initiated by the US Federal Highway Administration in 1993. Part 2 of this series presents recommendations for the design of single micropiles and groups of micropiles for different engineering applications. Their research discusses the ultimate axial and lateral capacity of micropiles, design guidelines for cohesionless soils, cohesive soils, and rocks, and group and network effects. The authors also evaluate existing analytical approaches by comparing them to experimental data on the engineering behavior of micropile groups and reticulated micropile networks under different loading conditions. The study provides a comprehensive overview of design guidelines and recommendations for micropile group systems based on field experiences and full-scale testing observations.

An experimental study was conducted by Sharma and Hussain (2019) to examine the effects of the relative density of sand, pile spacing, and length-to-diameter (L/D) ratio on the load capacity of micropile groups. The study involved testing micropile groups with different *L/D* ratios and center-to-center spacings installed in sand beds of relative densities of 30 percent, 50 percent, and 80 percent. The piles and the pile groups were subjected to different loading conditions to observe their response. The purpose of the study was to understand the impact of these factors on the performance of the pile group and particularly aimed to examine the effect of relative density of sand, pile spacing, and length-to-diameter ratio on the lateral load capacity of micropile groups. Results showed that for sand beds of 30 percent and 50 percent relative density, the highest group capacity was observed at 2D spacing, while for 80 percent relative density, it was observed at 6D spacing. For the 30 percent and 80 percent relative densities, a positive group effect was observed

at 2D and 6D spacing, respectively. Furthermore, for pile length-to-diameter ratio greater than 50, efficiency was found to be greater than 1 for all spacings and relative densities. The mode of failure of the micropile groups was influenced by the length-to-diameter ratio and relative density of sand but not by the spacing of the piles.

Capatti et al. (2019) conducted a comprehensive experimental study on a full-scale group of inclined injected micropiles in transitional silty soils, including ambient vibration, impact load, and forced vibration tests. The micropiles were inclined in only one direction, and tests were performed in both the direction of inclination and the orthogonal direction to capture the effects of inclination on system dynamics. The results of the tests allowed for the dynamic characterization of the soil-foundation system at both small and medium-high strain levels and showed the evolution of system behavior from linear to nonlinear. Permanent and movable instrumentation, consisting of strain gauges on the piles, accelerometers, and geophones, was used to measure pile strains and the acceleration of the cap and soil during the tests. The main findings from the experimental study are:

- By comparing the behavior of the soil-foundation system from impact load and ambient vibration tests in the direction of micropile inclination and the orthogonal direction, the effect of inclination on the fundamental frequencies of translational modes and relevant damping ratios can be determined. Specifically, the fundamental frequency in the inclination direction is approximately 18% higher than in the orthogonal direction.
- The nonlinear behavior observed in the soil-micropile system is consistent with the intermediate nature of the foundation soil, featuring both phenomena that are typical of cohesive soils (such as gap formation around the micropile shaft) and granular soils (such as the refilling of the gap with partial recovery of original dynamic properties).

- Reduction in the damping ratios associated with translational modes is observed in conjunction with a reduction in system frequencies. This effect, which is more pronounced in the direction of micropile inclination, is likely caused by the formation of gaps at the soil-micropile interface, reducing the system's ability to dissipate energy through radiation in the soil.

To examine the impact of inclination angle on the dynamic performance of a micropile system, Komak Panah et al. (2019) carried out shaking table experiments using a small-scale physical model of micropiles. The model consisted of a group of 4 x 4 micropiles embedded in a low-density sand fill and subjected to sine wave excitations as shown in Figure 2-7. The responses of various points in the model were recorded as sine waves were applied to its base. The analysis from the shaking table experiments revealed the following important observations and findings:

- The results of the experimental study revealed that when sine waves were applied to the micropile system at different inclination angles, the acceleration on both the soil surface and the micropile cap increased compared to the input excitation acceleration.
- When the micropiles were inclined, their highest acceleration response was lower than the maximum acceleration recorded on the soil surface. The ratio of acceleration at the micropile cap to the soil surface was less than 1, with the minimum value of this amplification ratio appearing when the micropiles were inclined 10° from the vertical direction.
- The results of the study showed that the amplification ratio of acceleration on the micropiles cap compared to the input acceleration decreased significantly due to the inclination of the micropiles. In simpler terms, when the micropiles were inclined within the range of angles studied, they experienced lower acceleration and displacement during

shaking events because the lateral stiffness and resistance of the group of micropiles to seismic lateral loading increased. As a result, the seismic performance of the micropile system in terms of horizontal acceleration was improved.

- The results of the study also provide evidence in support of the observation made post-earthquake and previous numerical investigations, which indicated improved seismic performance of inclined micropiles compared to vertical micropiles. These experimental findings justify the use of inclined micropile systems in seismic-prone areas. The results of the physical tests can also serve as useful references for future analytical advancements in the modeling of inclined micropile systems.

Figure 2-7: A view of the uniaxial earthquake shaking table facility in the Hong Kong Polytechnic University (After Komak Panah et al. 2019)

2.5.2 Numerical and Analytical Studies on Micropiles

The findings of the linear and nonlinear numerical analyses conducted by Kishishita (2000) revealed that the relative rigidity of pile and soil (E_p/E_s) has an impact on the horizontal displacement of the top structure and micropile cap. E_p and E_s represent the Young's modulus of the pile and soil, respectively. The analysis demonstrated that an increase in the relative rigidity (i.e., a softer soil) led to an increase in the displacement.

Research conducted by Kishishita (2000) and Juran et al. in 2001 showed that the horizontal movement of raked micropiles was less than that of vertical micropiles. As the inclination of the micropiles increased, the fundamental frequency of the system increased, as found by Juran et al. Sadek and Shahrour's (2003) seismic analysis showed that when the micropile inclination increased, lateral stiffness, bending moment, and axial force increased, but shear force and lateral acceleration at the cap and superstructure decreased.

Shahrour et al. (2001) conducted a series of 3-dimensional modeling using a finite element program called PECPLAS to analyze the behavior of micropiles. The analysis included a single micropile and a group of micropiles supporting a structure. The micropile group consisted of groups of 1×3, 3×3, and 3×5 micropiles, which were modeled as embedded in soil overlaying a rigid bedrock. The soil-pile-structure system was considered elastic with Rayleigh material damping, and the cross-section of the micropile was assumed to be square. The structure was modeled as a single degree-of-freedom system with a concentrated mass and column, and the soil was modeled with periodic conditions at the lateral boundaries for the displacement field. Seismic loading was applied at the base of the soil as a harmonic acceleration with its frequency equal to the fundamental frequency of the soil. Figure 2-8 illustrates the 3-D FEM Mesh used by Shahrour et al. to conduct FEM seismic analysis of a group of micropiles.

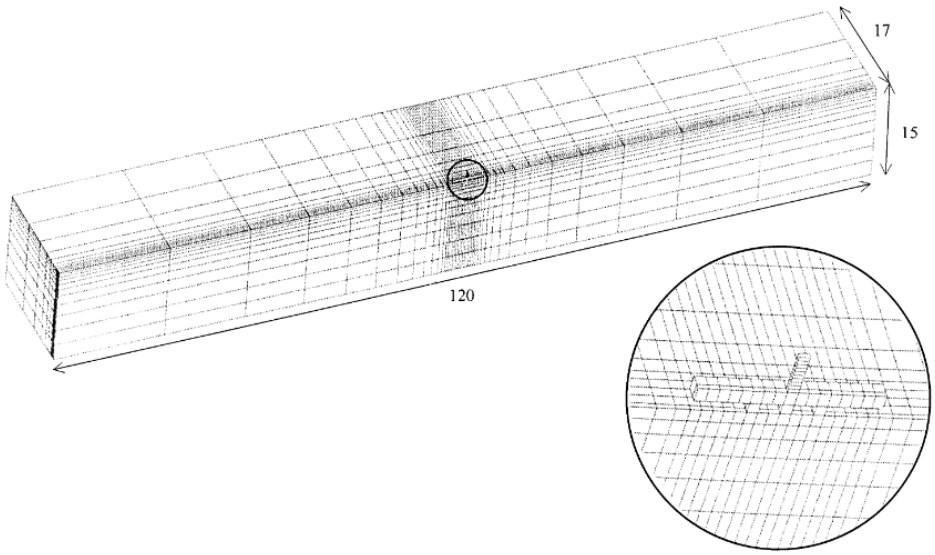

Figure 2-8: The FEM Mesh used for Finite Element analysis micropiles (after Ousta and Shahrour 2001)

Shahrour et al. (2001) found that the mass and frequency of the superstructure have a significant impact on inertial interactions in SSI problems. They showed that as the mass of the superstructure increased, the lateral displacement, bending moment, and shear force at the pile head also increased. Furthermore, when the frequency of the superstructure was close to the loading frequency, significant increases were observed in the horizontal displacement, bending moment, and shear force of the superstructure. These findings emphasize the important role that the frequency of the superstructure plays in the design of micropile foundation systems. Figure 2-10 illustrates the effect of fundamental frequency of superstructure on the lateral displacement in micropile and bending moment in micropiles. Figure 2-9 displays the effect of fundamental frequency of superstructure on lateral displacements as well as the shear forces and bending moments of micropile members in the group.

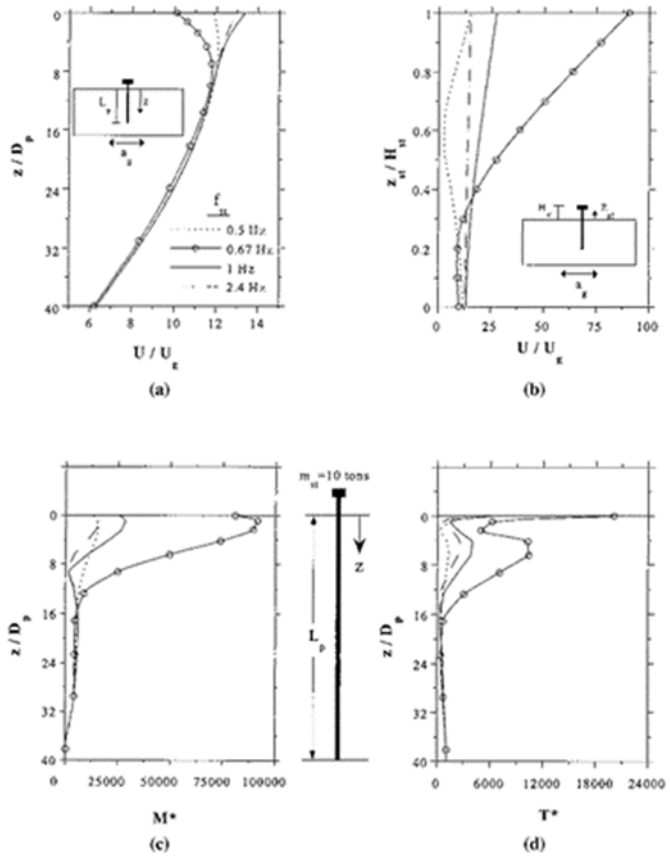

Figure 2-9: The effect of fundamental frequency of superstructure: (a) amplification of lateral displacement in micropile, (b) amplification of lateral displacement in superstructure, (c) bending moment in micropile, and (d) shearing force in micropile (after Shahrour et al., 2001)

Shahrour et al. (2001) and Ousta and Shahrour (2001) also found that the bending moment increased as the micropile spacing increased, which is due to frame action. However, they found that the micropile spacing has a negligible effect on the distribution of shear forces. They also found through their FE analyses that as the number of piles increased, the bending moment decreased. However, unlike in the case of pile spacing, the shear force increased with the increase in the number of piles.

The studies by Shahrour et al. (2001) and Juran et al. (2001) further indicated that there is a positive group effect in a micropile group. They found that the maximum bending moment at the central part of the micropile (around mid-height of micropile) decreases as the number of micropiles increases from 9 to 15. Similarly, Juran et al. (2001) observed a reduction in bending moments and displacements of micropile groups with s/D=3 compared to groups with s/D=5 when subjected to a selected frequency of excitation (a=0.3g). These findings highlight the positive impact of having multiple micropiles in a group. They further studied the position of the micropile within a group and that it affects the internal forces it experiences under seismic loading. According to the experimental data from Juran et al. (2001) and numerical analyses from Shahrour et al. (2001), the loads taken by corner micropiles are greater than those taken by the center micropile, meaning that the seismic load is not evenly distributed throughout the micropile group.

Kishishita (2000) found through numerical analysis that the pile type did not affect the horizontal displacements of the top structure and the micropile cap. Despite the use of four different pile types (precast, cast-in-situ, high-capacity micropiles, and raked high-capacity micropiles), the horizontal response was nearly the same at these two points. According to Kishishita, this is because the micropile cap moves in response to the soil. Another numerical simulation by Kishishita (2000) utilized a trilinear model for cast-in-situ piles, a modified Takeda model for precast piles, and a bilinear model for high-capacity micropiles. The results indicated that during a real earthquake, such as the Kobe earthquake, the high-capacity micropiles retained their linearity while the precast and cast-in-situ piles failed. This highlights the fact that high capacity micropiles have high resistance to earthquakes and provide higher ductility.

Sadek et al. (2008) conducted a study using a 3D finite element model to analyze the impact of the inclination of micropiles on their response to seismic loading. The study considered two cases:

micropiles in a soil layer with constant stiffness and micropiles in a soil layer with stiffness increasing with depth. Figure 2-10 shows a schematic of the FEM mesh used for soil–micropile–structure system.

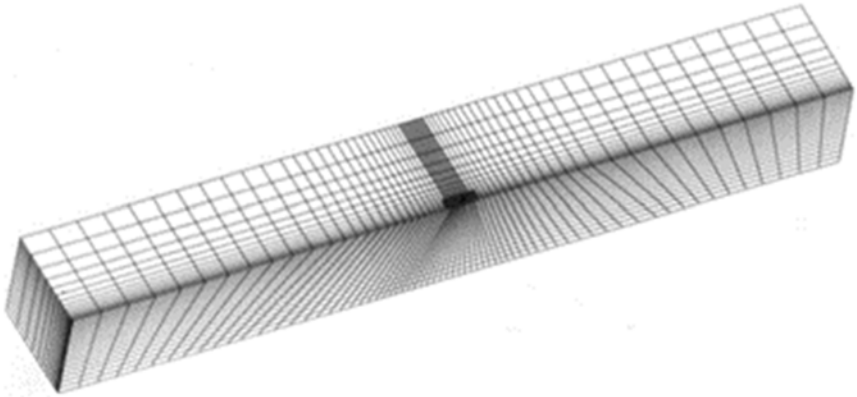

Figure 2-10: The FEM mesh used for soil–micropile–structure system (After Sadek et al. 2004)

The results showed that inclining the micropiles improves their performance in seismic loading and reduces both shearing forces and bending moments. The inclination results in an improved utilization of the axial stiffness of micropiles, leading to a decrease in shear forces and bending moments during seismic loading. The influence of inclination on the seismic response of the group of micropiles is shown in Figure 2-11.

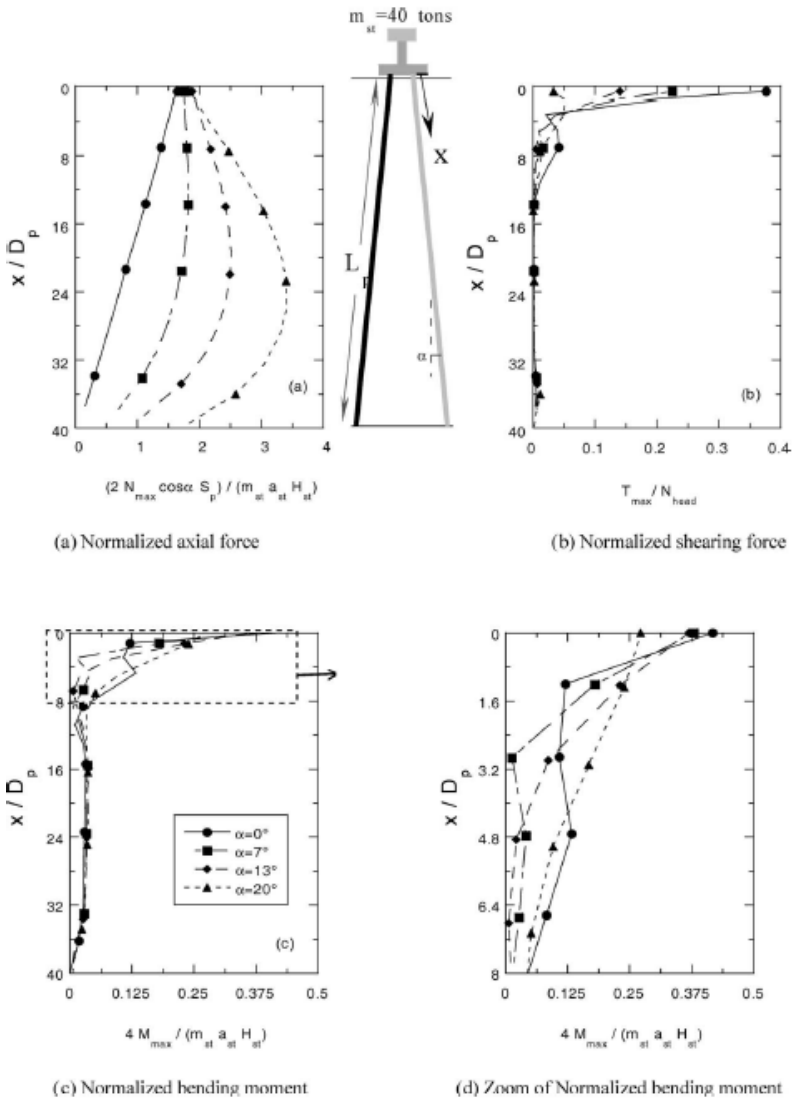

Figure 2-11: Influence of inclination on the seismic response of the group of micropiles

The numerical studies conducted by Teerawut (2002) on full-scale tests discovered that the impact of pile diameter on the stiffness of the p-y curves for piles in sand is influenced by the sand's relative density. For dense, weakly cemented sand, the pile diameter's effect on the p-y curves was minimal until the soil reached its maximum resistance. However, for loose sand, an increase in pile diameter led to an increase in the stiffness of the p-y curves. In essence, a higher

relative density will reduce the impact of pile diameter on the p-y curves. Figure 2-12 illustrates the FEM mesh developed for an individual pile for this study.

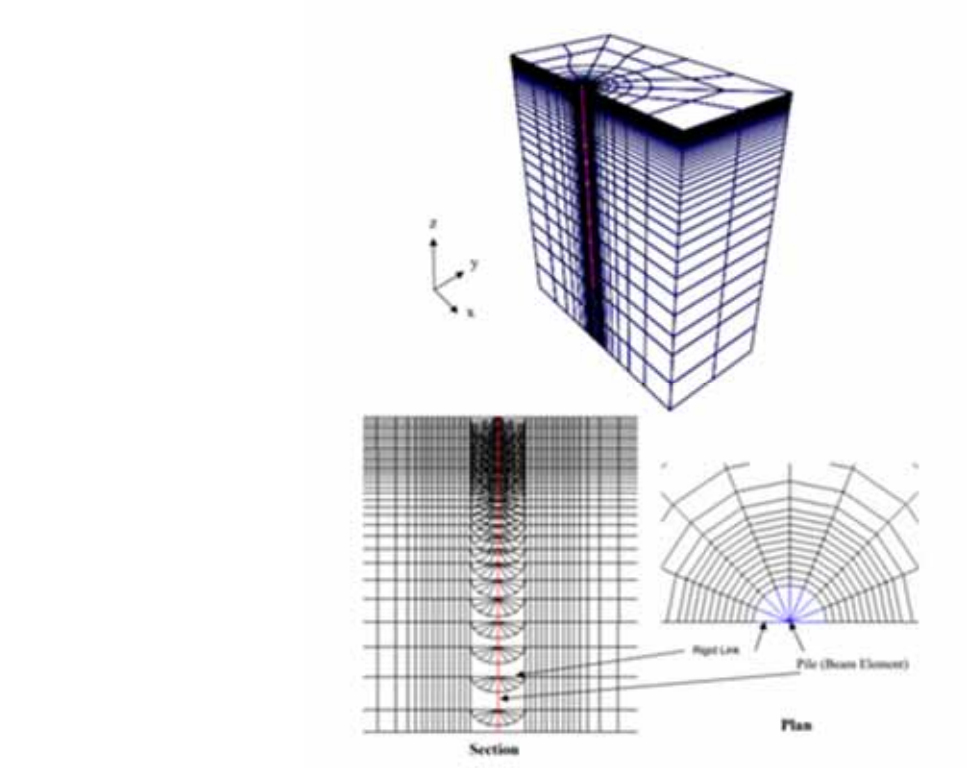

Figure 2-12: The FEM mesh used for Finite Element analysis of an individual pile (after Teerawut 2002)

It was also noted that as the pile diameter increased, the natural frequency of the soil-pile system increased due to an increase in its stiffness. Additionally, the damping ratio increased because the damping of the soil comes mainly from radiation damping, which is influenced by the contact area and excitation frequency. The radiation damping increases with an increase in the contact area between the pile and soil and with an increase in the excitation frequency.

Shu (2004) conducted a comprehensive study on the performance of micropiles in sands with different initial states, using a state-dependent constitutive model coded with C++ and implemented in the FLAC3D finite difference geotechnical software. The model was first verified

using laboratory triaxial tests on Toyoura, Ottawa, and Fontainbleau sands, and then validated with a full-scale test on a micropile group installed in Fontainbleau sand. The study revealed that the side resistance of micropiles is influenced by the initial normal stress and its positive increment due to shear-induced dilation of dilative sand, and negative increment due to contraction of contractive sand. Load transfer in a group of piles is controlled by overlap of stresses induced by adjacent piles and dilatancy, with positive group effects on side resistance and tip resistance. Inclination also affects pile resistance, with outward inclined network pile groups exhibiting higher resistance than inward inclined pile groups, depending on the sand state.

Wong et al. (2005) conducted thorough analysis of micropiles and developed finite element 2-D models using two different soil constitutive models: linear elastic and bounding surface plasticity (Figure 2-13). The interface between the micropile and soil was either modeled as a perfect bond or with interface elements that accounted for friction. In the case of dynamic loading, a superstructure with a single degree of freedom (SDOF) was placed on top of the micropiles. The study was conducted through a series of parametric tests, looking at the impact of various independent variables including load intensity, non-linearity of soil and soil stiffness for static cases, and soil non-linearity, input motion intensity, frequency contents of the input motion and the natural period of the superstructure for dynamic cases.

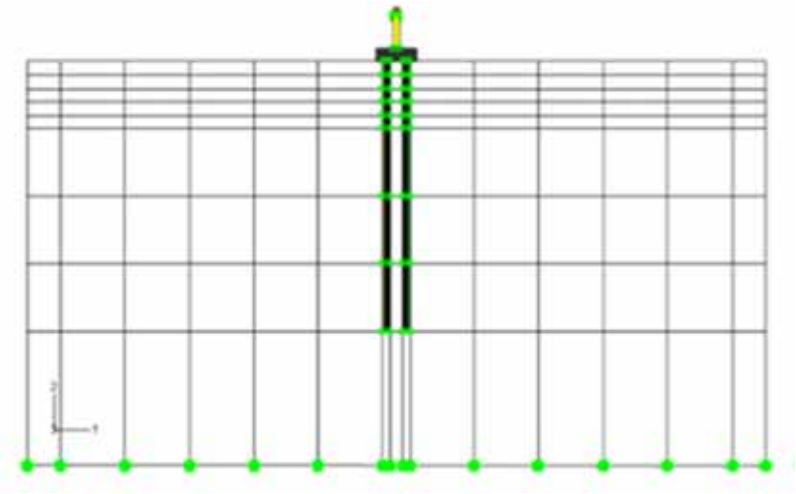

Figure 2-13: 2-D Finite Element model for two vertical micropiles under dynamic loading (after Wong et al. 2005)

The results of these tests showed indicated that increase in soil's non-linearity results in further increase in the displacements of micropiles, this is because soil with higher non-linearity exhibits a decrease in stiffness when subjected to larger strains, which results in higher deflections of the micropile even if both soils have the same initial stiffness (Figure 2-14). The bending moments in micropiles in soil with higher non-linearity are higher compared to those in soil with more elastic material, due to the lesser degree of load transfer from the micropile to the soil in the more non-linear material.

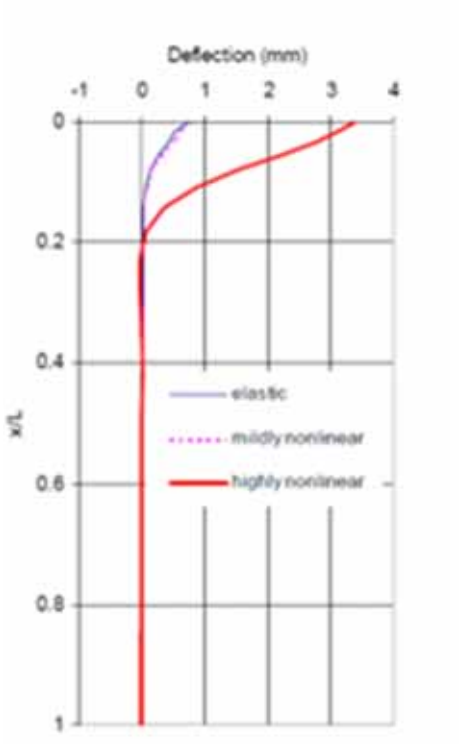

Figure 2-14: Variation of deflections with depth from elastic and inelastic soil materials with the load of 100 *kN* at the micropile head (after Wong et al. 2005)

Turan et al. (2008) conducted a series of dynamic and pseudo-static analyses on micropile groups. The objective of the dynamic and pseudo-static analyses was to study the implications of designing micropiles with an upper casing section compared to not using casing. They also carried out some sensitivity studies to evaluate the EI of the pile cap and the effects of a surface surcharge on the ground surface. The results indicated that the maximum values of the bending moments did not show significant change due to the flexural rigidity (EI) of the pile cap. The maximum gapping between the pile and soil for the flexible cap was 33% greater than that for the rigid pile cap case.

Also results showed that raising the surface surcharge from 0 to 50 KPa caused a 64% increase in the maximum bending moments in the pile due to a harmonically varying static lateral load. The findings indicated that increasing the surface surcharge reduced the pile-soil separation. The

pressures on the soil-pile interface remained largely unchanged with increasing surcharges up to a depth of 1.5 meters. However, the values increased with the increase of surface surcharge beyond 1.5 meters.

El Naggar et al. (2010) investigated the effect of increasing drill bit diameter and micropile spacing on the performance of Hollow Bar Micropile (HBMP) groups through field load testing and 3D finite element modeling. Four groups of HBMPs were tested in sand with different drill bit diameters and spacing to micropile diameter ratios. Results showed that micropile groups constructed with larger drill bits had higher stiffness and load capacity compared to those constructed with smaller bits. Group efficiency ratios were close to unity for all groups, and the ultimate skin friction values were higher than suggested by the US Federal Highway Administration for medium to very dense sand. The HBMP group settlement increased by 25% to 33% due to the group effect.

Theinat et al. (2015) conducted a study on a recently completed 5-span bridge along the Foothills Parkway of the Great Smoky Mountains, TN. The study aimed to examine the interaction between the ground and micropiles using both field data performance and numerical modeling. Two out of the four piers were instrumented with strain gauges to measure the load transfer in the foundations consisting of twenty 10-inch micropiles under the pile cap for each pier. The 3D computer model included the micropile foundation within the steep rock bedding planes and overburden soils. The study found that the load transfer behavior of a single micropile and group micropiles with s/D=3.9 were almost identical. Additionally, the load transfer was not significant in the overburden soil up to interface friction of 0.3 between the micropile and the ground. The study also found that the bond zone of long micropiles carries a small percentage of the load due to the intermediate value of stiffness, while short micropiles carry a much higher percentage of the

load because the high stiffness rock is closer to the load source. Finally, the study concluded that the load transfer mechanism is affected by friction and the elasticity modulus, and neither factor alone can guarantee good load transfer.

Rajkumar et al. (2015) investigated the design of foundations supporting rotary machines and the influence of soil-structure interaction (SSI) on their behavior. Depending on the soil conditions, loadings, and other requirements, these foundations can be supported on a raft or pile foundation. However, neglecting the effects of the Soil-Structure Interaction may not always be a safe practice, while conducting rigorous SSI analyses can be computationally expensive. To address this, the study used an analytical model with a lumped-mass approach and compared the results with a 3D finite-element (FE) model. The results showed that simplified methods could be used for foundations resting on rock-to-dense-soil conditions, but FE analysis was mandatory for stiff-to-soft soil conditions. The study also observed that SSI effects reduced the natural frequency significantly for a raft-supported framed-foundation on soft soil strata. Pile-supported framed-foundations were found to be a better solution for soft soil conditions in controlling the vibrations of the framed-foundation compared to raft foundations.

Elsawwaf et al. (2022) carried out a detailed numerical investigation on the performance of micropiled rafts subjected to both vertical and lateral loads when installed at an incline. The analysis was performed using a finite element method that was validated against actual field tests. Figure 2-15 displays the FEM mesh developed for the micropile rafts. The soil layer consisted of soft clay on top of a dense sand layer. The study examined the impact of several factors, including the magnitude of vertical loading, the type of reinforcement, the inclination angle of the micropiles, and the number of inclined micropiles. The results showed that an increase in vertical load led to a consistent decrease in the lateral load capacity of the micropiled rafts. When all the micropiles

were inclined, the positively inclined micropiles took 79-86% of the total lateral load, while the negatively inclined ones carried 14-21%. Inclined micropiles provided a greater lateral load sharing ratio compared to vertical micropiles, with the maximum value achieved at an inclination angle of 45 degrees. Figure 2-16 shows the effect ratio of lateral load of a micropile to total lateral load carried by micropiles. The effect of micropile reinforcement on improving lateral performance was found to be relatively low compared to the effect of the inclination angle of the micropiles.

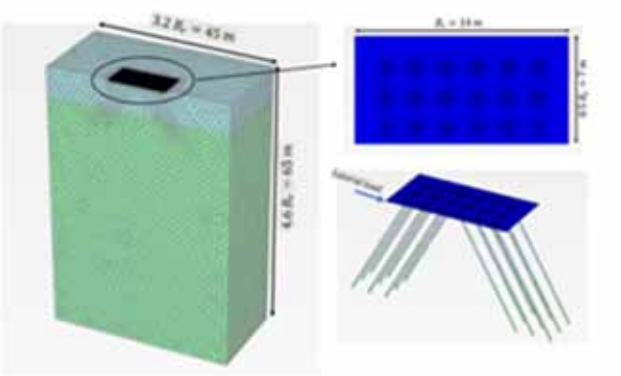

Figure 2-15: The FEM Mesh used for Finite Element analysis of rafted micropiles (after Elsawwaf et al., 2022)

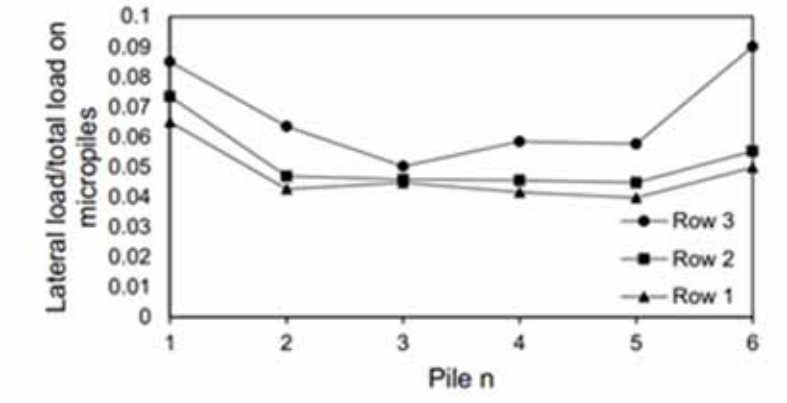

Figure 2-16: Ratio of lateral load of a micropile to total lateral load carried by micropiles (after Elsawwaf et al., 2022)

Ossama (2015) conducted a three-dimensional finite element study of the soil-pile system with viscous boundaries to determine the dynamic stiffness and damping generated by soil-pile interaction. The study investigated the vertical vibration characteristics of a pile response to a vertical harmonic loading at the pile head, considering factors such as the dimensionless frequency, soil and pile properties, as well as the length and axial load on the pile head. The pile was embedded in a linearly elastic, homogeneous soil layer with constant material damping. The results of the study indicated how spacing and soil shear stiffness can affect performance of the pile groups. The studies revealed that in strong soils, the vertical static stiffness of pile groups increased with increasing soil shear modulus and spacing of the piles as it can be observed from Figure 2-17. The increase in stiffness was attributed to the load sharing between the piles within the groups and the soils around the piles. For a group of piles embedded in weak soils, the piles acted as end bearing piles and transferred the load to the surrounding soil. As the soil shear modulus increased, the load was gradually transferred to the surrounding soil, and the piles acted as friction piles in strong soils.

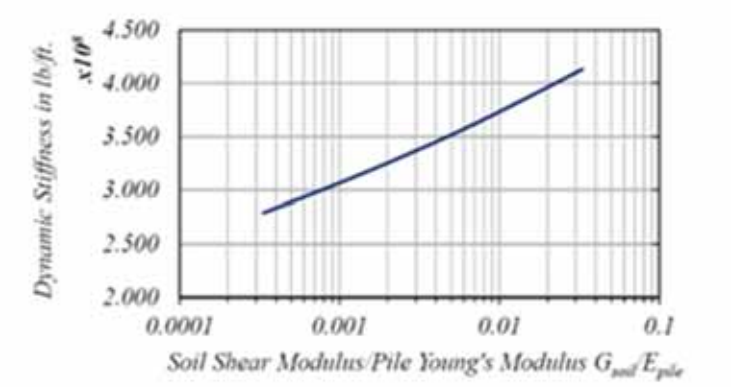

Figure 2-17: Effect of Soil Shear Modulus/Pile Young Modulus on Dynamic Stiffness of the Piles (After Ossama et al., 2015)

Also, the results of this research revealed that the pile group under dynamic loading exhibited behavior similar to that of static loading, with the pile cap's stiffness producing the same vertical displacement of the piles. However, the forces transmitted to each pile were different. In weaker soils, all piles carried an equal load at resonance, while in stronger soils, the corner pile carried the highest load, followed by the edge pile, and the middle pile carried the lowest load.

2.6. Present Codes for Design of Micropiles

According to FHWA Supported Structures Research for Seismic Behavior of Micropiles (Rodriguez-Marek A., Balasingam Muhunthan, 2005) there are currently two design guidelines documents on micropiles that have been published in the United States:

- Drilled and Grouted Micropiles – State-of-Practice Review: Volume 2: Design by the U.S. Department of Commerce National Technical Information Service (1997) reviewing the current design practices for drilled and grouted micropiles.
- Micropile Design and Construction Guidelines Implementation Manual by the Federal Highway Administration (2000) providing a summary of the geotechnical aspects of micropile design from these two documents will be provided below.

2.6.1 Federal Highway Administration (FHWA): Drilled and Grouted Micropiles - State-of-Practice Review: Volume II: Design

This document introduces a new classification system for micropiles, based on two criteria: the design philosophy (behavior) and the method of grouting (construction). The system categorizes

micropiles into two types: CASE 1 and CASE 2. CASE 1 micropiles are single or group elements that are loaded directly and are primarily supported by the steel reinforcement and the bond between the grout and ground. On the other hand, CASE 2 micropiles function as a reinforced soil composite to resist loads and are usually less reinforced than CASE 1 micropiles. The majority of micropile usage in the United States is CASE 1 and this is the focus of the study. The geotechnical capacity of micropiles subjected to axial, lateral, or combined loading must be evaluated by determining the grout-ground interface parameters and the initial stress state in the ground after micropile installation, which is influenced by the grouting pressure. The geotechnical design guidelines for single micropiles under axial loading are based on ultimate load capacity and vertical displacement control. The design method can be selected from empirical methods for predicting ultimate load, load-transfer interface models for estimating vertical displacement, and site-specific loading tests. Currently in the US, there are no design codes for the four types of micropiles as discussed in this Chapter (A, B, C, and D). For Type A micropiles, design usually adheres to established specifications for large-diameter drilled shafts, such as AASHTO 1992 or Caltrans 1994. On the other hand, for types B, C, and D micropiles, the British Standard BS 8081 (1989), referencing Littlejohn and Bruce (1977), and the French code (CCTG 1993), based on the work of Bustamante and Doix (1985), would be applicable.

For micropile groups and networks, there is currently no specific design code in the United States. Similar to single micropiles, the design criteria used for these structures involves determining the ultimate load capacity and displacement control. The ultimate load capacity and displacement of micropiles are affected by factors such as the spacing between piles, soil and site conditions, and the type of micropile and pile cap used. The group efficiency factor, which is an

important factor in determining the ultimate load capacity of a group of micropiles, is also very reliant on the method of installation.

Therefore, it can be concluded that ultimate axial loading capacity of micropile groups and networks does not have a well-established design code for determination and generalization in the industry. AASHTO (1992) provides a method following Terzaghi and Peck (1948), which has been used for conventional piles and calculates the axial group capacity as either the sum of the individual piles' capacities or the axial load capacity for the group's block failure. Another code that can be used for a preliminary estimate is the French CCTG (1993), which has a conservative equation for determining the group efficiency factor based on Converse-Labarre group efficiency equation. The followings are methods that have been used to estimate the vertical displacement of pile groups (Rodriguez-Marek A., Balasingam Muhunthan, 2005):

- Empirical correlations: This method uses empirical correlations based on the observation of the vertical displacement of pile groups and that of a single pile. Some of the commonly used correlations are by Skempton (1953), Vesic (1969), Meyerhof (1976), and Fleming et al. (1985).
- Continuum Elastic Methods: This method uses Mindlin's equations to describe the behavior of pile groups. The methods were used by Butterfield and Banerjee (1971), Randolph and Wroth (1979), Poulos and Davis (1980), and Yamashita et al. (1987).
- Load-transfer Models and Hybrid Methods: This method involves the use of load-transfer models and hybrid methods to estimate the vertical displacement of pile groups. O'Neill et al. (1977), Chow (1986), Lee (1993), and Maleki and Frank (1994) are some of the researchers who have used this method.

- Pure Shear Interface Model: This method assumes no radial movement and was developed by Randolph and Wroth (1979).

2.6.2 Federal Highway Administration (FHWA): Micropile Design and Construction Guidelines: Implementation Manual

Per FHWA Supported Structures Research guidelines, the implementation manual provides general guidance on the design of micropiles in accordance with the 1996 AASHTO Standard Specifications for Highway Bridges, 16th edition. The SLD and LFD methods are used to estimate the load capacity and displacement of the micropiles. The design of micropiles is primarily based on the grout-to-ground skin friction, with the exception of when the micropile is embedded in rock, and no end bearing is considered. The manual presents some design guidelines and considerations but does not provide a step-by-step design procedure. The also manual provides guidelines for determining the geotechnical load capacity of a micropile. It includes estimating the load transfer parameters between the grout and the ground for different soil layers, determining the bond length of the micropile to support the load, and evaluating the group effect for axially loaded micropiles. The manual also highlights the sensitivity of the micropile's geotechnical load capacity to the pile construction process, especially the techniques used for drilling, flushing, and grouting the pile. The manual includes a table with estimated unit values for the bond strength between the grout and the ground for various installation methods and soil conditions. These values are based on the experience of local contractors or engineers. The bond length is determined based on the estimated bond strength, and it is noted that group effects in micropiles tend to be beneficial in granular soils due to the compaction from pressure grouting. The manual considers various geotechnical factors in its design guidelines such as the expected structural axial displacement, long-term ground creep

displacement, settlement of the pile group, stability against buckling, and considerations for both downdrag and uplift (Rodriguez-Marek A., Balasingam Muhunthan, 2005).

2.7. Conclusion of Literature Review

Through a thorough literature review, it was found that there are very limited studies, if any, that have investigated the behavior of micropile groups supporting machine foundation systems. This lack of understanding is concerning as it can lead to faulty design and construction, resulting in severe economic and safety implications. Therefore, this study aims to fill this knowledge gap and provide some insights into the behavior of micropile groups under machine foundation loads.

It is worth noting that micropiles have unique properties that distinguish them from traditional piles. They are characterized by their small diameter, high strength, and grouted bond zone. The bond zone can have a significant impact on the overall performance of the micropile group, which is not the case with traditional bored or driven piles. Therefore, studying the behavior of micropiles under machine foundation loads is of paramount importance, not only to better understand the nonlinearity of the system but also to provide guidance for proper design and construction practices.

Furthermore, the nonlinearity of the micropile group system must be carefully taken into consideration when analyzing its behavior under machine foundation loads. The presence of the grouted bond zone adds significant complexity to the system, making it difficult to predict its behavior using traditional linear analysis methods. Therefore, a comprehensive study using advanced numerical techniques such as three-dimensional finite element analysis (3D FEA) is

required to gain a better understanding of the micropile group's behavior under machine foundation loads.

Chapter 3 - Numerical Modeling and Soil Constitutive Law

3.1. Introduction

In the previous chapter, a summary of the micropile systems and the important studies pertaining to the behavior of micropiles under dynamic loading were reviewed. In this chapter, the numerical modeling of the soil-micropile system is presented. Numerical methods offer great advantages such as cost-effectiveness, the ability to accurately model the soil and the structural elements behavior and therefore can be a great tool to analyze these structures under various loading conditions.

The chapter focuses on using ABAQUS, a finite element module, to model the soil-micropile system for a group of micropiles subjected to dynamic loading. ABAQUS is a multipurpose software that can perform a variety of analyses and computational studies including linear and nonlinear dynamic analysis. It has a wide range of element types to model the soil as continuum as well as structures and the soil-structure interfaces. The chapter explains the details of the numerical modeling, including the elements used to model the soil and the micropile, their interface and the modeling of the boundary conditions. Additionally, a parametric study is conducted to investigate the impact of the various soil boundaries on the vertical dynamic response of the micropile group. In addition, in this chapter, the nonlinear constitutive model used for the soil in the finite element models is also described.

3.2. Numerical Module : ABAQUS

In this research, the software ABAQUS was used to model the soil medium as a continuum, as well as the micropile groups. ABAQUS is a finite element analysis and simulation software for

modeling and analyzing complex engineering problems. It is widely used in various industries, such as aerospace, automotive, and construction, to predict the behavior of structures under different loads, temperatures, and environmental conditions. The software can handle a wide range of problems, including linear and nonlinear static and dynamic analysis, heat transfer, and fluid dynamics. It also provides a robust set of post-processing tools to visualize and interpret simulation results.

The software ABAQUS has the capability to simulate complex engineering models and can also use models created in other software, such as AutoCAD, to export to ABAQUS. Engineering models can be generated in multiple portions and assembled in ABAQUS using geometry features. In addition, the physical properties, such as linear or nonlinear, are incorporated into the software through various engineering models. Different network meshes and types can be created for a model in ABAQUS. Additionally, the software is capable of defining interface contacts between different bodies or surfaces, which can be defined between them based on the type of interaction. For solid mechanics problems, various boundary conditions can be applied, such as displacement, velocity, acceleration, and various types of forces, such as pressure, body forces, line loads, surface loads, or concentrated loads. The boundary conditions and forces can be defined for each node, element, or the entire model and can have various forms or ranges of application. Analysis can be defined in multiple stages based on the type of problem, loading, and boundary conditions. ABAQUS employs a number of advanced algorithms, such as explicit and implicit time integration methods, as well as nonlinear solution procedures, to ensure accurate and efficient solutions for complex engineering problems.

3.2.1 ABAQUS Problem Solving Algorithm:

As discussed earlier, the finite element module ABAQUS has two solver algorithms to analyze engineering problems: ABAQUS/Explicit, which solves explicit dynamic problems, and ABAQUS/Standard, which solves both static and dynamic problems in an implicit mode. ABAQUS/Explicit and ABAQUS/Standard are capable of solving a wide range of engineering problems. The properties of implicit and explicit procedures determine which method is suitable for a particular problem. In this section, these two algorithms are expanded.

3.2.1.1 ABAQUS/Standard (Implicit) analysis

ABAQUS/Standard (Implicit) analysis in ABAQUS is based on discretizing a continuous system into a finite number of smaller elements, which can be analyzed individually. In implicit analysis, the time derivatives (accelerations and velocities) are solved simultaneously with the other unknown variables in the problem. This requires the solution of a large system of nonlinear equations at each time step. The basic equation used in implicit analysis is Newton's equation of motion, which states that the acceleration of a body is proportional to the net force acting on it. In the context of finite element analysis, this equation can be written as follows:

$$[K]_i\{C\}_i = \{R\}_i - \{F\}_i - [M]_i\{\ddot{u}\}_i \qquad \text{Equation 3.1}$$

where M is the mass matrix, K is the stiffness matrix, u is the vector of nodal displacements, and F is the vector of external forces. The mass and stiffness matrices depend on the properties and geometric configuration of the elements, while the external forces depend on the loading conditions. Newton's method aims to achieve dynamic equilibrium at the end of the increment at

time $(t + \Delta t)$ and determine the displacements simultaneously. The time increment Δt used in this method is relatively larger compared to the explicit method as the implicit approach is unconditionally stable. In solving nonlinear problems, it typically takes several iterations per increment to get a solution that meets the required tolerances. During each Newton iteration, a correction $\{C\}_i$ is found to the incremental displacements $\{\ddot{u}\}_i$. This process involves solving a set of equations simultaneously. It is worth mentioning that in the Standard method, it is not possible to apply the load once to reach equilibrium and the load must be applied in increments and gradually to the body. That is, the total load is applied to the model in the form of incremental loads so that the equilibrium at the end of a time increment is written as follows. Therefore, the solution of the implicit equation involves an iterative procedure, in which an initial estimate of the solution is repeated until convergence is achieved.

Due to large deflections in the model, excessive reiteration is required in order to achieve the convergence and the time increment should be very small (usually less than 10^{-5}). This small-time increment makes the solution time and cost unrealistic for large models. For a nonlinear problem, each time increment requires several iterations to bring the computational margin of error within the range of interest. If the model has discontinuities or bodies that interface with one another, a large number of iterations may be required. For all these reasons, the explicit method is seen as a more suitable tool for analyzing nonlinear engineering problems with large deflections. Although the time increment in the implicit method may be equal to that used for explicit analysis, due to the simultaneous solution of equations, the cost of iterations in the implicit method will be much higher and convergence may not be achieved in some cases. Each iteration in the implicit method may require solving a large set of linear system equations, which may require considerable amount of computation and memory. Especially when the size of the mesh becomes very large, the

requirements for solving the equations increase significantly, which in practice, given the computer limited memory, it may not be feasible.

3.2.1.2 ABAQUS Explicit analysis

The ABAQUS Explicit Dynamics is a useful method for solving nonlinear solid and structural mechanics problems quickly. The three main stages of an ABAQUS/Explicit analysis are: preprocessing, simulation, and postprocessing. These stages are connected through a set of files that provide input and output data for each stage. The preprocessing stage is responsible for defining the geometry of the model, assigning properties to the materials, and defining the boundary conditions. The simulation stage is where the actual analysis is performed, and the postprocessing stage is used to interpret the results and extract meaningful information. These three stages are linked together by files as shown in Figure 3-1.

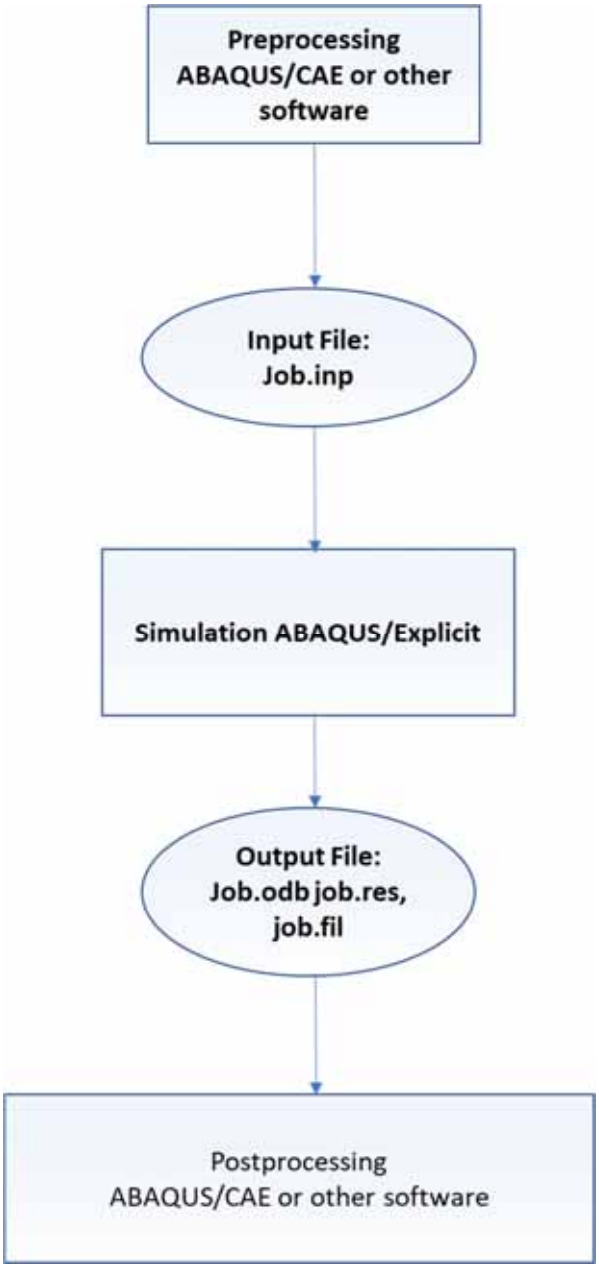

Figure 3-1: : ABAQUS Explicit Analysis Stages (ABAQUS Documentation, 2008)

The explicit method involves breaking down the problem into small time increments that are based only on the highest natural frequencies of the model, regardless of the type and duration of loading. Typically, the simulations require between 10,000 and 1,000,000 increments, but each increment has a low computational cost.

The equations of motion are integrated over time using the central difference method in ABAQUS/Explicit module. This process involves using the movement conditions at one time step to determine the conditions in the next step. At the start of each time step, the program calculates the dynamic equilibrium by solving for the balance between the nodal mass matrix and the nodal accelerations, taking into account both external forces applied and internal forces within the elements.

$$M\ddot{u} = P - I \qquad \text{Equation 3.2}$$

The calculation of the accelerations at the start of the current time step is determined by dividing the difference between the total external forces and internal forces by the nodal mass matrix:

$$\ddot{u}|_{(t)} = (M)^{-1}.\ (P - I)|_{(t)} \qquad \text{Equation 3.3}$$

In the Explicit method, the nodal accelerations are calculated easily because a diagonal mass matrix is always used. This means that there is no need to solve a set of simultaneous equations. Each node's acceleration is determined simply by its mass and the total force acting on it, making the nodal calculations very cost-effective. Acceleration is used to calculate the change in velocity by assuming that it is constant. This change in velocity is then added to the velocity from the previous increment to get the current velocity. This is done using the central difference rule.

$$\dot{u}|_{(t+\frac{\Delta t}{2})} = \dot{u}|_{(t-\frac{\Delta t}{2})} + \frac{(\Delta t|_{(t+\Delta t)} + \Delta t|_{(t)})}{2}\ddot{u}|_{(t)} \qquad \text{Equation 3.4}$$

The integration of velocities through time is performed by adding the velocities to the initial displacements. This results in the calculation of the final displacements at the end of the current increment.

$$u|_{(t+\Delta t)} = u|_{(t)} + \Delta t|_{(t+\Delta t)} \dot{u}|_{(t+\frac{\Delta t}{2})} \qquad \text{Equation 3.5}$$

To solve the equation of the motion, the dynamic equilibrium at the start of each increment is used to calculate the accelerations. Having the knowledge of the accelerations, velocities and displacements are advanced "explicitly" through time. This method is called Explicit since it depends only on the conditions at the beginning of each increment, including the displacements, velocities, and accelerations. To obtain accurate results, the time increments must be kept small to ensure that the acceleration remains constant. This often requires a large number of increments, but each one is relatively inexpensive to compute as there are no simultaneous equations to solve. The majority of the computational expenses comes from determining the internal forces acting on the nodes, which involves calculating element strains and applying material constitutive relationships to find the stresses and internal forces. The flowchart in Figure 3-2 demonstrates the summary of ABAQUS/Explicit algorithm that is used for this research:

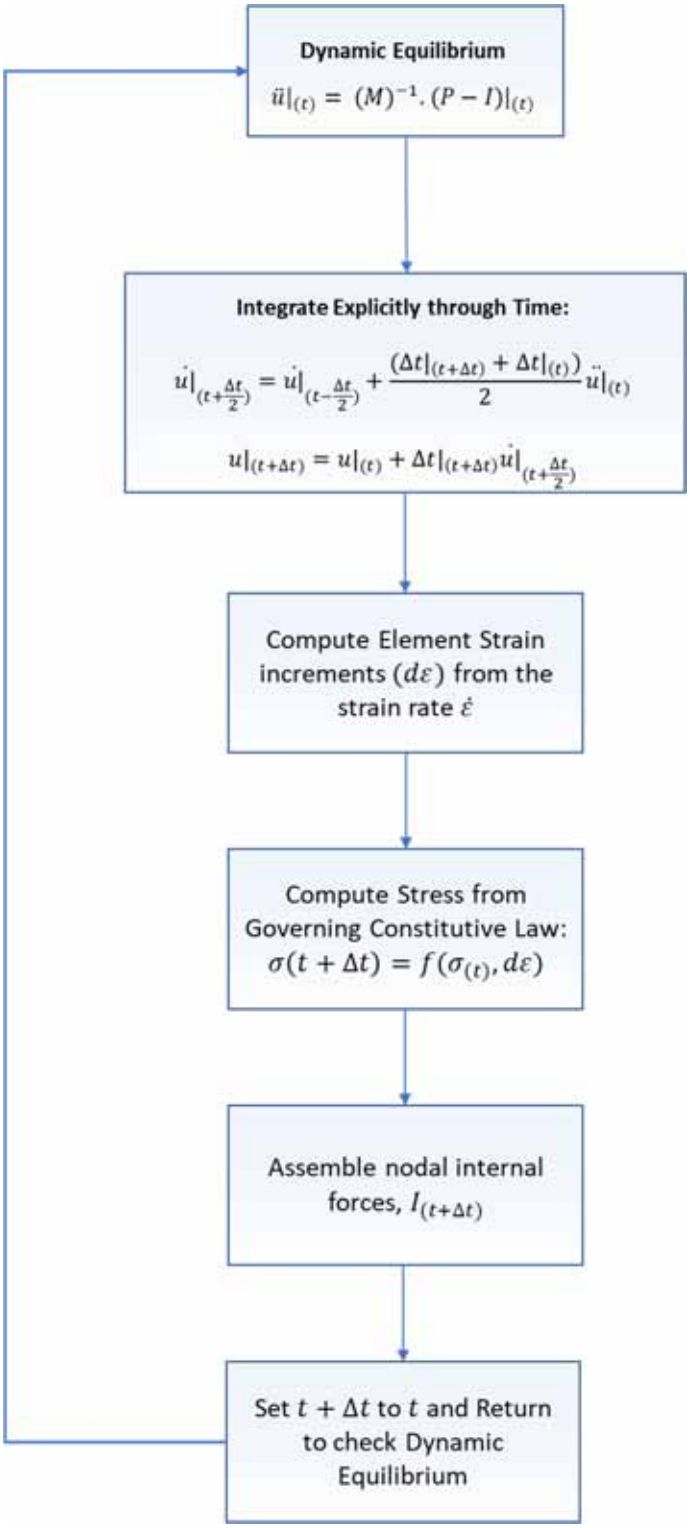

Figure 3-2: ABAQUS/Explicit Dynamic Analysis Algorithm (ABAQUS Documentation, 2008)

In this research the Explicit Method has been chosen to conduct a three-dimensional analysis of the group of micropiles subject to dynamic loads. The Explicit method is well-suited to solving dynamic events that occur fast and require a high level of accuracy in the solution. When the event is short in duration, the Explicit method can produce results quickly and efficiently. The Explicit method has the advantage of easily solving contact conditions and discontinuous events. This is achieved by enforcing them on a node-by-node basis without the need for iteration. The nodal accelerations can be adjusted to balance the external and internal forces during the event. As elaborated earlier, one of the advantages of the Explicit method is that it differs from Implicit methods in that it does not require a global tangent stiffness matrix. This makes it simpler and more efficient, as there's no need for iterations or tolerances. The Explicit method is well-suited for solving high-speed dynamic events and handling contact conditions and discontinuous events. (ABAQUS Documentation, 2008)

3.2.1.2.1 State of Stability Limit in Explicit Dynamic Analysis

The stability limit sets the upper limit for the time step utilized by the ABAQUS/Explicit solver, and it plays a crucial role in determining the efficiency and accuracy of ABAQUS/Explicit analysis. In this method, the condition of the model is updated over a certain time interval, based on its initial state at the start of that interval. The amount of time that the model's state can be updated while still maintaining an accurate representation of the problem is typically short. If the time increment exceeds this maximum limit, it is referred to as exceeding the stability limit.
The stability limit is established in relation to the highest frequency present in the system ω_{max}. In the absence of damping, it is determined by the following formula:

$$\Delta t_{stable} = \frac{2}{\omega_{max}} \qquad \text{Equation 3.6}$$

The stability limit with damping is defined by a different expression, taking into account the effects of damping on the system:

$$\Delta t_{stable} = \frac{2}{\omega_{max}} (\sqrt{1 + \xi^2} - \xi) \qquad \text{Equation 3.7}$$

In the above equation, ξ is defined as fraction of critical damping in the mode with highest frequency. The determination of the actual highest frequency in the system is complex and cannot be calculated with computational feasibility. As an alternative, a conservative estimate is made by evaluating the highest frequency of each element in the model separately. This highest frequency, related to the dilatational mode, is always higher than the highest frequency in the entire finite element model when determined in this manner. The stability limit is recalculated using the element-by-element estimate of the highest frequency in the system, with the element length L^e and wave speed of the material c_d as the main determining factors.

$$\Delta t_{stable} = \frac{L^e}{c_d} \qquad \text{Equation 3.8}$$

For majority of Element types in ABAQUS, the above equation is an approximation of the stability limit, and its accuracy can vary, as it is based on the shortest distance within the element. A shorter element length results in a lower stability limit. The wave speed, which is a characteristic of the

material, is used in the calculation. For linear elastic materials with a Poisson's ratio of zero, the wave speed can be determined.

$$c_d = \sqrt{\frac{E}{\rho}} \qquad \text{Equation 3.9}$$

The stability limit is influenced by the wave speed of the material c_d, which is determined by its Young's modulus E and mass density ρ. Stiffer materials typically lead to a higher wave speed, resulting in a smaller stability limit. Conversely, a higher density results in a lower wave speed, leading to a larger stability limit. It is worth noting, the stability limit is determined by the amount of time it takes for a dilatational wave to travel the length of the characteristic element. By knowing the smallest dimension of the elements and the wave speed of the material, it is possible to calculate an estimate of the stability limit. For instance, if the smallest dimension of the elements is 5 *mm* and the dilatational wave speed is 5000 *m/s*, the stability limit would be approximately 10^{-6} seconds (ABAQUS Documentation, 2008)

3.3. Finite Element Modeling Technique

A finite element model (FEM) is a numerical representation of a physical system or process that is used to solve engineering problems. The model is created by dividing the system into small, manageable elements (finite elements) and representing the behavior of each element mathematically. The interactions between elements are then used to predict the behavior of the entire system. The FEM approach is used in many fields, including structural engineering and geotechnical engineering to simulate and analyze complex physical phenomena, such as stress and

deformation. In general, modeling and analyzing a model using software ABAQUS involves several steps as summarized here:

- Problem Definition and Selection of Appropriate Elements: The first step is to clearly define the problem desired to solve and select the appropriate elements to model the structure or system.
- Model Generation: A 3-D model of the system is created by defining its geometry, material properties, and boundary conditions. The model can also be created using the built-in CAD tools or import an existing model.
- Mesh Generation: The model is divided into a finite number of small elements. This process is also known as mesh generation. Various meshing algorithms are available in ABAQUS to generate the desired mesh.
- Assigning Properties: The model properties are assigned to each element, properties such as material, loading, and boundary conditions to the elements in the model.
- Analysis Setup: The analysis type, such as static, dynamic, or thermal analysis, and define the analysis parameters such as the time step, load increments, etc. The geostatic step is conducted as a part of this step for a soil-micropile system problem. The Geostatic step involves analyzing the static behavior of soil, including soil-structure interaction and is typically performed prior to a dynamic analysis to determine the initial soil deformation and stress state.
- Solution: ABAQUS uses numerical techniques to solve the governing equations and obtain the response of the model to the applied loads.
- Post-Processing and Results Analysis: The results obtained from the solution are visualized and analyzed. The results for further analysis can also be exported in other software to create plots and diagrams.

- Verification and Validation: The accuracy of the results is verified, and the model is validated using experimental data or other practical methods. This step is important to ensure that the results obtained from the simulation are reliable.

Finite elements make up the fundamental components of an ABAQUS model. The extensive element library in ABAQUS provides a powerful set of tools for solving a variety of problems with its range of available elements. To conduct a finite element modeling of soil-micropile system a number of different elements is required. These elements include Solid (continuum) elements that represent the soil medium, Beam elements that represent the structural elements such as piles and Interface elements that model interaction behavior between the soil and micropile.

3.3.1 Solid (Continuum) Elements

The solid or continuum elements are among the most versatile as they can be used to model a wide range of components. These elements work by representing small sections of a component and they can be connected to other elements on any face, allowing for the creation of models of almost any shape and subject to various types of loading. In this section, variety of elements used to model the soil-micropile system are discussed in further detail:

3-D Brick (Hexahedral) Elements, also known as hexahedral elements, are a type of finite element frequently used in ABAQUS. They are called "brick" elements because they are shaped like a rectangular brick and are used to represent a small portion of the entire model. These elements have a minimum of eight nodes, each of which can be used to apply loads and constraints and are connected by edges and faces. The displacement field within a 3-D brick element can be

described by linear or quadratic polynomials, which allows for the representation of complex geometries and material behaviors.

Modified Tetrahedral Elements are a type of three-dimensional solid element that are used to model continuum materials in a finite element analysis. Tetrahedral elements are made up of four vertices, and each vertex is connected to its neighbors by an edge. The element shape is defined by a tetrahedron, which is a three-dimensional shape made up of four triangular faces. The use of tetrahedral elements in ABAQUS provides a flexible and efficient means for modeling complex and intricate geometries. These elements are ideal for simulating the behavior of solid materials, such as metals, plastics, and ceramics, under various loading conditions.

The choice of 3-D brick elements over other types of finite elements, such as tetrahedral elements, is typically based on the specific needs of the analysis, including the type of loading, the geometry of the structure, and the level of detail required in the analysis. In the finite element modeling of soil-micropile system both elements type has been deployed but due to better convergence rate of hexahedral elements and the sensitivity of the results to irregularities of Tetrahedral elements most of the parametric studies are conducted using second order hexahedral elements. Figure 3-3 illustrated the three-dimensional geometry of the solid elements utilized in software ABAQUS.

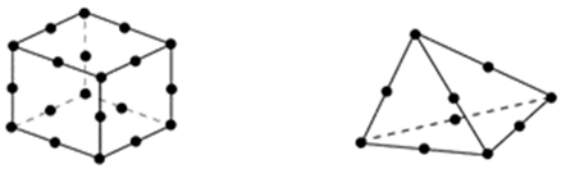

(a) (b)

Figure 3-3: (a) 3-D brick Quadratic (Hexahedral) Element (C3D20), (b) Tetrahedron Element (C3D10M) - (ABAQUS Documentation, 2008)

3.3.2 BEAM Elements:

The BEAM element is a one-dimensional element that is used to model slender, linear, or non-linear, flexible, or rigid members subjected to axial loads, transverse loads, bending moments as well as torsion. The beam element is suitable for modeling structures such as columns, beams, and thin-walled sections and piles. The beam element models the deformation of the beam using nodal displacement and rotations. Beam elements provide extra flexibility with regards to the shear deformation that occurs between the axis of the beam and the directions of its cross-section. Figure 3-4 illustrate a BEAM element and the behavior of a transverse beam section. The element uses a variety of mathematical formulations to describe the relationship between the element's nodal displacement and rotations and the applied loads and restraints. When modeling with BEAM elements in ABAQUS, selecting the appropriate cross section is important for obtaining accurate results. The choice of cross section can affect the beam's stiffness, stress distribution, and deformation behavior. There are various methods for defining a cross section in ABAQUS, including using predefined shapes such as circular, rectangular, or I-beam, as well as defining a custom cross section using a cross-sectional area and moment of inertia. It's crucial to choose a cross section that accurately represents the real-world cross section of the beam being modeled and to consider the effects of any geometric imperfections or material nonlinearities. In the case of a micropile, since micropiles are typically composed of a hollow bar filled with concrete a cross section representing strength characteristics of a micropile is defined in ABAQUS using pre-defined shapes feature.

It is worth mentioning that BEAM element can incorporate various nonlinear behaviors, including large deformations, plasticity, and creep, as well as dynamic effects like frequency and damping. However, in our analyses the behavior of micropiles is assumed to be elastic and therefore none

of the aforementioned effects are assumed in the micropile behavior. Due to relative slenderness of micropile elements, it is believed that their axial and flexural behavior align very well with BEAM elements and therefore in the analyses a BEAM element is employed for modeling the micropiles.

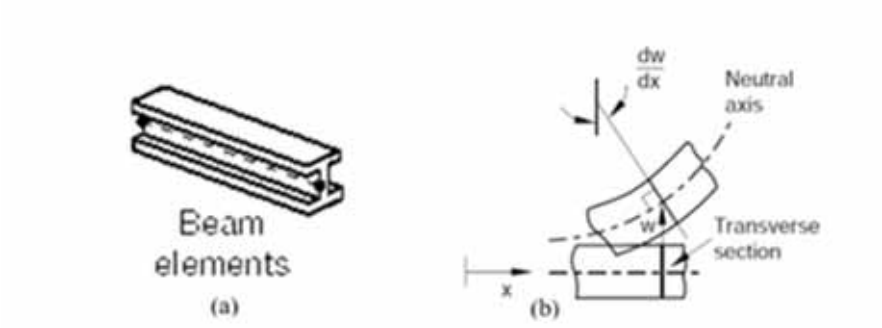

Figure 3-4: a) Schematic view of BEAM Elements in ABAQUS b) Behavior of transverse beam sections in slender beams - (ABAQUS Documentation, 2008)

3.3.3 Element Size

Element size is a measure of the size of the elements in a finite element mesh and is often described as the characteristic length of an element. The choice of the element size in a finite element analysis is crucial because it determines the level of detail that is captured in the model. A smaller element size will result in a model with more detail but will also require more computational expenses. On the other hand, a larger element size will result in a model with less detail but will be computationally less expensive. The choice of element size will also affect the accuracy of the results, with smaller elements generally providing more accurate results. It is important to choose an appropriate element size that balances the level of detail and computational resources needed to achieve the desired accuracy of the results. One commonly used criterion for

determining the appropriate element size in soil-structure interaction problems is the Lysmer criterion. It states that the element size should be small enough so that the deformation of the soil element is not larger than one-sixth of its length. In ABAQUS, the element size for a soil-structure interaction problem can be calculated using the following steps, if the frequency of the shear wave is not known:

- Estimation of the shear wave velocity of the soil; The shear wave velocity of the soil can be estimated through field tests such as Standard Penetration Test (SPT), Cone Penetration Test (CPT), or Seismic Refraction Test. It typically ranges from 400 *ft/sec* to 4000 *ft/sec*.
- Calculate the wavelength of the shear wave (λ) in the model; The wavelength (λ) that should be captured depends on the frequency content of the loads (*f*) applied to the machine foundation:

$$\lambda_{shear} = \frac{v}{f} \qquad \text{Equation 3.10}$$

  Assuming a machine foundation highest range of frequency at 50 *Hz*, leads to wavelength range of:

$$8\ ft. < \lambda_{shear} < 80\ ft$$

- Calculate the Element Size; per recommendation Lysmer, the element size can be calculated as one fifth to one tenth of the shear wavelength, it states that the element size should be small enough so that the deformation of the soil element is not larger than one-fifth of its length. This criterion helps to ensure that the soil response is accurately captured in the finite element model. Therefore, we have:

$$L_e = \left(\frac{1}{10} \sim \frac{1}{5}\right)\lambda_{shear} \qquad \text{Equation 3.11}$$

$$L_e = 0.8 \sim 1.6\ ft.$$

3.3.4 Contact Modeling

The goal of contact modeling in ABAQUS is to accurately simulate the behavior of the surfaces during contact, taking into account the complex interactions between the surfaces, such as friction, adhesion, normal forces, and relative motion. The simulation results provide insight into the contact behavior and can be used to optimize the design, improve performance, and prevent failure. There are two main approaches for contact modeling:

Nodal-based Contact Modeling: This approach involves defining the contact between nodes in the model and specifying the contact behavior between them. There are two types of nodal-based contact modeling in ABAQUS: Penetration contact and Tied node contact.

Surface-based Contact Modeling: This approach involves defining the contact surfaces and the behavior of these surfaces as they come into contact with each other and also by specifying the contact properties and conditions between two sets of surfaces. ABAQUS automatically generates appropriate contact elements, and the contact conditions specify how the surfaces should interact. The contact properties describe the behavior of the surfaces during contact, for example, the type of friction, the stiffness and damping of the contact, and the constitutive behavior of the surfaces. As elaborated above, there are two types of surface-based contact modeling in ABAQUS: frictional contact and tied contact.

The surface-based approach is widely recommended in ABAQUS software for simulating contact surfaces. In this study, the surface-based contact mode was considered for analyses. Generally, contact surface modeling involves the following steps:

- Determining the surfaces that are effectively in contact with each other,
- The condition in which the surfaces interact with each other,

- Determining the mechanical properties (friction and normal), and the type of interaction between two bodies,
- Modeling the interaction between two bodies,

In a contact-based surface approach, two surfaces are chosen based on their stiffness and referred to as the reference surface and the slave surface. Surfaces with higher stiffness are referred to as reference surfaces and surfaces that undergo more deformation are referred to as slave surfaces. The reference surfaces should only be referred to as surfaces based on elements, while the slave surfaces can be referred to as surfaces based on elements or nodes. There are two algorithms for determining the behavior of surfaces on each other and the dependence of the deformation of two surfaces on each other, the Pure Master Slave algorithm, and the Balanced Master Slave algorithm as shown in Figure 3-5 and Figure 3-6. ABAQUS provides two types of contact behavior for surface-based contact, referred to as frictional contact and tied contact. In ABAQUS/Explicit, Coulomb's law of friction is used for frictional contact and hard contact is used for tied contact.

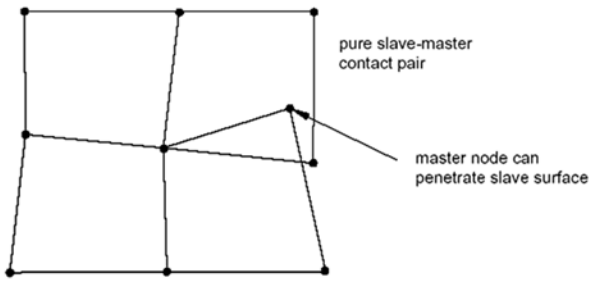

Figure 3-5: Schematic view of contact pairs using the Balanced Master Slave algorithm (ABAQUS Documentation, 2008)

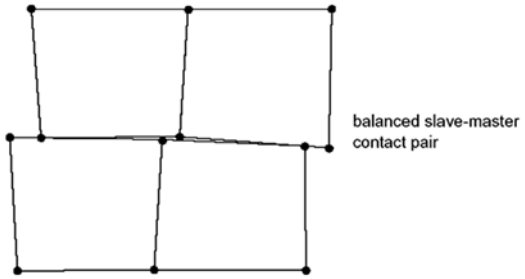

Figure 3-6: Schematic view of contact pairs using the Pure Master Slave algorithm (ABAQUS Documentation, 2008)

Different options are available to incorporate the tangential contact behavior between two bodies in ABAQUS. By default, the option of no contact is activated in order to define the properties between the two bodies. When the surfaces are in contact, in addition to the normal forces, shear forces are also applied to each other, so in the analyses, the contact forces that prevent slipping between surfaces should also be taken into account. The most common method used to describe the contact between surfaces is Coulomb's law of friction. In the context of the Coulomb friction model in ABAQUS, there are several approaches to consider slip. The most common approach is to use the stick-slip behavior, which means that there is no slip until the friction force reaches a certain level [the friction coefficient (μ) multiplied by the normal force (p)]. Figure 3-7 displays slip regions for the basic Coulomb friction model and Figure 3-8 shows the slip regions for the friction model with a limit on the critical shear stress.

Another approach is to use a rate-independent slip, where the slip is proportional to the relative velocity of the surfaces. Additionally, there is a user-defined option, where the user can write a subroutine to specify the friction behavior based on their specific requirements. The "penalty" option in ABAQUS is related to the Coulomb law of friction as it is used to model the friction between surfaces in contact. The Coulomb law states that the maximum tangential force between

two bodies in contact is proportional to the normal force and is limited by the coefficient of friction. The "penalty" option uses a numerical approach, known as the penalty method, to enforce this relationship between the normal and tangential forces. This option applies a stiffness proportional to the normal force to model the friction between the surfaces and is a simple and efficient method for modeling friction in ABAQUS.

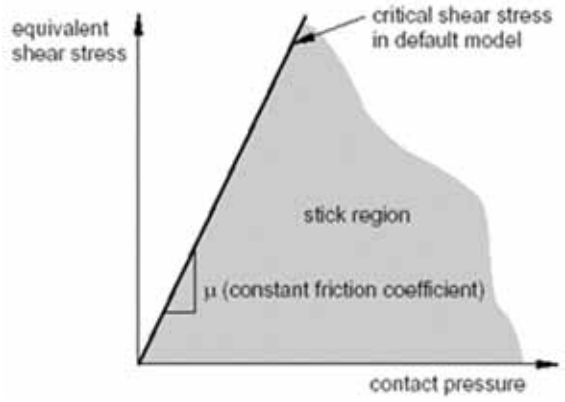

Figure 3-7: Slip regions for the basic Coulomb friction model (ABAQUS Documentation, 2006)

It is worth noting that equivalent shear stress (τ) can be limited using the "penalty" feature in the contact analysis. The shear stress limit is used in situations where the contact pressure stress is high, and the Coulomb law gives an excessive shear stress at the interface that exceeds the material's yield stress beneath the contact surface. A commonly used estimate for the upper bound of this stress limit (τ_{max}) is the $\sigma_y/\sqrt{3}$ in which σ_y is Mises yield stress and this limit is also used to define the maximum contact surfaces friction between soil and micropiles in dynamic analyses in this research (ABAQUS Documentation, 2008).

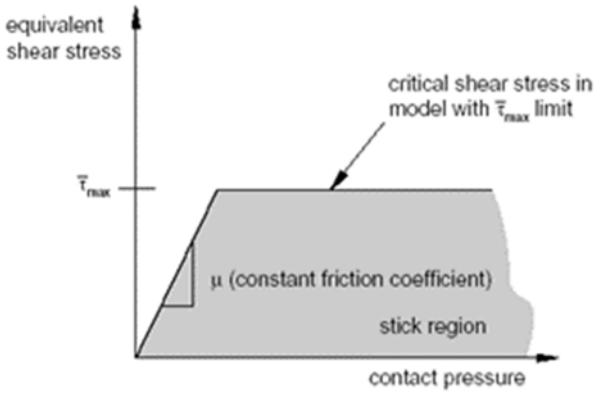

Figure 3-8: Slip regions for the friction model with a limit on the critical shear stress. (ABAQUS Documentation, 2006)

3.3.4.1 Surfaces Interaction

The interaction between surfaces is modeled using contact algorithms in ABAQUS. There are two main contact algorithms available in ABAQUS: General Contact and Contact Pair.

General Contact: The General Contact method in ABAQUS is based on finite element method and algorithms for modeling the interaction between surfaces. It solves the contact problem using a semi-implicit formulation that combines a penalty method for handling the normal forces with a Lagrange multiplier method for handling the tangential forces. The General Contact method can solve a wide range of contact problems, including large deformation, friction, and separation. The method also has options for controlling the mesh density and mesh update in the contact region, as well as options for handling contact that occurs between different material types.

The theory behind the General Contact method is based on the Lagrange multiplier method, which is used to enforce the constraints that arise from the contact conditions. The method introduces Lagrange multipliers as additional unknowns in the finite element analysis, which are used to enforce the contact constraints at the nodes of the contact surface. This allows the method to

handle the normal and tangential contact forces, and to enforce the contact conditions in a robust and accurate way. The General Contact method also includes a variety of options for controlling the numerical behavior of the contact, such as the stiffness and damping of the contact formulation, and the choice of integration method for the Lagrange multipliers. Figure 3-9 illustrates a schematic view of the General contact domain with ABAQUS including edge-to-edge contact.

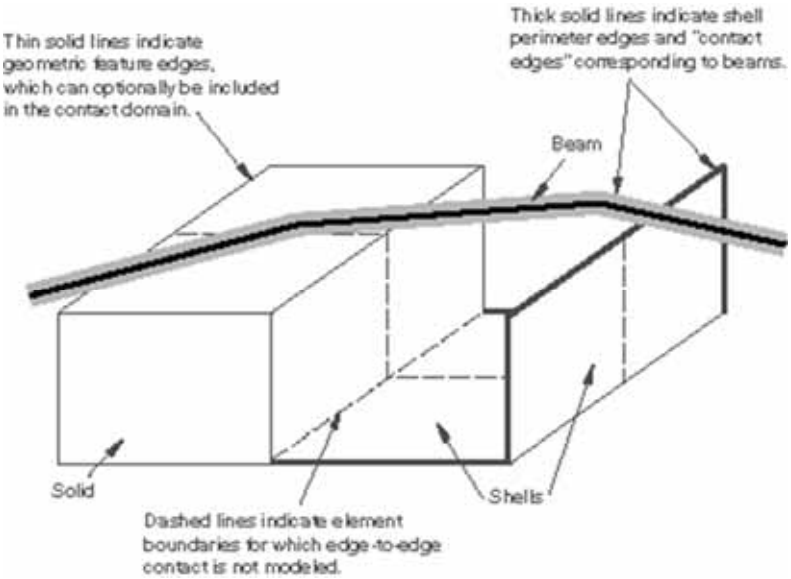

Figure 3-9: General contact domain, including edge-to-edge contact (ABAQUS Documentation, 2006)

Contact Pair: ABAQUS provides the Contact Pair method as an alternative to using General Contact to model the interaction between two surfaces or between a surface and a solid body. This method is based on the friction laws that govern the behavior of the contact interface. Contact Pair allows specifying the type of contact and the associated parameters, such as the friction coefficient, normal stiffness, and normal and tangential dissipations. There are two methods available in ABAQUS for modeling the contact pair:

- Limited Slip Contact: This method is used to model contacts where sliding is limited. The friction force is proportional to the normal force and is limited by the friction coefficient. The contact behavior is defined by the Coulomb friction law.
- Small Slip Contact: This method is used to model contacts where the sliding is not limited, but the relative motion between the two surfaces is small. The tangential force is proportional to the relative velocity between the two surfaces. This method is based on the normal spring-slider model.

In both methods, the contact behavior can be specified, such as the friction coefficient, normal stiffness, and normal and tangential dissipations. The contact surface type, such as rough or smooth, and the geometry of the contact region can also be specified. In addition, there are various features in ABAQUS, such as user-defined subroutines that can be used to customize the contact behavior to meet the specific needs of the analysis (ABAQUS Documentation, 2008).

3.4. Soil Constitutive Model

In any numerical modeling, it is crucial to select an appropriate constitutive model for the model components. The accuracy of the results depends on how well the chosen stress-strain behavior of the soil continuum in the model represents the actual characteristics of the soil in the field. In this research, the soil behavior under dynamic loading conditions was modeled using both linear and nonlinear soil models. An elastoplastic constitutive model known as Modified Drucker Prager with Cap was chosen to represent soil behavior in parametric studies. Parameters selected for each soil model are discussed in further detail in Chapter 4. In this section, the governing equations of the Modified Drucker Prager with Cap is further discussed.

3.4.1 Modified Drucker-Prager with Cap

The modified Drucker-Prager/Cap plasticity/Creep model is a commonly used soil model in geotechnical engineering, particularly for simulating the behavior of soils and rocks under dynamic loading conditions. This model is non-linear, and it accounts for the pressure-dependent yield behavior of geological materials; it is based on the Drucker-Prager plasticity model, and it extends the original model by adding a cap yield surface. This cap yield surface accounts for plastic compaction and helps to control volume dilatancy that occurs when the material yields in shear. This soil model has been successfully used in different loading conditions and has been shown to provide a good response to large stress reversals. This makes it a useful tool for understanding the behavior of geological materials and predicting how they will respond to different loads and conditions.

3.4.1.1 Modified Drucker-Prager Yield and Failure Surface Equations

The Drucker-Prager yield surface is a soil model that has two main segments: a pressure-dependent Drucker-Prager shear failure segment and a compression cap segment as shown in Figure 3-10. The Drucker-Prager failure segment is a plastic yield surface that, when plastic flow occurs, causes an inelastic volume increase (dilation). On the other hand, plastic flow on the cap surface results in material compaction. The model includes an inelastic hardening mechanism to account for plastic compaction and helps control volume dilatancy when the material yields in shear. Figure 3-11 illustrates the typical Modified Drucker-Prager Cap Model yield surface.

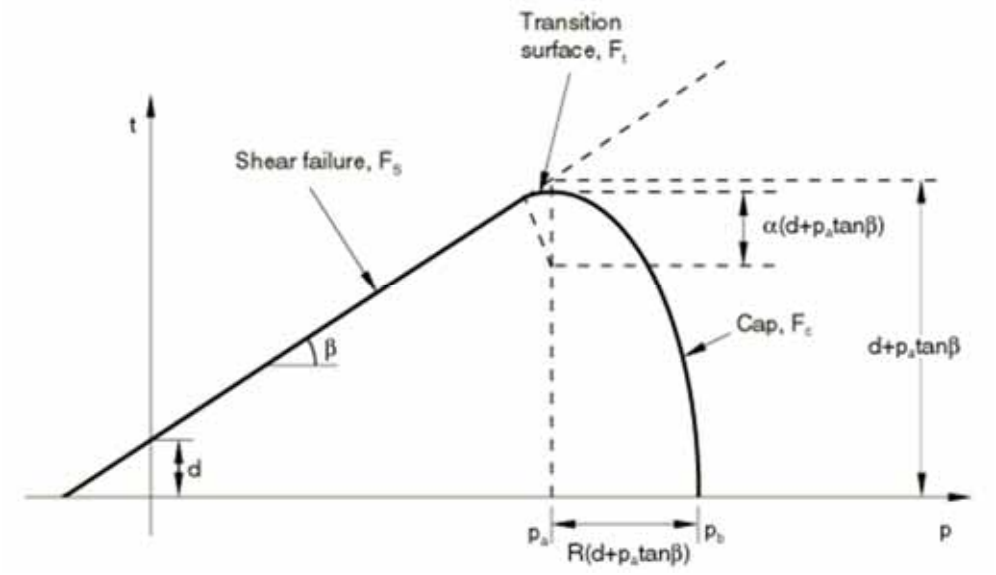

Figure 3-10: Modified Drucker-Prager/Cap model: yield surfaces in the p–t plane. (ABAQUS Documentation, 2006)

The Drucker-Prager model in ABAQUS/Standard models the behavior of materials that exhibit long-term inelastic deformation through the use of a cohesion creep mechanism in the shear failure region and a consolidation creep mechanism in the cap region. The soil's elastic behavior is modeled using linear elasticity and Hooke's law, which defines the elastic model using the volumetric elastic stiffness to capture the stress-strain changes within the model. The plastic behavior is determined by the Drucker-Prager failure surface, which is defined by an equation that accounts for the pressure-dependent shear failure and compression cap segments.

$$F_s = t - P\,tan\,\beta - d = 0 \qquad \text{Equation 3.12}$$

where β and d represent the angle of friction of the material and its cohesion, respectively, and may depend on temperature (θ) and other predefined parameters. The deviatoric stress measure, *t* can be defined as:

$$t = \left(q/2\right)\left[1+1/K-\left(1-1/K\right)\left(r/q\right)^3\right] \qquad \text{Equation 3.13}$$

The material parameter K depends on temperature, θ and other factors that have been previously defined. The use of deviatoric stress as a measure allows for the matching of different stress values under tension and compression in the deviatoric plane, providing more flexibility in matching the results with experiments.

The Cap yield surface is an elliptical shape with a constant eccentricity in the meridional plane as shown in Figure 3-11 and includes a dependence on the third stress invariant in the deviatoric plane. It can either harden or soften based on the volumetric plastic strain - hardening occurs with volumetric plastic compaction from yielding on the cap, while softening occurs with volumetric plastic dilation from yielding on the shear failure surface. The addition of the Cap yield surface to the Drucker-Prager model serves to account for:

- It bounds the yield surface in hydrostatic compression, resulting in an inelastic hardening process to depict plastic compaction.
- It helps control volume dilatancy when the material yields in shear by offering softening based on the inelastic volume increase generated as the material yields on the Drucker-Prager shear failure surface.

The cap yield surface can be written as:

$$F_c = \sqrt{(P - P_a)^2 + \left(\frac{Rt}{1+\alpha-\frac{\alpha}{Cos\beta}}\right)^2} - R(d + P_a \tan\beta) = 0 \qquad \text{Equation 3.14}$$

where R is a material parameter controlling the shape of the Cap, α is a small number typically in the range of 0.01 to 0.015 and is used to define a smooth transition surface between shear failure surface and the cap. P_a is an evolution parameter representing the volumetric plastic strain driven

hardening/softening. The relationship between the hydrostatic compression yield stress P_b and the volumetric inelastic (plastic and/or creep) strain is a user defined piecewise linear function and is used to control the hardening or softening of the material (as shown in Figure 3-12). The evolution parameter, P_a, is written as:

$$P_a = \frac{P_b - Rd}{1 + R\,tan\,\beta} \qquad \text{Equation 3.15}$$

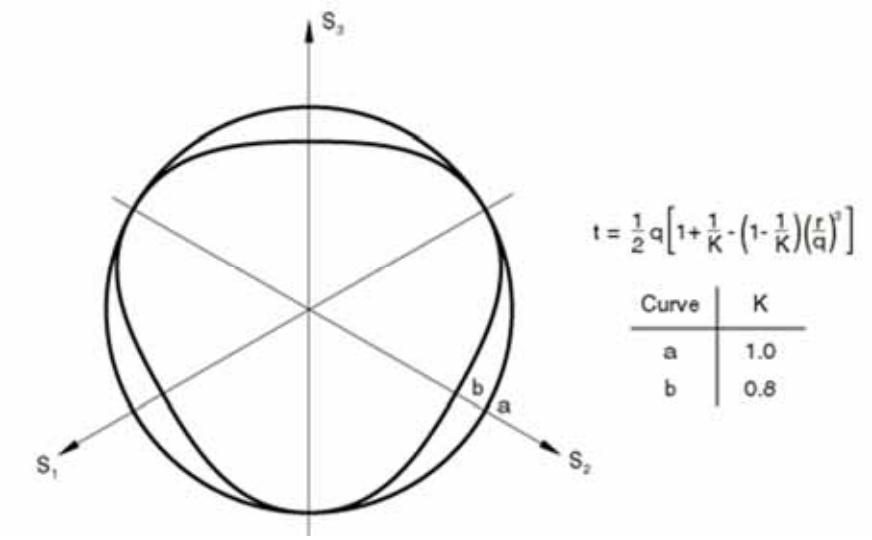

Figure 3-11: Typical yield/flow surfaces in the deviatoric plane. (ABAQUS Documentation, 2006)

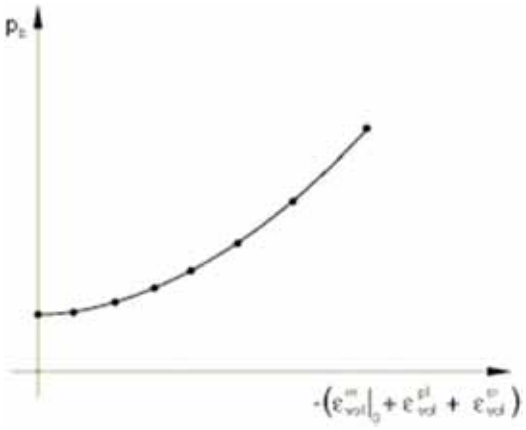

Figure 3-12: Typical Cap hardening (ABAQUS Documentation, 2006)

3.4.1.2 Flow Rule

The plastic flow in the model is characterized by a flow potential, which is associated on the cap and non-associated on the failure and transition yield surfaces. The reason for the non-association of these surfaces is due to the shape of the flow potential in the meridional plane, which is depicted in Figure 3-13:

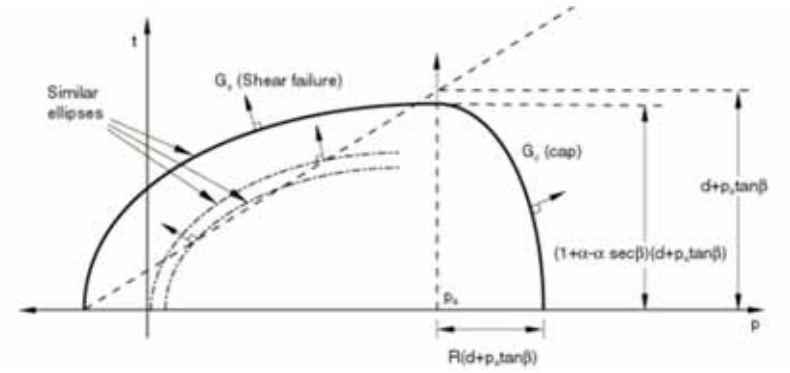

Figure 3-13: Modified Drucker-Prager/Cap model: flow potential in the p–t plane. (ABAQUS Documentation, 2006)

The Plastic flow has an elliptical portion in the cap region that is identical to the cap yield surface and can be written as:

$$G_c = \sqrt{(P - P_a)^2 + \left(\frac{Rt}{1 + \alpha - \frac{\alpha}{Cos\beta}}\right)^2} \qquad \text{Equation 3.16}$$

The flow potential in the failure and transition regions is also defined by an elliptical portion, which contributes to the non-associated flow component in the model:

$$G_s = \sqrt{[(P - P_a)^2 \, tan\,\beta]^2 + \left(\frac{t}{1 + \alpha - \frac{\alpha}{Cos\beta}}\right)^2} \qquad \text{Equation 3.17}$$

The flow potential surface is therefore composed of two elliptical parts, G_c and G_s, which combine to create a continuous and smooth potential surface. The material stiffness matrix for non-associated flow is not symmetric, so the unsymmetric solver should be utilized. However, if the area in which non-associated inelastic deformation is occurring is limited, a symmetric approximation of the material stiffness matrix may provide a sufficient convergence rate, in which case the unsymmetric solver may not be necessary.

3.4.2 Model Parameters

Now that the constitutive soil model is outlined, the model requires the parameters as input for the model. To achieve this, results of three triaxial pressure tests to determine the parameters *d* and *β* are required. The shear failure conditions obtained from these test results can be plotted on a the *p*-*t* plane to determine these parameters. The intersection of the plotted line with the *t* axis determines *d*, and the slope of the line determines *β*. Additionally, the results of a uniaxial test with different loading-unloading cycles is also needed. This can be used to evaluate the hardening-softening law, which is a piecewise linear function related to the hydrostatic pressure P_b and the corresponding plastic volume deformation. The loading-unloading slope can be used to calculate the elastic volume deformation, which should be subtracted from the total volume deformation to obtain the plastic volume deformation. The data obtained from triaxial compression tests on sands as part of a Master of Science coursework are used to obtain the

Modified Drucker-Prager with Cap model parameters and the model parameters are summarized in Chapter 4.

3.5. Boundary Conditions

In dynamic soil structure interaction problems, the loads and constraints are typically time-varying and can be modeled as excitations such as ground motions, earthquakes, or impact loading. In contrast, in static problems, the loads and constraints are considered constant over time. This means that the boundary conditions in dynamic conditions are more complex compared to static ones. Additionally, dynamic problems also involve the modeling of the response of the system under these excitations, including the effects of damping, mass, and stiffness. These factors require specialized techniques to accurately predict the response of the system in dynamic problems. Thus, the modeling of boundary conditions in dynamic problems requires a deeper understanding of the physical and mathematical principles involved.

A boundary condition in ABAQUS is a set of conditions or constraints applied on a part or all of the model's geometry to define the response of the structure to loads or other external excitations. These conditions specify the type and magnitude of the displacement, velocity, or acceleration that must be maintained at a specific location on the model, and can include fixed, pinned, roller, and other types of conditions or constraints. The choice of boundary condition depends on the type of structure being modeled and the loading conditions and plays a critical role in determining the overall behavior and response of the structure. ABAQUS supports variety of boundary conditions to define various situations in static and dynamic problems:

Kelvin-Voigt Model (Boundary Conditions) which is used to model the behavior of an ideal spring-slider system in dynamic problems. The Kelvin boundary condition is modeled as a spring-slider element that is attached to a node at one end and is free to move in the direction of the spring axis at the other end. Spring is characterized by its stiffness constant, which defines the relationship between the spring displacement and the force applied. The Kelvin boundary condition is used to represent the behavior of a soil-structure system, where the soil is modeled as a spring-slider system and the structure is modeled as a mass-spring system. This boundary condition can be used to simulate the interaction between the soil and the structure, including the effects of soil-structure interaction on the response of the structure. The equation for this boundary condition can be written as:

$$F = K * X + C * dX/dt \qquad \text{Equation 3.18}$$

Where, F is the force on the boundary, X is the displacement of the boundary, K is the spring constant, C is the dashpot (viscous) damping constant, and dX/dt is the velocity of the boundary. The equation expresses the equilibrium between the spring and dashpot elements, reflecting the interaction between the system and its environment. The spring element represents the elasticity of the boundary, and the dashpot component represents its viscous damping. The values of K and C can be specified to reflect different boundary conditions based on the desired behavior of the boundary.

Infinite Boundary Condition (IBC) is a type of boundary condition that is used to simulate an idealized semi-infinite domain. This type of boundary condition is typically used to model the behavior of a soil or rock mass when it is subjected to an infinite load, such as in the case of a soil deposit that is subject to an external pressure. In this boundary condition, the material is assumed

to behave as an idealized homogeneous and isotropic continuum, with no variation in its mechanical properties. Infinite Boundary Conditions are characterized by its stress-strain behavior, which is defined by the material's stiffness, strength, and failure criteria. The response of the material to an applied load is determined by solving the equations of motion that describe the behavior of the continuum. Infinite Boundary Conditions in ABAQUS is modeled using a combination of finite elements and numerical processes, with the goal of accurately simulating the behavior of the soil or rock mass under the applied load. The IBC can be used in both static and dynamic conditions, and it is often used in geotechnical engineering applications, such as slope stability analysis, foundation design, and excavation design.

Viscous Boundary Condition is used to model the dissipation of energy that occurs due to friction between adjacent layers or due to material damping. This type of boundary condition is typically used in dynamic analyses cases such as time-history analysis or seismic response analysis or structural vibration analysis, where the system's response to time-sensitive loads is of interest. The governing equations for viscous boundary conditions in ABAQUS are based on the equations of motion for a damped linear system. These equations describe the relationship between the displacement, velocity, and acceleration of a mass-spring-damper system, where the damping is represented as a frictional force proportional to the velocity of the mass. The proportional constant represents the magnitude of the damping and can be adjusted to match the desired level of damping for the system being modeled. Lysmer and Kuhlemeyer (1969) proposed a set of relationships for soil damping ratios in dynamic soil-structure interaction problems. These relationships are based on the assumption that soil damping can be modeled as a combination of viscous and hysteretic damping. These relationships provide a way to estimate the soil damping ratios from the soil and structure parameters, such as soil density, shear wave speeds, and the strain rate in the soil. Using

these relationships, the damper ratios in the vertical and horizontal directions can be calculated through the following equations:

$$c_n = \rho_S V_p A \qquad \text{Equation 3.19}$$

$$c_t = \rho_S V_S A \qquad \text{Equation 3.20}$$

Where, c_n and c_t are normal and tangential damping ratios in soil dynamics, which relate the damping ratios to soil parameters such as the soil density (ρ_S), shear wave velocity (V_S), and the compressional wave velocity (V_p).

In this study, a series of viscous boundary conditions are applied to all the 3-D models developed in ABAQUS. The viscous elements that are composed of infinitesimal dashpots are oriented normal or parallel to the soil continuum boundaries and are designed to control energy dissipation in the system. The equations governing dashpots in terms of stresses are described below. Figure 3-15 and 3-15 illustrates the schematic view of the spring damper elements at the boundaries.

$$\sigma_{xx} = -\rho_s c_p \dot{u}_x \qquad \text{Equation 3.21}$$

$$\sigma_{xy} = -\rho_s c_s \dot{u}_y \qquad \text{Equation 3.22}$$

$$\sigma_{xz} = -\rho_s c_s \dot{u}_z \qquad \text{Equation 3.23}$$

Where σ_{xx} is the normal stress and σ_{xy} and σ_{xz} are shear stresses at the boundaries, and $\dot{u}_x$ and $\dot{u}_y$ and $\dot{u}_z$ are velocities in each direction and c_p and c_s are coefficient of viscosity in the normal direction and the tangential direction respectively.

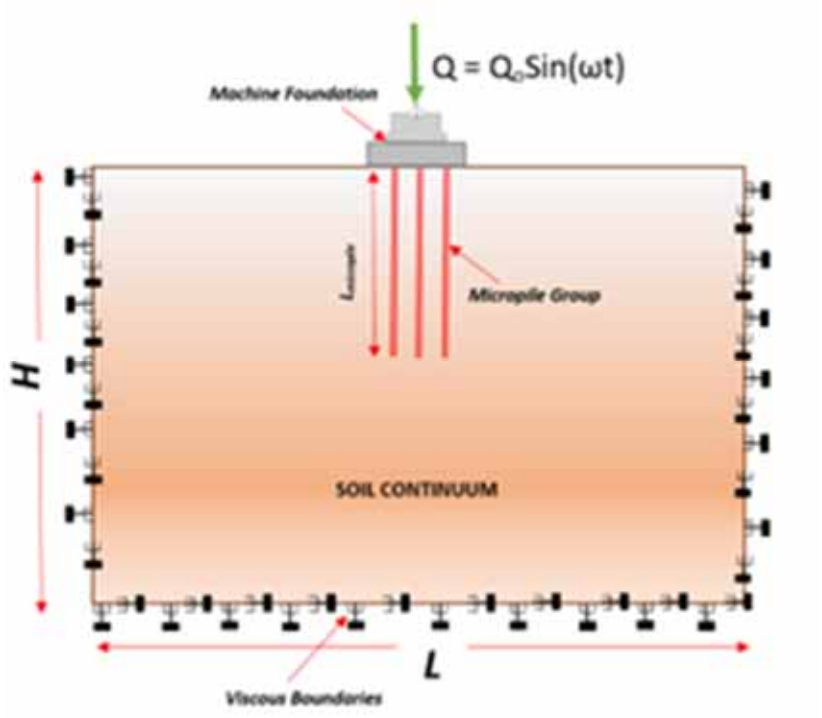

Figure 3-14: Sectional Overview of the Micropile Group with Viscous Boundary Conditions

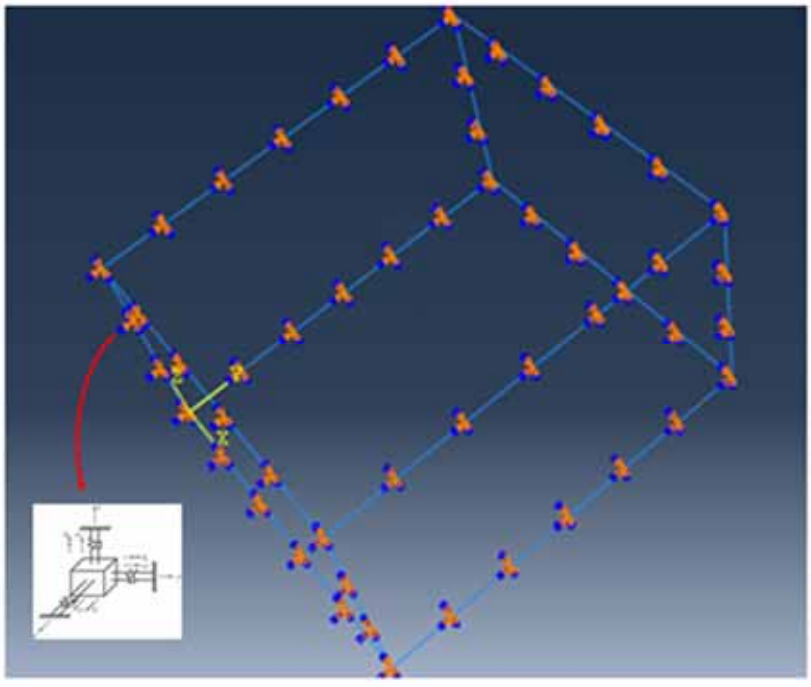

Figure 3-15: Schematic view of the viscous boundary conditions at the extreme limits of the FEM model

3.5.1 Boundary Conditions Verification

To verify the effectiveness of the used boundary conditions in the model, a two-dimensional FEM model of group of micropiles has been developed in the ABAQUS. This model has been analyzed by deploying two (2) type of boundary conditions:

- Boundary conditions composed of viscous dampers (i.e., vertical dampers and tangent dampers) to the boundary implemented via ABAQUS special purpose elements.
- Boundary conditions composed of infinite elements implemented via ABAQUS.

It is further assumed that the micropile behavior is elastic and the soil behaves as a nonlinear continuum modeled under modified Drucker-Prager model with a Cap. The micropile head displacements for the two boundary conditions as outlined above are measured as output and illustrated in Figure 3-16. As it is evident in these figures, both boundary conditions delivered close displacements at the micropile head with a discrepancy of less than 6 percent. Considering results of these analyses, in all the FEM models developed in this research, the viscous elements are deployed to represent boundary conditions under vertical dynamic analyses.

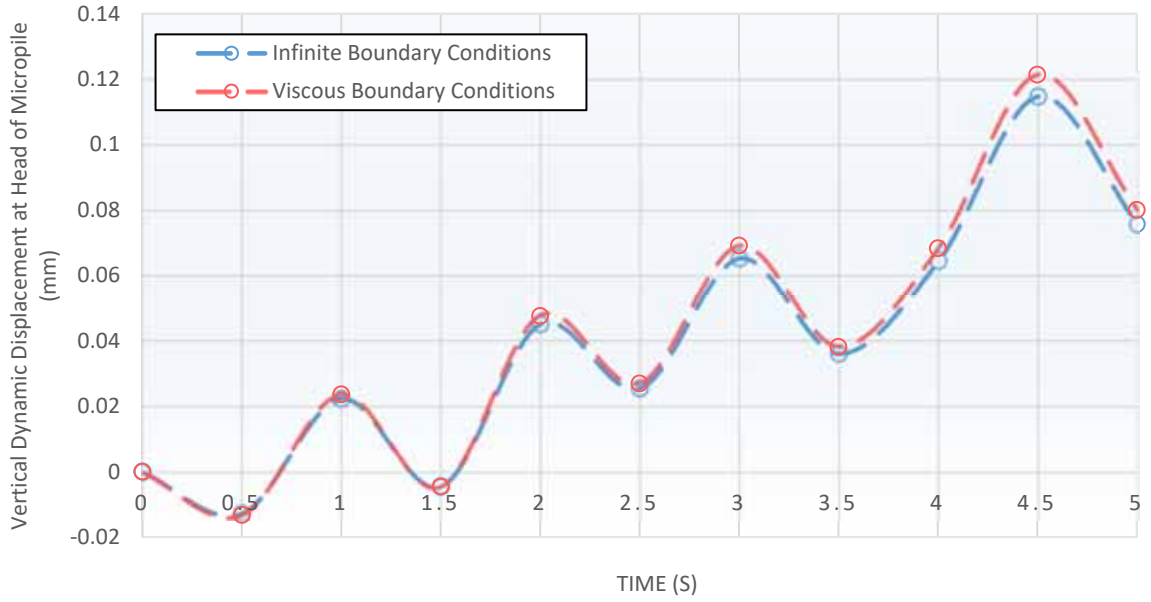

Figure 3-16: Vertical Dynamic Displacement at Head of Micropile (ft.) for Viscous and Infinite Boundary Conditions

3.6. Rayleigh Damping

The Rayleigh damping model is used frequently in the field of time history response analysis to model damping conditions for many engineering problems. It is represented as a linear relationship between mass (m) and stiffness (k), expressed as two coefficients (a coefficient proportional to the mass α, and a coefficient proportional to stiffness, β). The Rayleigh damping coefficients can be calculated at any phase angle (ω) of the system based on the assumption of proportionality between damping and mass or stiffness:

$$C = \alpha m + \beta k \qquad \text{Equation 3.24}$$

The linear damping component in the system can be calculated as:

$$C_n = \alpha M_n \qquad \text{Equation 3.25}$$

The above equation states that the Rayleigh damping coefficient (α) is proportional to the modal mass (M_n), therefore the damping ratio (ξ_n) can be calculated as the ratio of the Rayleigh damping coefficient to twice the natural frequency (ω_n) of the system, so we have:

$$\xi_n = \frac{\alpha}{2\omega_n} \qquad \text{Equation 3.26}$$

The nonlinear damping component in the system can be calculated as:

$$C_n = \beta {\omega_n}^2 M_n \qquad \text{Equation 3.27}$$

The above equation states that the damping coefficient (β) is proportional to the square of the natural frequency (ω_n) multiplied by the modal mass (M_n), and the damping ratio (ξ_n) can be calculated as half of the product of the damping coefficient and the natural frequency of the system, therefore we can write:

$$\xi_n = \frac{\beta \omega_n}{2} \qquad \text{Equation 3.28}$$

The damping ratio in the presence of both linear and nonlinear damping can be expressed as below:

$$\xi_n = \frac{\alpha}{2\omega_n} + \frac{\beta \omega_n}{2} \qquad \text{Equation 3.29}$$

where α and β are the coefficients for the linear and nonlinear damping, respectively, ω_n is the natural frequency of the system, and ξ_n is the damping ratio. Solving the equation for two different natural frequencies ω_i and ω_j would give values for the damping ratio, ξ_i and ξ_j, corresponding to those frequencies. These values would take into account both the linear and nonlinear damping

in the system and would be used to describe the damping behavior of the system for each of these frequencies. We have:

$$\xi_i = \frac{\alpha}{2\omega_i} + \frac{\beta\omega_i}{2} \quad , \quad \xi_j = \frac{\alpha}{2\omega_j} + \frac{\beta\omega_j}{2} \qquad \text{Equation 3.30}$$

The damping coefficients can now be calculated as following:

$$\begin{Bmatrix}\alpha \\ \beta\end{Bmatrix} = 2\begin{bmatrix}\omega_j & -\omega_i \\ -\frac{1}{\omega_j} & \frac{1}{\omega_i}\end{bmatrix}\frac{\omega_i\omega_j}{\omega_j^2 - \omega_i^2}\begin{Bmatrix}\xi_i \\ \xi_j\end{Bmatrix} \qquad \text{Equation 3.31}$$

Based on the above equations we can write:

$$\xi_{min} = (\alpha\beta)^{\frac{1}{2}} \quad , \quad \omega_{min} = \left(\frac{\alpha}{\beta}\right)^{\frac{1}{2}} \qquad \text{Equation 3.32}$$

The above equations represent the relationship between the minimum damping ratio ξ_{min} and the corresponding natural frequency ω_{min} for a system. These equations describe the tradeoff between damping and frequency in a system, where increasing damping will decrease the natural frequency and vice versa. The minimum damping ratio of the soils is used to determine the seismic response of the system. A lower damping ratio indicates that the soil has a lower ability to absorb energy, which can result in higher seismic response and greater damage to structures. The minimum damping ratio is typically less than 5 percent for most soils. ABAQUS supports the implementation of Rayleigh damping in the 3-D models. The damping ratio can be specified as a combination of proportional and derivative damping, based on the Rayleigh damping model. The proportional damping ratio can be defined as a constant value, while the derivative damping ratio can be defined as a function of frequency. The amount of damping can be specified as a fraction of critical damping, which is the minimum amount of damping required to prevent oscillations in

the system. The Rayleigh damping will be added to the overall damping matrix of the system, which contributes to the damping of the system's response (ABAQUS Documentation, 2006).

Chapter 4 - Numerical Analyses, Parametric Studies, Results and Discussion

4.1. Introduction

In the previous chapters, a comprehensive review of past studies on the behavior of micropiles under dynamic loading and the methodology of numerical modeling and soil constitutive relationship was presented in detail. This chapter focuses on evaluating and validating the numerical models developed against available field data. To achieve this, the accuracy of the developed numerical models built under 3D-FEM is compared against corresponding field data.

Moreover, a series of parametric studies are conducted to investigate the effects of various salient parameters on the response of soil-micropile systems under vertical dynamic loads. The nonlinearity of the soil, micropile inclination angle (i), micropile spacing ratio (s/D), soil shear stiffness ratio (R), machine foundation mass (m), and operating frequency of the machine foundation (f) are considered as the key parameters that affect the system's response. Through these studies, the effects of each parameter are analyzed in detail, and the results are compared and discussed in light of the existing literature.

Overall, this chapter presents a detailed analysis of the behavior of soil-micropile systems under vertical dynamic loads of machines, taking into account the influence of different parameters and using a nonlinear stress-strain behavior for the soil and soil-structure interaction (SSI). The findings can provide a better understanding of the response of micropile-supported machine foundations and offer insights for the design and further analysis of these systems.

4.2. Equation of Motion for a Micropile Group Supporting Machine Foundation

The equation of motion for a machine foundation supported by a group of micropiles can be expressed as following:

$$m\frac{d^2u}{dt^2} + c\frac{du}{dt} + ku = Q \qquad \text{Equation 4.1}$$

Where, *m*, *u*, *c*, *k*, and Q are total mass of the foundation and machine, displacement of the foundation, damping coefficient, stiffness coefficient of the micropiles and amplitude of the harmonic dynamic load applied to the machine foundation. Assuming that the amplitude of the load is given by:

$$Q = Q_0\, Sin(\omega t) \qquad \text{Equation 4.2}$$

where Q_0 is the peak amplitude of the harmonic dynamic load of machine, and ω is the angular frequency of the machine load, then the equation of motion can be rewritten as:

$$m\frac{d^2u}{dt^2} + c\frac{du}{dt} + ku = Q_0\, Sin(\omega t) \qquad \text{Equation 4.3}$$

This is the equation of motion for a machine foundation supported by a group of micropiles, operating at a frequency of *f* and subjected to a sinusoidal load with peak amplitude load of Q_0. The solution of this equation can be obtained using numerical methods, such as finite element

analysis or finite difference method in order to determine the displacement, velocity, and acceleration of the micropiles under dynamic loading. A more detailed discussion of the soil dynamics and the concept of the equation of motion has been provided in the Chapter 7 – Appendix of this dissertation.

4.3. Numerical Modeling Verifications

Before conducting parametric studies on a group of micropiles to investigate the effects of different factors, it is crucial to first verify the accuracy of the numerical model using actual field data. To ensure the reliability of the numerical results, a verification model is created in a finite element software, and its output is compared with the field data obtained from micropile loading under vertical loads. This step is necessary to establish the credibility of the numerical model and to ensure that the subsequent analyses accurately capture the behavior of the micropile system.

4.3.1 Static Loading Field Tests – French National project (FOREVER) Full-Scale tests on the experimental site (CEBTP site)

The FOndations de REacteurs à VErsailles et à Romans also known as FOREVER project was a national initiative that aimed to improve the design and performance of micropile foundations in France. The program was a research program funded by the French National Research Agency (ANR) that aimed to develop a comprehensive and systematic understanding of micropile behavior in various soil conditions and applications.

One of the key aspects of the FOREVER project was to investigate the performance of micropiles under both static and dynamic loading. To achieve this objective, a series of tests were conducted on the CEBTP (Centre d'Études et de Recherches du Bâtiment et des Travaux Publics) experimental site located in Saint-Rémy-lès-Chevreuse, France. The site consists of a controlled sand mass of Fontainebleau sandstone measuring 10m × 10m × 6m, which allowed for controlled testing conditions. These tests aimed to provide a better understanding of the behavior of micropiles and their interactions with the surrounding soil in different loading conditions. The experiments were conducted using various configurations of micropiles, including single micropiles, isolated micropile groups, and interconnected micropile networks. The tests were carried out under both static, centrifuge and dynamic loading conditions, and the results were analyzed to develop a comprehensive understanding of the micropile behavior in different soil and loading conditions.

As part of the numerical modeling verification, one of the micropile groups from the CEBTP site was selected to be modeled in the FEM software. The properties of the micropile group, such as dimensions, material properties, and installation method, were carefully chosen based on the information obtained from the field tests and published literature (Estephan, 2003). It is worth noting that the scaling factor did not matter since the tests were conducted in real scale. The sand and Micropile properties are presented in Table 4-1:

Table 4-1: Soil and Micropile Properties at CEBTP site	
Sand Properties	
Dry Density	14.4 $kN/m^3 < \gamma_d < 14.82\ kN/m^3$
Density Index	$0.53 < I_D < 0.62$ (Avg: 0.57)

Water content	7.9% < ω < 10.8%
Pressuremeter Modulus	2.2 MPa < EM < 6.3 MPa
Tip resistance	0.9 MPa < q_d < 3.0 MPa
Micropile Properties	
Anchored length	L = 5 *m*
Diameter	B = 100 *mm*
Micropile Spacing	3~4B
Steel tube inner/outer diameter:	40/50 mm
E_{steel}	200,000 *MPa*
E_{grout}	10,000 *MPa*

Figure 4-1 illustrates the overall site view and configuration of one of the vertical groups of micropiles used in the CEBTP site for this study. The group of micropiles consists of four (4) vertical type II micropiles spaced at approximately 3 to 4B (micropile diameter) and inserted and connected at the top through a micropile cap.

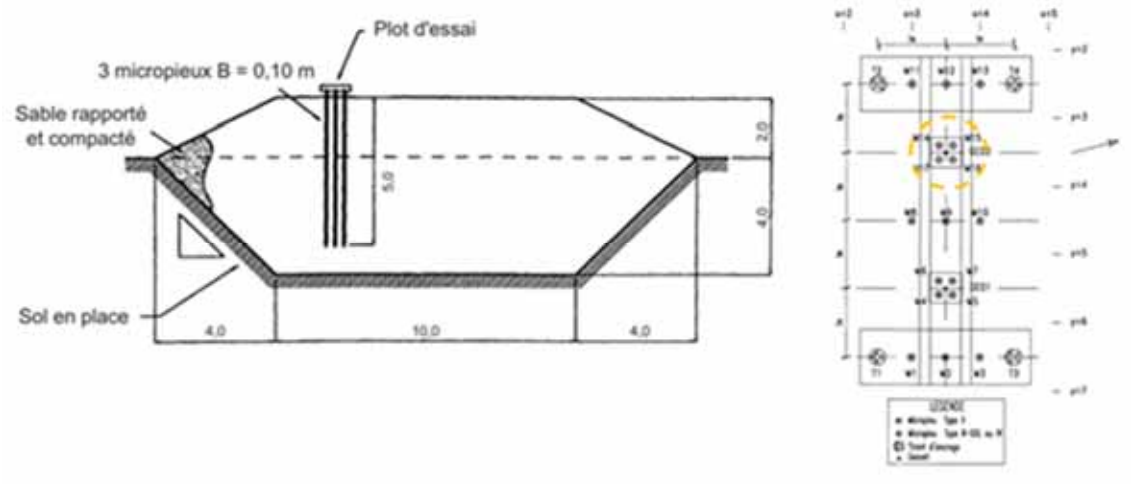

Figure 4-1: a) View of Experimental site of Saint Rémy-lès-Chevreuse (CEBTP site) b) schematic view of group of 2 × 2 micropiles in the CEBTP - FOREVER project (After Estephan, 2003)

Figure 4-2: General 3-Dimensional Finite Element Mesh used for group of micropiles inserted in homogenous sand at (French Forever Project – CEBTP site)

The numerical modeling of the micropile groups inserted in the Fontainebleau sand was done using the finite element software. A finite element mesh to include a 2 × 2 micropile group was prepared in the FEM software. Micropiles were simulated via the structural BEAM elements as supported by software. Figure 4-2 illustrates the three-dimensional finite element mesh of the model CEBTP micropile group with cap. The results of FEM analysis for the 2 × 2 micropile group using two different models of linear elastic, Modified Drucker-Prager with Cap are presented in Figure 4-3 and Figure 4-4 for two vertical loads of 60 *kN* and 100 *kN* respectively. The figures display the vertical displacement contours at the micropile cap and in Figure 4-5 the vertical displacements at the center micropiles for the three aforementioned models are derived for various micropile cap loads and compared against the CEBTP field measurements. At the vertical load of 100 *kN*, the settlement at the center of the micropile in the model using linear elastic model was predicted to be around 44% lower than the field measurement. Using the Modified Drucker-Prager model the settlements were noted to be about 27% lower than the field measurement respectively. Overall,

results obtained from the FEM models are within reasonable agreement of field measurements and the nonlinearity of the soil response at high loads was better captured by the Drucker-Prager, which resulted in higher displacements compared to the Linear Elastic model. The discrepancy between the numerical results and field measurements could be attributed to the interaction effects from adjacent isolated micropiles (Type R-Sol) that may influence the responses and complicate the soil-structure interaction behavior, and also uncertainties from the field measurements to estimate the soil strength properties.

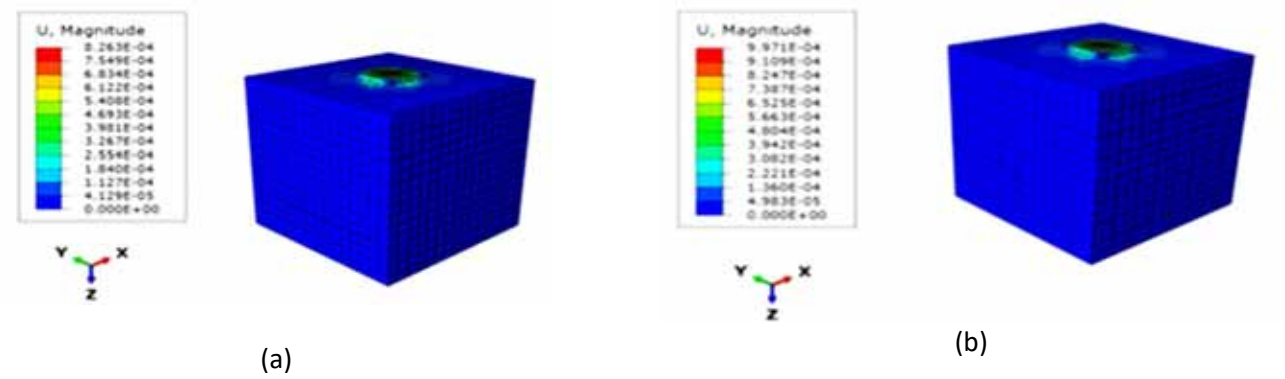

Figure 4-3: Displacement Contours for Group of 2 × 2 Grouted Micropiles under Vertical Load of 60 *kN* at CEBTP site (FOREVER project) – a) Linear Elastic Model – b) Modified Drucker-Prager Model

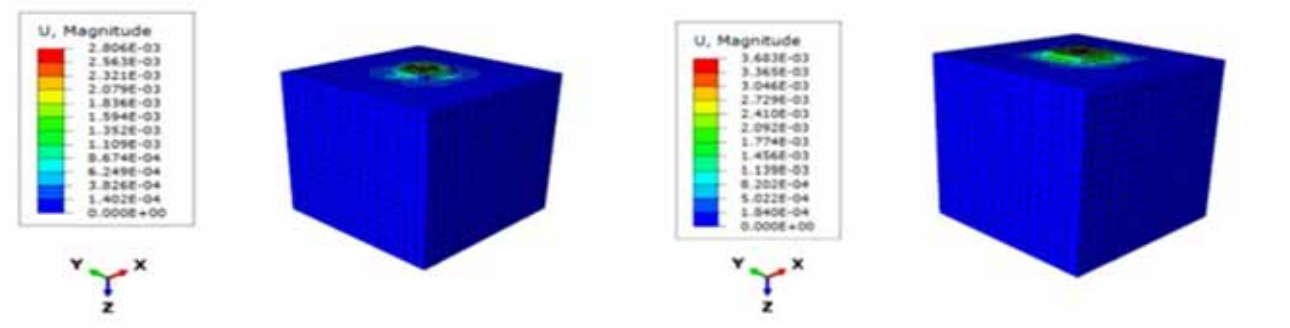

Figure 4-4: Displacement Contours for Group of 2 × 2 Grouted Micropiles under Vertical Load of 100 *kN* at CEBTP site (FOREVER project) – a) Linear Elastic Model – b) Modified Drucker-Prager Model

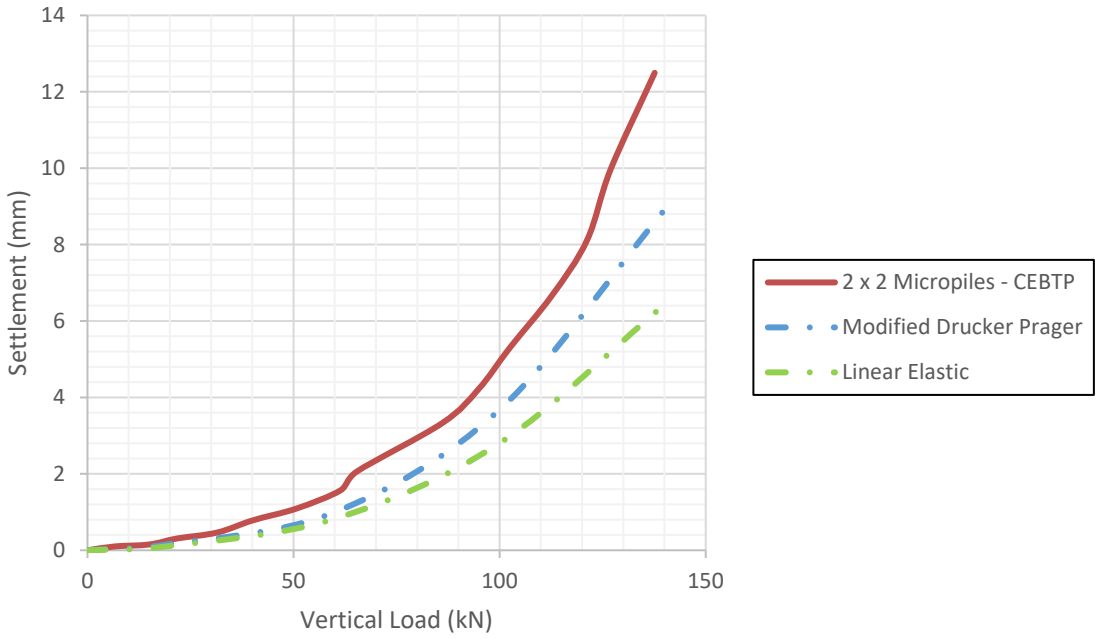

Figure 4-5: Comparison Between Field Data of CEBTP site experiments at French National Project (FOREVER) and 3-D FEM Modeling (Group of 2 × 2 Grouted Micropiles Under Vertical Loading)

4.3.2 Dynamic Loading Field Tests (Reduced Scale Shaking Table Experiments on the Group of Micropiles)

In this section, a series of analyses are conducted to validate the three-dimensional FEM modeling against field experiments that studied micropile groups dynamic response. A group of researchers (Komak Panah, et al. 2018) used micropiles groups in the CEBTP site of Saint Remy-lès-Chevreuse in the French Foundations Reinforced Vertically (FOREVER) national project as a prototype and built a reduced-scale physical model of micropile groups and performed a number of 1-*g* shaking table tests. The dimensions, geometrical properties and instrumentation used for the shaking table tests are shown in Figure 4-6 and Figure 4-7. The scaling law of 1-*g* was chosen per theoretical consideration to the similitude for shaking tables test (Iai 1989; Iai et al. 2005; Hokmabadi et al. 2015) in the gravitational field. Based on the similitude requirements for the proposed prototype model as well as the characteristics of the model, a scaling factor of *n* equal to 8.5 was chosen for these experiments. Accordingly, the soil and micropile elements specifications were chosen as summarized in Table 4-2 with special consideration to the appropriate scaling laws. The scaling laws dictate that certain physical properties, such as soil properties, and boundary conditions, must be scaled appropriately to ensure that the experiment accurately represents the behavior of the full-scale system. When modeling the reduced scale to the FEM, the model must reflect the scaling laws by appropriately scaling the physical properties and boundary conditions. Hence, it is necessary that the scaling laws and similarity requirements are accurately reflected in the FEM model. This means the same relationships between physical properties that exist in the prototype must be maintained in the FEM model.

The uniaxial earthquake shaking table facility was based in the Hong Kong Polytechnic University and was used for these experiments. Figure 4-8 illustrates the small-scale physical model used at

this facility. The results of the shaking table tests on group of micropiles provided insight on how these groups behave under dynamic excitations. The team developed a physical model including a 4 × 4 micropile system inserted in sandy soil with a relatively low-density. A sine wave was applied at the base of the physical model as an input motion and acceleration response at the micropile group cap as well as the soil surface has been measured (See Figure 4-10). Three (3) groups of 4 x 4 micropiles with vertical, and inclination angles of 10 and 20 degrees are developed. The sine wave with the frequency (12 *Hz*), a duration of 14 *sec*, and peak acceleration of 0.17*g* is applied to the base of the model. To capture an amplified response of the micropile groups, the frequency of the input excitation was selected close to the natural frequency of vibration of free field. Figure 4-10 illustrates the time-history for the sine wave applied at the base of the model. (Komak Panel et al. 2019)

As part of numerical verification of dynamic studies, four (4) numerical models were developed in a Finite Element Method (FEM) software to simulate the behavior of these shaking table tests under base excitations. The first (2) two models accounted for vertical and inclined micropile groups and considered the soil continuum as a linear elastic material, while the second two (2) models were developed for vertical and inclined micropiles with a nonlinear constitutive model to account for the soil's nonlinearity and nonlinear SSI. Both models' characteristics were defined using the shaking table test data, and the parameters for the constitutive models were determined by using this data and in accordance with the scaling laws and conducting sensitivity analyses. Figure 4-9: 3-D Finite Element Mesh use for Hong Kong University Shaking Table tests on Micropiles Groups illustrates the three-dimensional FEM mesh developed in the Finite Element software.

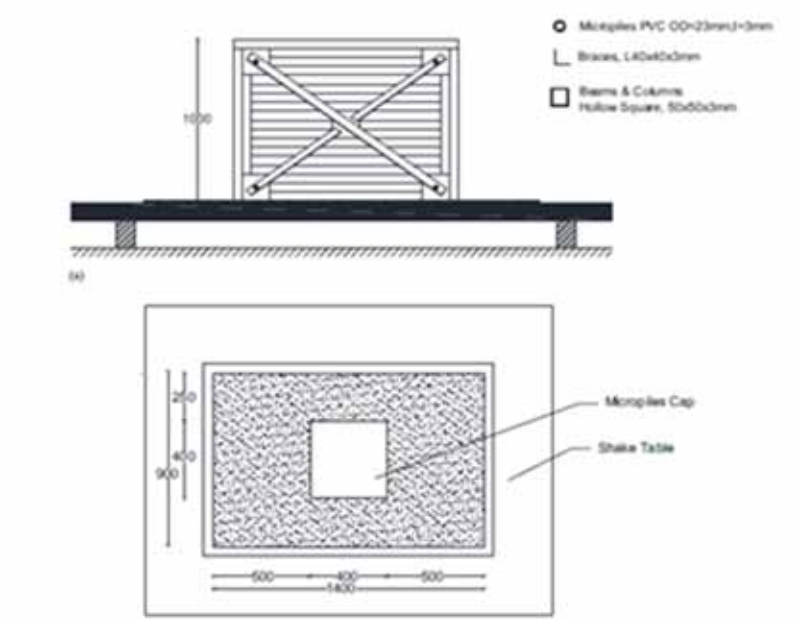

Figure 4-6: The physical model used for shaking table tests (dimensions in mm): (a) side view; (b) plan view; (after Komak Panah et al. 2018)

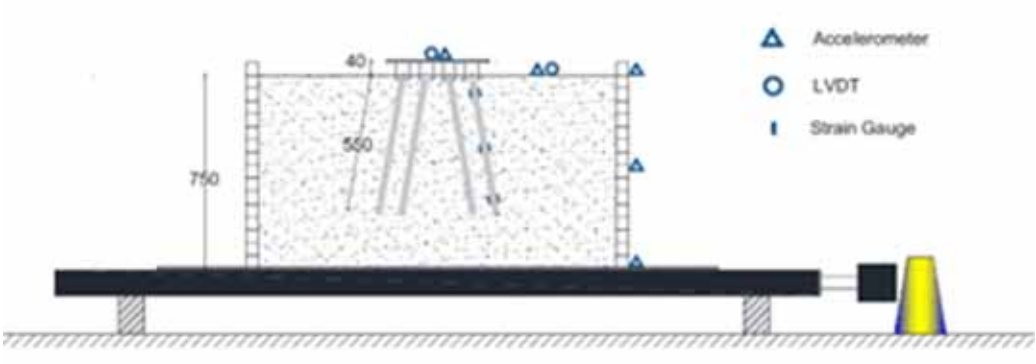

Figure 4-7: Shaking Table tests instrumentations (after Komak Panah et al. 2018)

Figure 4-8: The physical model used for shaking table tests (after Komak Panah et al. 2018)

Table 4-2: Shaking Table Tests Micropile Group Characteristics (Soil)	
Specific Gravity, *Gs*	2.625
Void Ratio, *e*	0.76
Relative Density, D_r	32.48%
Cohesion, *C*	3.32 *kPa*
Internal Friction Angle (φ)	32°
EI of pile/width	$1/n^{3.5}$
Poisson's Ratio (ν)	0.28
Scaling factor (n)	8.5
Modified Drucker-Prager with Cap Parameters	
d = 0	Initial Yield = 0.05
R = 1.2	K = 1
$e_{0_{min}}$ = 0.59	$e_{0_{max}}$ = 0.89
Shaking Table Tests Micropile Group Characteristics (Micropile)	

Scaling Factor, n	8.5
Micropile Length, L	550 *mm*
Diameter (Outer), d	23 *mm*

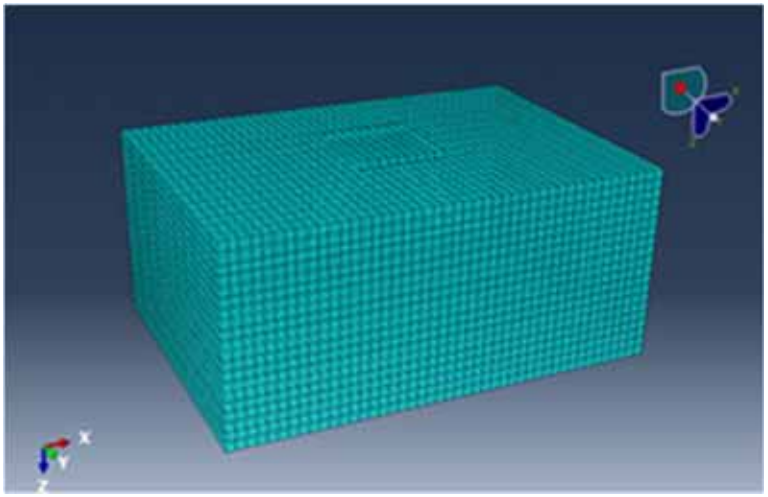

Figure 4-9: 3-D Finite Element Mesh use for Hong Kong University Shaking Table tests on Micropiles Groups

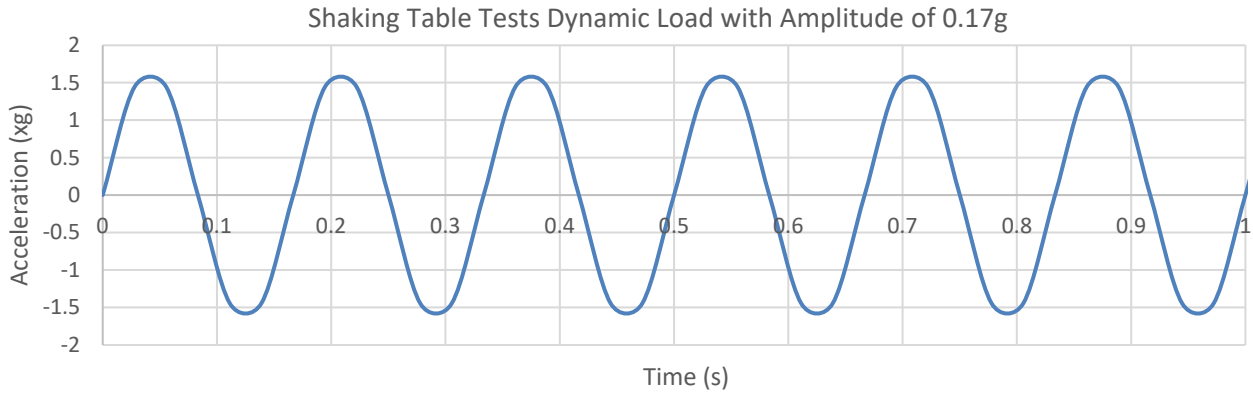

Figure 4-10: Acceleration Spectra of Dynamic Base Excitation for Hong Kong Polytechnique University Shaking Table Tests

The results of the numerical models were compared with the shaking table test data in terms of spectral acceleration response at the soil surface and micropile cap. Figure 4-11 display spectral dynamic acceleration contours of groups of vertical micropiles at the location of micropile/soil surface at resonance. The FEM analyses carried out revealed that the peak response acceleration for both the group of vertical and inclined micropiles were lower than the measured acceleration from the experiment. The spectral response curve for a group of vertical and inclined micropiles at the location of soil surface and cap is illustrated in Figure 4-12 and Figure 4-13. As it can be noted the reduction in the spectral acceleration response at micropile cap was more significant for the linear elastic model compared to the nonlinear Modified Drucker-Prager model for both groups of micropiles. The reduction was noted to be at 37 percent for the linear elastic model and 13 percent for the Modified Drucker-Prager model in the case of the vertical micropiles. Similarly, for the inclined micropiles, the reduction was around 29 percent for the linear elastic model and 8 percent for the Modified Drucker-Prager model. In comparison to the linear elastic model, the nonlinear Modified Drucker-Prager model has demonstrated to provide more consistent and accurate results for both the vertical and inclined micropiles, as it marginally underestimated the resonant frequency and peak spectral acceleration, and its results are within reasonable agreement of the actual experiments data.

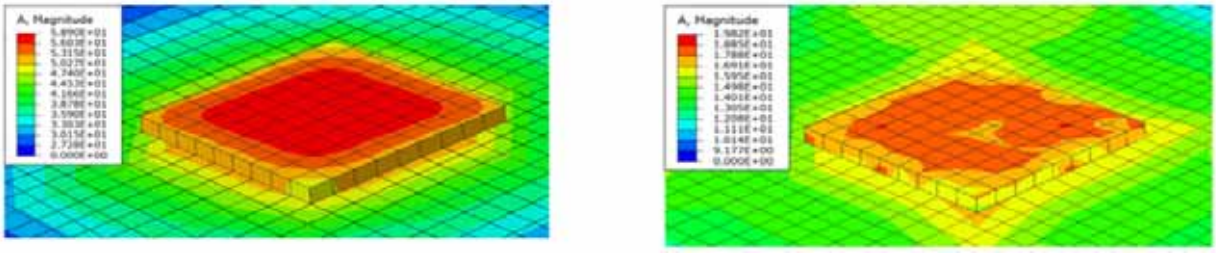

Figure 4-11: 3D-FEM analysis Spectral Acceleration contours for group of a) vertical micropiles b) inclined micropiles at micropile cap/soil surface at resonance

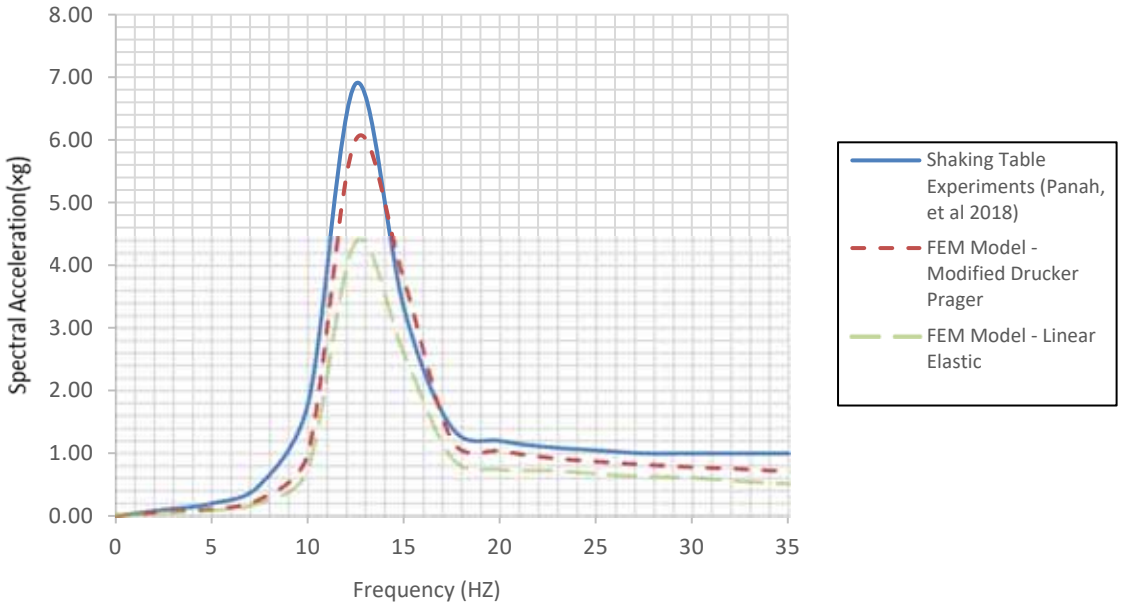

Figure 4-12: Comparison Between Shaking Table Tests (After Komak Panah et al.) and 3-D FEM Analysis Spectral Accelerations Analysis at Micropile Cap – (Vertical Micropiles)

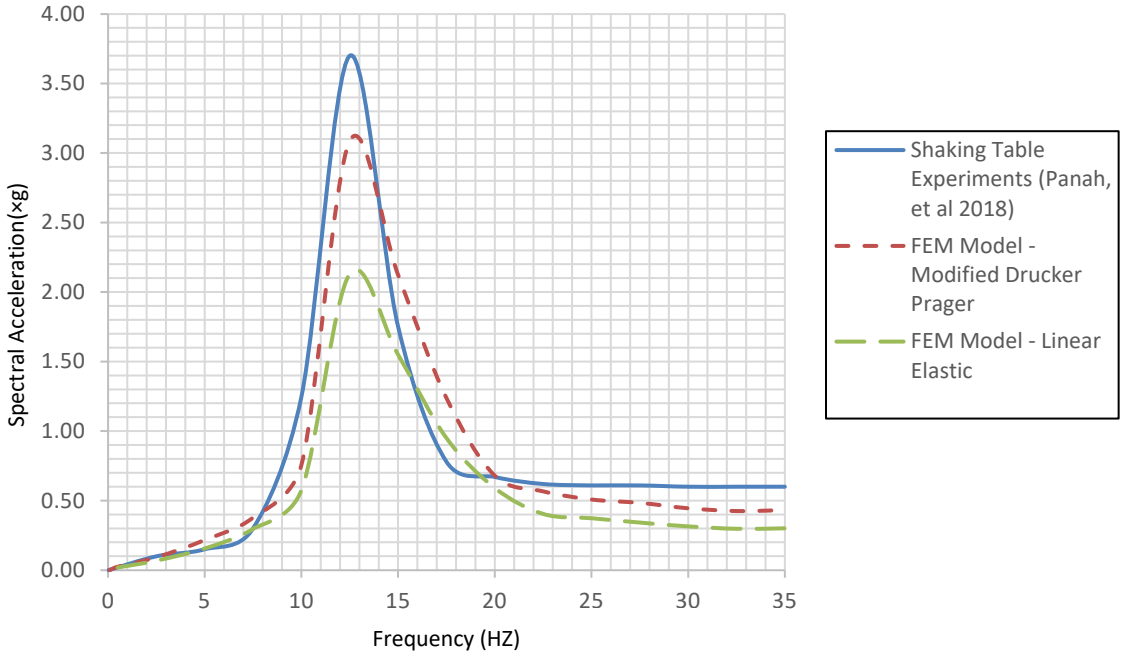

Figure 4-13: Comparison Between Shaking Table Tests (After Komak Panah et al.) and 3-D FEM Analysis Spectral Accelerations Analysis at Soil Surface – (Vertical Micropiles)

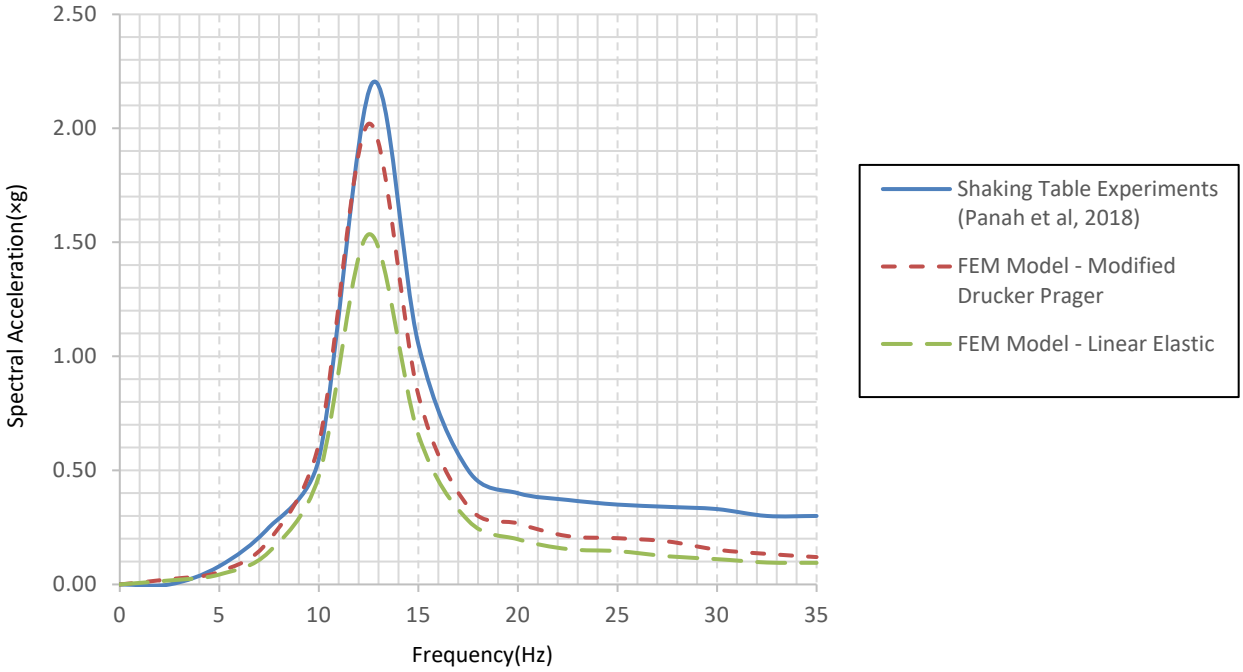

Figure 4-14: Comparison Between Shaking Table Tests (After Komak Panah et al.) and 3-D FEM Analysis Spectral Accelerations Analysis at Micropile Cap – (Inclined at 20 degrees)

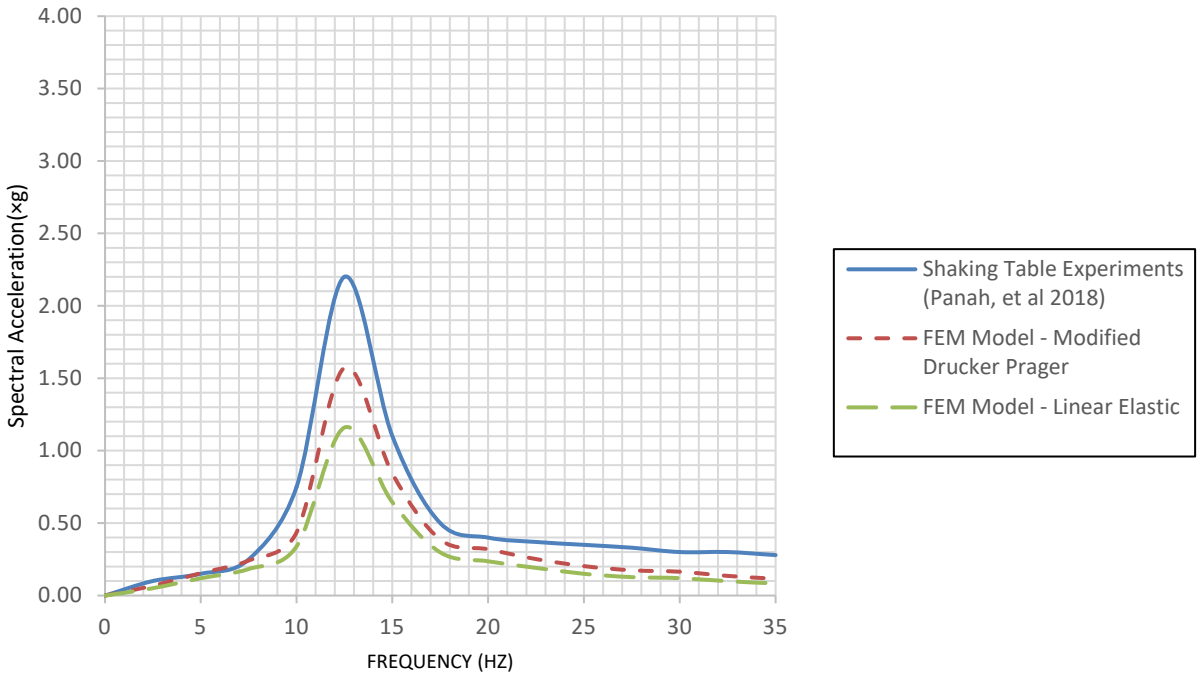

Figure 4-15: Comparison Between Shaking Table Tests (After Komak Panah et al.) and 3-D FEM Analysis Spectral Accelerations Analysis at Soil Surface – (Inclined at 20 degrees)

4.4. Parametric Studies: Performance of Micropile Groups under Vertical Dynamic Loading using 3D-FEM and Soil Nonlinear Stress-Strain Behavior

In this section, a series of parametric studies has been conducted to investigate the behavior of a group of micropiles under vertical dynamic loading from machine foundations. The results of parametric studies will provide more insight about the performance of micropiles in different engineering applications such as foundation supports. The effect of parameters such as, soil nonlinearity, the machine foundation mass (m), soil shear modulus/pile stiffness ratio (R), the operating frequency of machine foundation (f), the inclination angle of the micropile (i), the micropile spacings (s/D) on the dynamic behavior of the micropiles have been further studied.

4.4.1 Effect of Soil Nonlinearity on the Response of Micropile Groups subject to Vertical Dynamic Load of Machine Foundations

As discussed in Chapter 3, soil nonlinear stress-strain behavior can have a significant impact on the performance of deep foundation systems such as micropile groups subject to dynamic loads including vertical dynamic loads from machine foundations. Nonlinear stress-strain behavior can arise from various factors, including soil composition, density, and moisture content, as well as dynamic loading characteristics such as hysteresis, amplitude, and frequency content. Thus, the nonlinear behavior of soil can result to changes in its stiffness and damping properties, which can affect the dynamic response of the soil-micropile system. When subjected to dynamic loads from machine foundations, micropile groups experience both inertial and kinematic effects. Inertial effects are associated with the mass of the system and its response to external forces, while kinematic effects are associated with the displacement and deformation of the soil and the

micropiles themselves. The dynamic response of the system is strongly influenced by the stiffness and damping properties of the soil and the micropiles, which can vary significantly depending on the nonlinear behavior of the soil.

One of the key challenges in designing micropile foundations for machine foundations is to account for this nonlinear behavior as well as nonlinear soil-micropile interaction behavior which prompts engineers and scholars to seek a thorough understanding of the soil and SSI interface properties and how they will respond to complicated loading conditions. In addition, it is crucial to understand the dynamic properties of the micropile group itself, including its natural frequency and damping characteristics, as well as the interactions between the individual micropiles in the group. In Chapter 2, previous studies pertaining to behavior of micropiles under dynamic loading were extensively discussed and a summary of literature was presented. Amongst these studies, very few have drawn attention to the effect of nonlinear soil stress-strain behavior on micropile systems response while subjected to a vertical dynamic load. As the main purpose of this study was to understand the effect of soil nonlinearity on response of a soil-micropile system, this section has focused on this aspect. Two (2) three-dimensional (3-D) finite models are developed with introducing both linear and nonlinear constitutive models to the soil continuum and SSI interface for each model. A series of viscous boundary conditions are also applied to all models. The viscous elements that are composed of infinitesimal dashpots are oriented normal or parallel to the soil continuum boundaries and are designed to control energy dissipation in the system.

Table 4-3 summarizes the chosen soil characteristics for the constitutive models, i.e., linear elastic model and nonlinear Modified Drucker-Prager with cap model. The geometric configuration of the model is illustrated in Figure 4-16 with a group of 3 × 3 micropiles spaced at five times of the

micropile diameter (*s/D* = 5). The Finite Element Mesh developed to represent the micropile groups as well as the boundary conditions are illustrated in Figure 4-17.

The micropiles are connected at the top through a rigid cap. The harmonic dynamic load due to machine foundation operation is applied at the center of the rigid micropile cap and is governed by per Equation 4.2:

$$Q = Q_0 Sin(\omega t)$$

In this equation, ω is the angular frequency of the harmonic motion, t is time and Q_0 is the amplitude of the harmonic motion.

After completing the model geometry and property definition in FEM software and defining the necessary steps for Dynamic Explicit analysis, the load and boundary conditions are introduced to the model, then the model mesh is generated, and the simulation is submitted for analysis. The results of these dynamic analyses will shed light on how constitutive models can affect performance of the micropile groups. It is worth mentioning that per review of literature and previous studies, it is realized that soil and structural elements (micropiles) will sustain gapping while undergoing dynamic loads (Wong, 2005), and therefore in this research it is best to consider the effects of sliding and separation while modeling micropile groups subject to vertical dynamic loads.

Table 4-3: Soil Constitutive Model Parameters for Linear (Elastic) and Nonlinear (Mod. Drucker-Prager) Models and Micropile Structural Properties

Elastic Model (Linear) Properties			
$E(MPa)$	100	$\gamma\ (kN)$	17.7
ν	0.20	e_0	0.89

Modified Drucker-Prager with Cap (Nonlinear) Properties			
$E(MPa)$	100	d (kPa)	108
ν	0.20	R	1.2
$\gamma\ (kN)$	17.7	Initial yield	0
e_0	0.89	α	0.05
$\beta(deg)$	50	K	1
ξ	0.05	-	-

Micropile Properties	
$E = 25{,}000\ MPa$	$D = 0.3\ (m)$
$\gamma = 23.50$ kN	$v = 0.25$

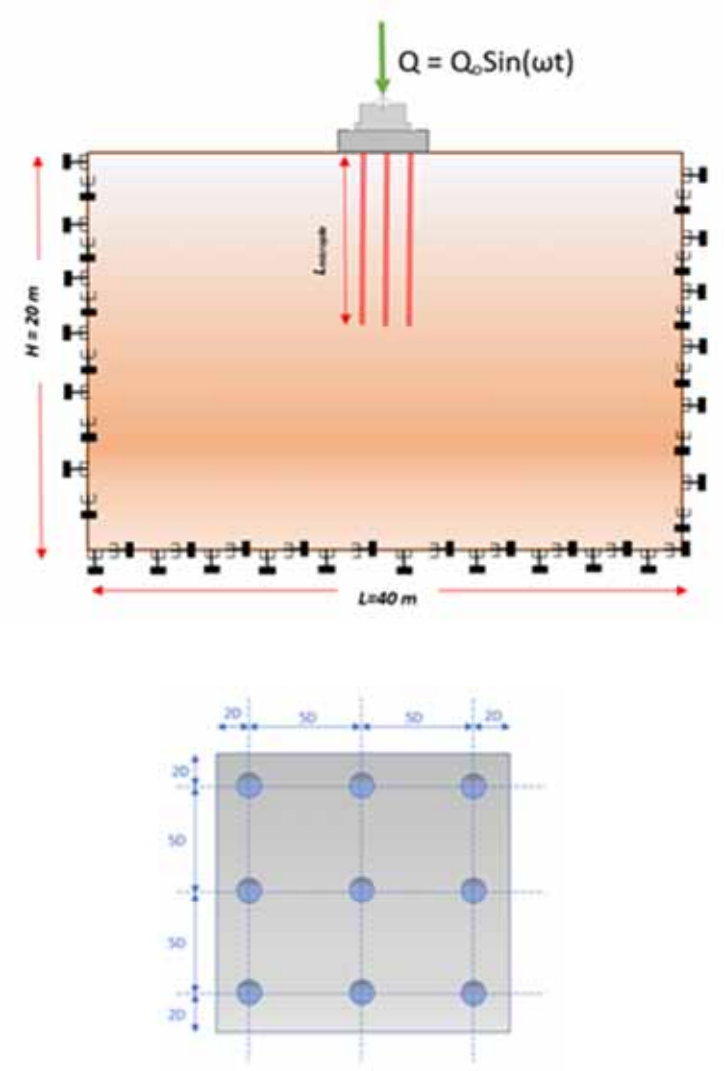

Figure 4-16: Schematic view of micropile group geometry and individual micropile configuration

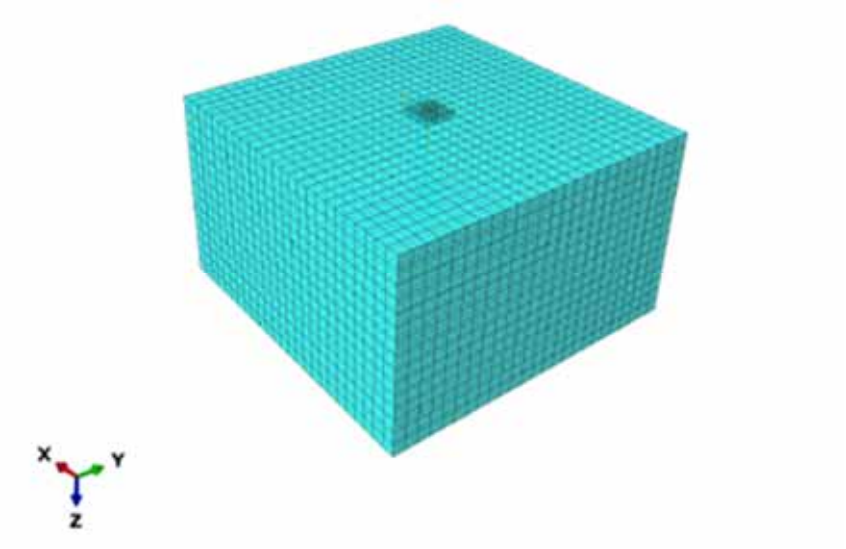

(a)

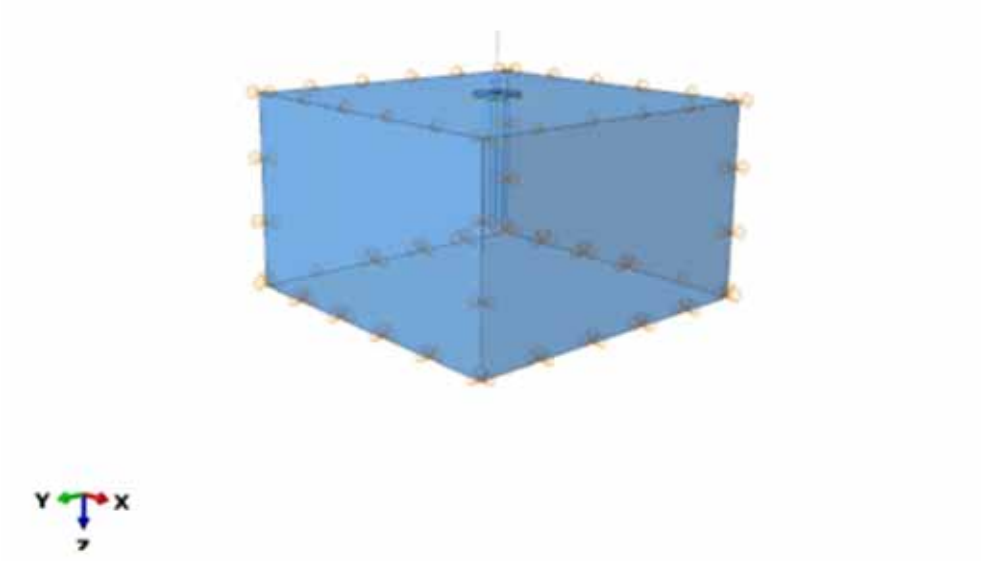

(b)

Figure 4-17: a) The FEM Mesh used to represent the micropile groups in soil - b) the boundary conditions at the FEM model.

Figure 4-18 displays the dynamic displacement at the location of the micropile cap for machine foundations subject to vertical dynamic loads for both linear elastic and nonlinear modified Drucker-Prager with Cap soil model. These figures indicate that the micropile groups with a nonlinear soil model exhibit higher magnitudes of displacements compared to the group modeled using a linear soil model. This could be because, during dynamic vertical loads of machine foundations, the soil undergoes plastic deformation due to the cyclic nature of the load of machine foundations.

The plastic deformation from the cyclic loads leads to a reduction in the system stiffness, which results in larger displacements compared to the linear elastic model. In other words, the response of soil subjected to vertical dynamic cyclic loads from machines is affected by hysteresis, meaning that the soil behaves differently during loading and unloading from machine cyclic loads. This phenomenon should be taken into account in the analysis of micropile-supported machine foundations.

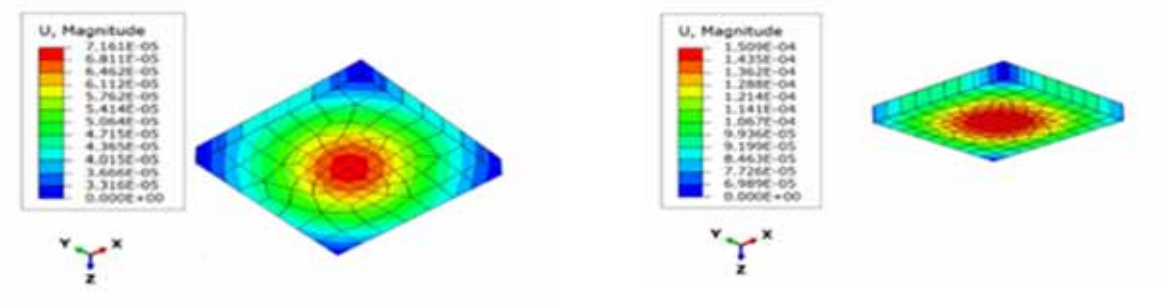

(a) (b)

Figure 4-18: Dynamic Displacement Contours at the location of Micropile Cap for Machine Foundations subject to Vertical Dynamic Loads using a) Linear (Elastic) Soil Model, b) Nonlinear (Modified Drucker-Prager) Soil Model at Resonance.

Figure 4-19 and Figure 4-20 show the variations of the dynamic displacement and spectral acceleration at the micropile cap location in the micropile group subject to vertical dynamic machine load with the amplitude of load ranging from 25 *kN* to 100 *kN* modeled under both linear elastic and nonlinear Modified Drucker-Prager with Cap models. As it is evident in these figures, it is observed that the nonlinear model predicts higher displacements compared to the elastic model for all of the applied dynamic loads. This is due to the fact that during dynamic loading, soil behavior becomes more nonlinear and plastic, leading to larger deformations.

Another observation is that as the amplitude of the applied dynamic load increases, the peak dynamic displacement also increases for both linear and nonlinear models. However, the rate of increase is higher for the nonlinear model than for the elastic model. This could be due to the fact that as the load increases, the soil experiences higher stress and strain levels, resulting in significant plastic deformations and formations of hysteresis loops. Therefore, it is crucial to consider the potential effects of the amplitude of machine load on the response of the micropile groups and

design the soil-micropile system accordingly to ensure its safety and structural integrity under various loading scenarios.

As the amplitude of the dynamic load rises, the dynamic displacements, and spectral accelerations at the micropile head also increase. The dynamic displacements and acceleration response for soil with an elastic model increase proportionally with the increase in the amplitude of the cyclic load. However, for the nonlinear soil behavior, i.e., the Modified Drucker-Prager model, the rate of change is greater at the higher amplitude of dynamic load. At a load amplitude lower than 50 *kN*, the soil's response is nearly pseudo-elastic, and accelerations will increase proportionally to the amplitude of the load. As the machine load amplitude exceeds 50 *kN*, the soil surpasses its yield strength, the response becomes more nonlinear, and plastic strains will not be directly proportional to the stresses. Therefore, the increase in amplitude may cause the soil to surpass its yield strength sooner, resulting in larger dynamic displacement and accelerations at the top of the soil surface.

Figure 4-21 shows the changes in dynamic displacement along the micropile profile for the two linear and nonlinear soil constitutive models. As can be observed from this figure, the displacement along the profile of micropile for the nonlinear soil constitutive model is greater than that of the elastic soil model. The nonlinear stress-strain relationship of the soil results in greater stresses being transferred from the micropile to the surrounding soil and, as a result, larger displacements along the micropile profile. The presence of grout bond zones between the micropile and soil can also significantly affect the interaction behavior of the micropile-soil system under vertical dynamic loading, further compounding the effect of the nonlinear stress-strain relationship between soil and soil-structure interaction elements. This adds up more nonlinearity and can result in larger stresses being transferred from the micropile to the surrounding soil, leading to larger displacements along the micropile profile.

Figure 4-22 shows the dynamic displacement amplitude response for linear and nonlinear soil constitutive models in the center micropile. As noted, the linear soil model yields lower amplitudes of dynamic displacements. Figure 4-23 displays the variations of the micropile axial forces at resonance with the amplitude of load ranging from 25 *kN* to 100 *kN* using linear elastic and nonlinear Modified Drucker-Prager with Cap models. These results acknowledge that the nonlinear soil behavior significantly affects the micropile axial forces at resonance, particularly at higher amplitudes. The difference in micropile axial forces between the linear elastic and nonlinear models is more pronounced at amplitudes of Q_0 higher than 50 *kN*. For lower amplitudes, the soil behavior is perceived to remain pseudo-elastic. This again reinforces the conclusion that nonlinear soil behavior becomes more important at higher loads.

In Figure 4-24, the axial force envelope at resonance for both linear and nonlinear soil models are compared, and in Figure 4-25, the axial force amplitude response for linear and nonlinear soil behavior are illustrated.

In conclusion, the nonlinear Modified Drucker-Prager model captures the behavior of the soil more accurately than linear models, especially at higher amplitudes of loads. The soil behavior behaves more nonlinear, and its response becomes more significant as the amplitude of the dynamic load increases. However, for lower machine loads ($Q_0 < 50$ *kN*), the difference in the responses between the two models is not as significant. This may indicate that the soil behavior is relatively linear or pseudo-elastic in lower amplitude. Therefore, in the case of micropile groups subject to high vertical dynamic loads from machine foundations, using a nonlinear model for the soil model will make sense as it can provide more accurate predictions of the soil-micropile system response.

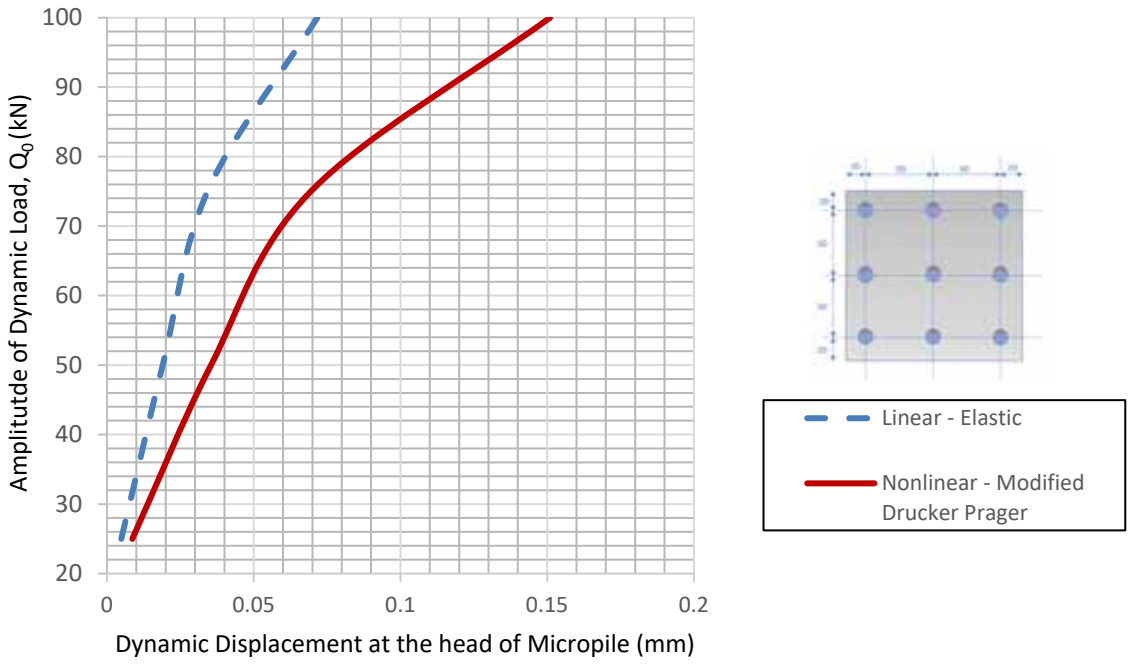

Figure 4-19: Effect of Soil Nonlinear Behavior on Dynamic Displacement at the head of Micropile in Micropile Groups Subject to Varying Amplitude of Dynamic Loads of Machine Foundation

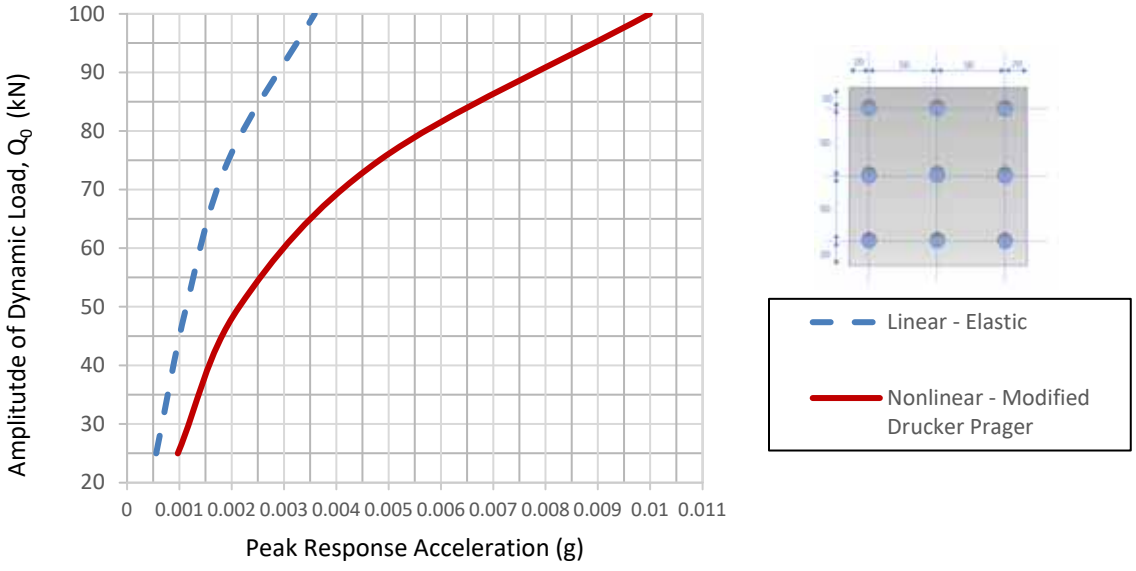

Figure 4-20: Effect of Soil Nonlinear Behavior on Acceleration Response at the Micropile cap in the Micropile Groups Subject to Varying Amplitudes of Dynamic Loads of Machine Foundation

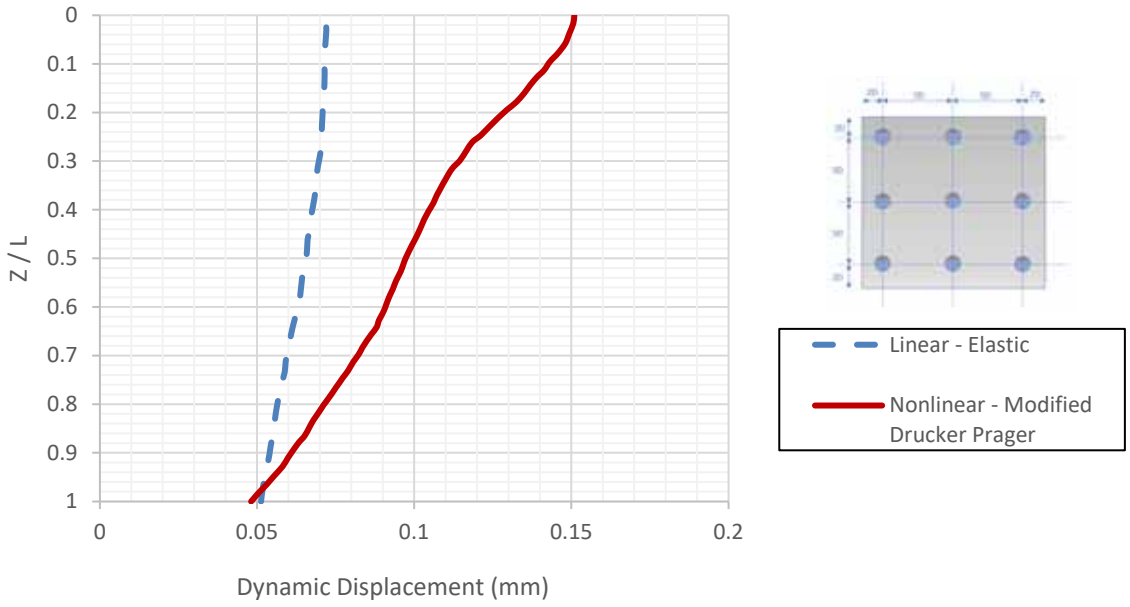

Figure 4-21: Dynamic Displacements Along the Micropile Profile in the Micropile Group for Linear and Nonlinear Soil Constitutive Models at Resonance (Center Micropile)

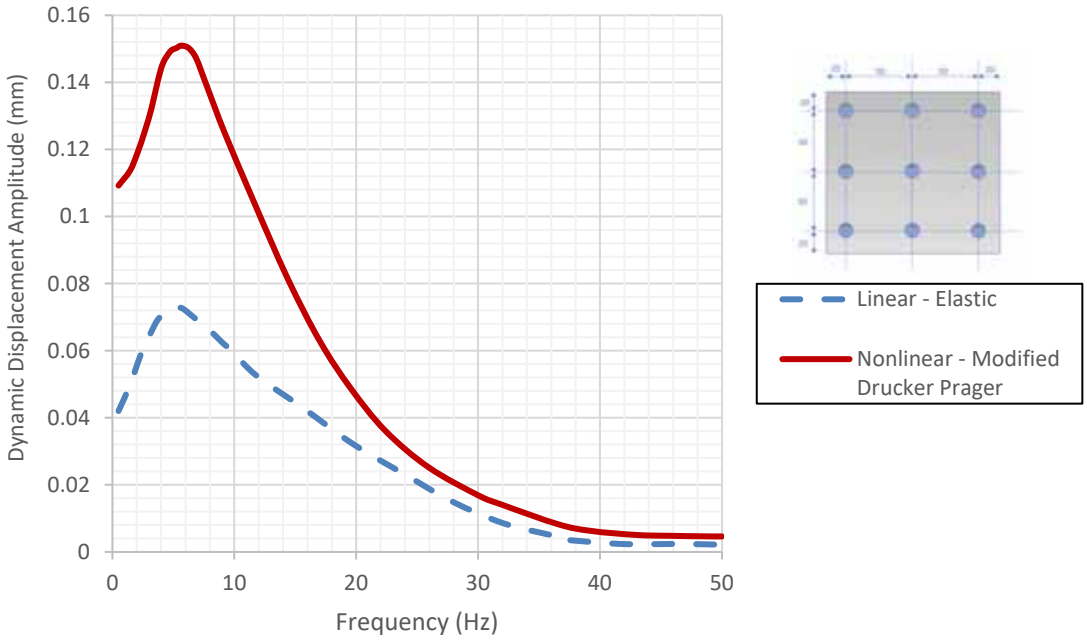

Figure 4-22: Comparison of Dynamic Displacement Amplitude Response for Linear and Nonlinear Soil Constitutive Models - (Center Micropile)

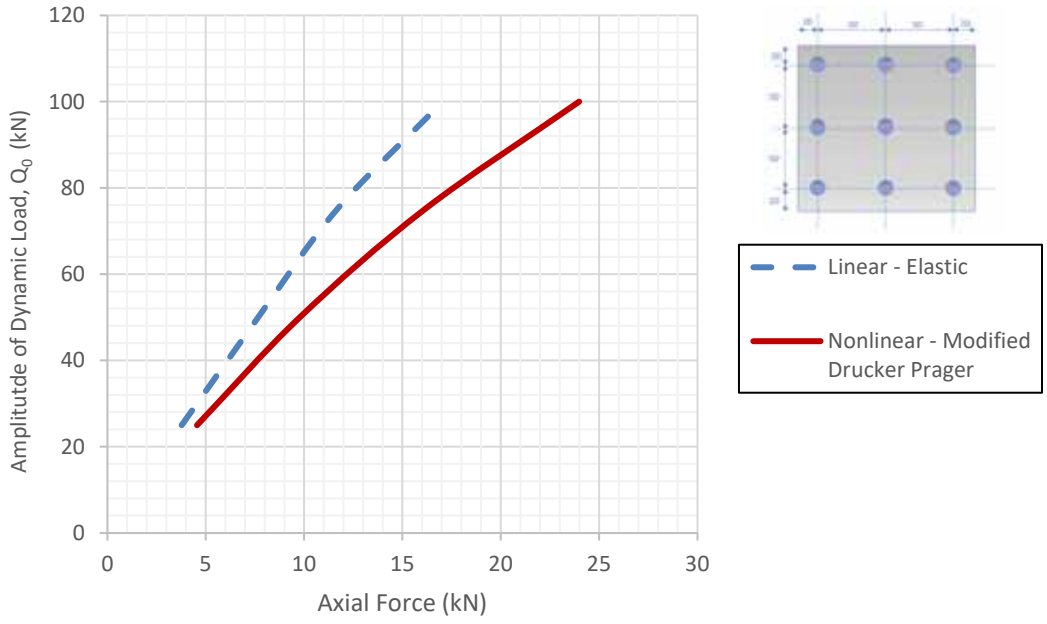

Figure 4-23: Effect of Soil Nonlinear Behavior on Axial Force of Micropile in Micropile Groups Subject to Varying Amplitude of Dynamic Loads of Machine Foundation

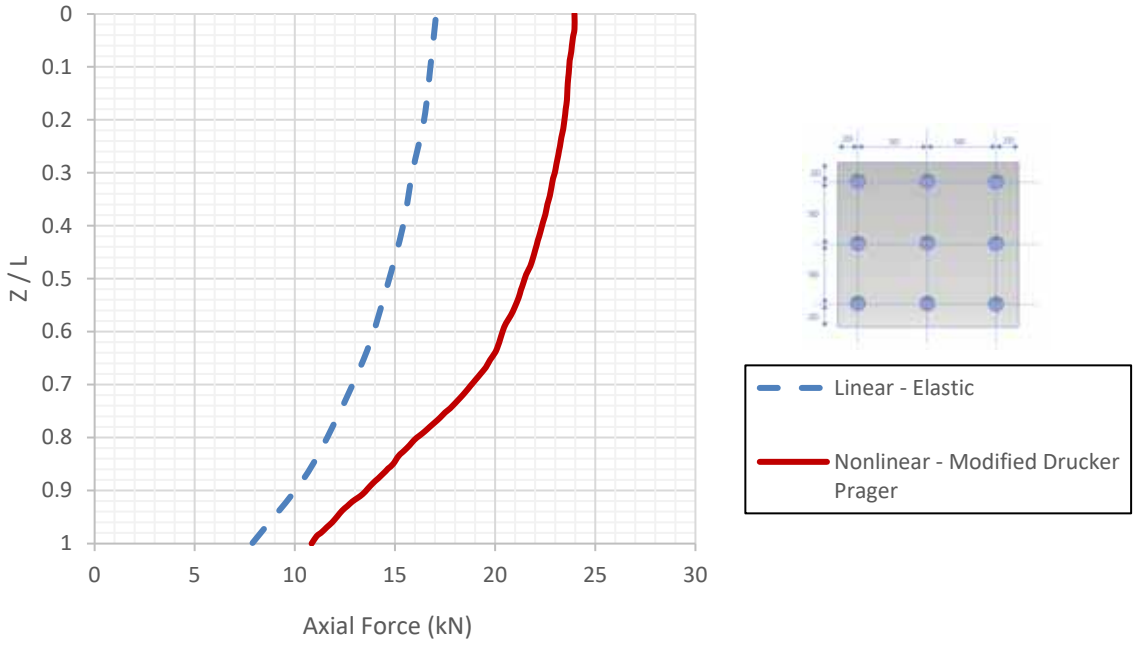

Figure 4-24: Comparison of Axial Force Envelope for Linear and Nonlinear Soil Behavior at Resonance

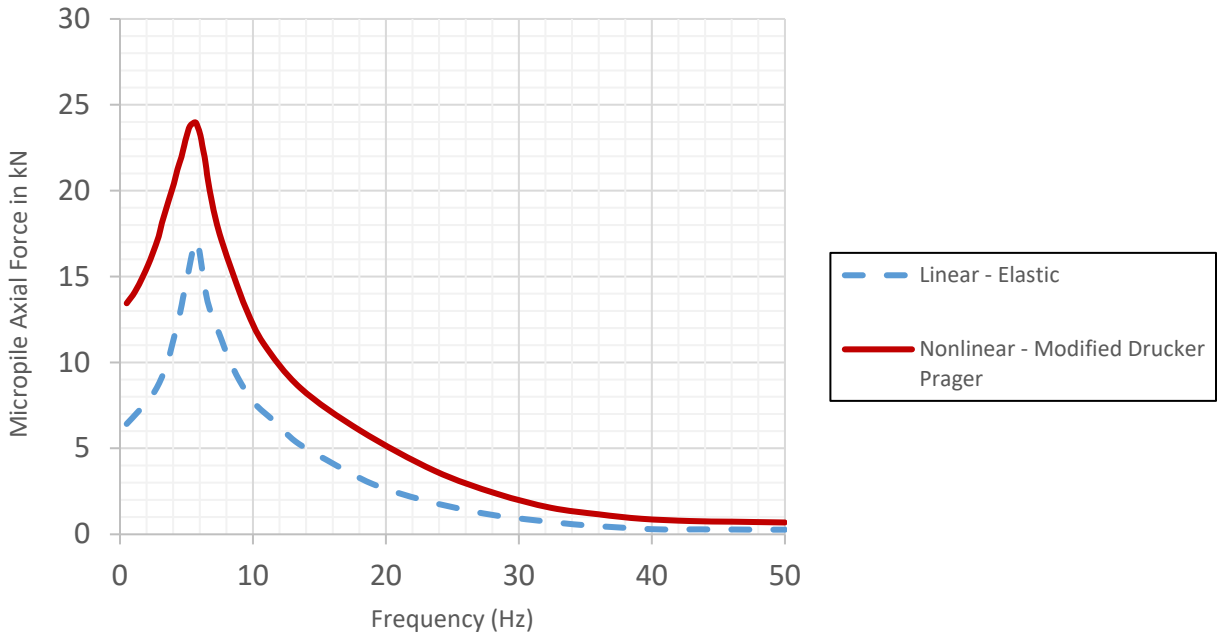

Figure 4-25: Comparison of Axial Force Amplitude Response for Linear and Nonlinear Soil Behavior

4.4.2 Effect of Machine Operating Frequency (f) on the Response of Micropile Groups subject to Vertical Dynamic Load of Machine Foundations

In this section, the effect of the machine operating frequency on the response of the machine foundation is examined. To understand this, the dynamic response of a group of vertical micropiles subjected to a machine load with amplitude of 100 *kN* and with varying range of operating frequencies was studied using the FEM technique and taking into consideration the nonlinear soil behavior. The results of the study can provide more insights into the behavior of the micropile system subject to a range of frequencies and can aid in the design and optimization of machine foundations. In order to assess the accuracy of the Finite Element Method (FEM) results and gain a better understanding of the dynamic response of the vertical micropile group, it is also useful to calculate the natural frequency of the system using available literature empirical equations and compare against the numerical results. The natural frequency is the frequency at which the system will vibrate if displaced from its equilibrium position and released and is an important parameter for the analysis of the dynamic behavior of the system. The natural frequency of the micropile-supported machine foundation system can be derived using following equation:

$$f = 1/(2\pi\sqrt{k/m}) \qquad \text{Equation 4.4}$$

where m is the mass of the micropile group and machine foundation, and k is the stiffness of the soil and can be calculated as:

$$k = \frac{Q_s A_p}{u_s} \qquad \text{Equation 4.5}$$

In this equation, Q_s is the amplitude of the dynamic load, A_p is the cross-section area of the micropile and u_s is the displacement of the micropile at the static phase. Also, from conducting a

Geostatic analysis in the FEM software, the static displacement at the location of micropile cap/soil surface were found at approximately 0.145 mm. Therefore, we can write:

$$k = \frac{Q_s A_p}{u_s} = \frac{(100{,}000\ N)(\frac{\pi}{4}(0.3^2))}{0.145 \times 10^{-3}} = 4.87 \times 10^7\ \ N/m$$

Assuming the micropile elements have negligible weight, we can take the foundation weight equal to mass of the machine foundation and therefore we have:

$$f_n = \frac{1}{2\pi}\sqrt{\frac{k}{M}} = \frac{1}{2\pi}\sqrt{\frac{4.87 \times 10^7}{50968}} = 4.92\ Hz$$

The value of 4.92 *Hz* can serve as a benchmark for comparison with the numerical results obtained using finite element analyses. The comparison of these values provides insights into the accuracy of the numerical model and helps to validate the assumptions and parameters used in the analysis.

Figure 4-26 show the dynamic displacement contours for machine operating frequencies ranged from 1 to 20 *Hz*. These contours show the distribution of deformations across the micropile-cap near and far from the natural frequency. In Figure 4-27 and Figure 4-28 the dynamic displacements along the micropile profile and spectral acceleration response at the micropile cap are shown. Based on these results, it can be noted that the system will be at resonance at the frequency of approximately 5.8 *Hz*. As the operating frequency deviates from the natural frequency, the dynamic displacement and acceleration magnitudes subside substantially.

Figure 4-29 illustrates the axial force profile for range of machine foundation operating frequencies, and it is observed that as the machine frequency operates farther from the natural frequency of the system (i.e., 5.8 *Hz*), less axial forces are mobilized along the micropiles. At

frequencies beyond resonance region (i.e., 11.6 *Hz*), the axial forces developed along the micropiles are nearly more than 60 percent less than the axial forces mobilized near or at resonance.

At the resonance, the micropile's natural frequency coincides with the applied load's frequency, resulting in the micropiles absorbing the maximum amount of energy from the machine load vibrations. This leads to the amplitude of the micropile group vibrations increasing significantly, which, in turn, causes peak axial forces to develop along the micropiles. In contrast, as machine frequency goes farther than the natural frequency, the forces in the micropile gradually reduce, and they become very small or negligible for frequencies beyond the resonance region as the micropile is not absorbing much of the energy from the machine vibrations. Also, at high frequencies, the amount of damping required to reduce the amplitude of vibration in the system significantly may be higher, therefore, resulting in negligible axial forces along the micropiles.

The determination of the resonance region is based on the system's response, particularly the dynamic displacement amplitude response curve. The natural frequency is typically identified at the peak amplitude of the curve, and the resonance region is usually determined based on the width of the peak and the amplitudes of the surrounding frequencies. The resonance region was identified as a frequency range beyond the natural frequency where the displacement amplitudes were reduced substantially, typically by 50 percent or more. Per a literature review, this range can vary from 1.2 to 2 times the natural frequency depending on the other characteristic of the system (Rajkumar, 2020). In this study, the width of the resonance region was determined to be around two (2) times the natural frequency.

In conclusion, the natural frequency plays an important role on the system's response and in determining the extent of reduction in axial forces along the micropiles, with a substantial decrease occurring at frequencies beyond the resonance region. Understanding the resonance response of the micropile group supporting a machine foundation is crucial for accurately predicting the system's behavior and design decision-making.

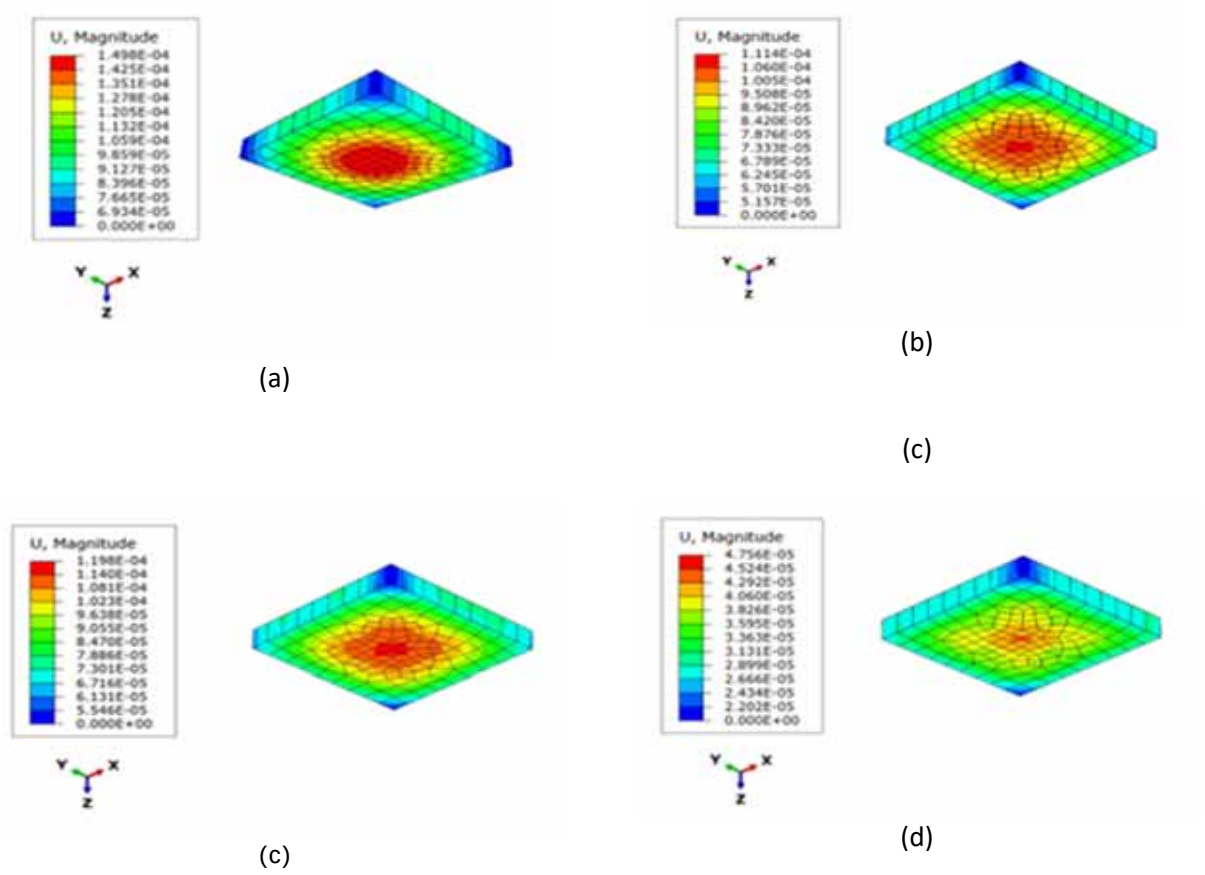

Figure 4-26: Dynamic Displacement Contours at the location of Micropile Cap for Various Machine Foundations Operating Frequencies a) f = 1 *Hz*, b) f = 5 *Hz*, c) f = 10 *Hz*, d) f = 20 *Hz*

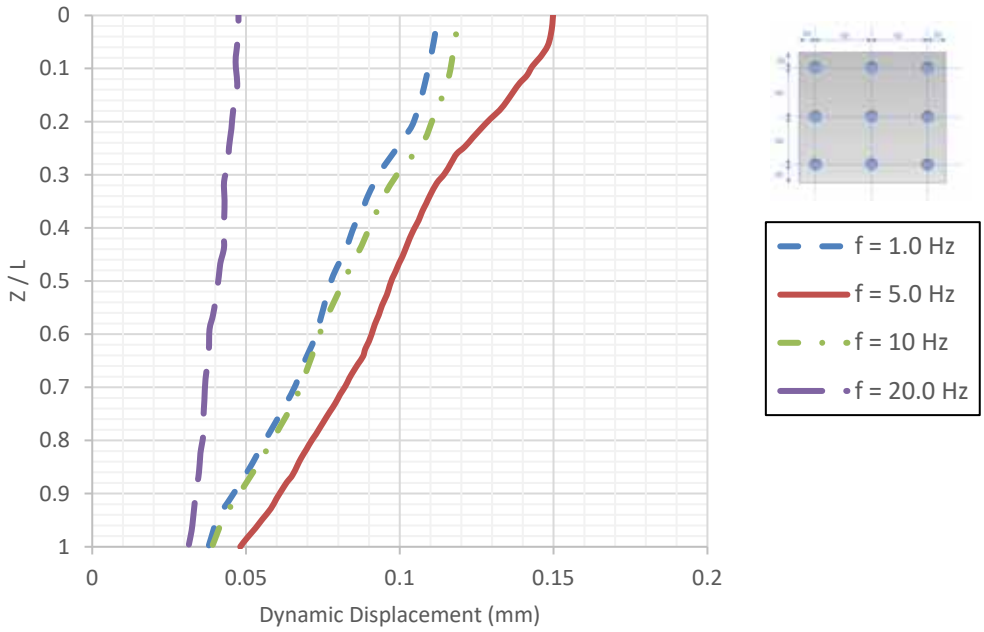

Figure 4-27: Dynamic Displacements along the Micropile Profile in the Micropile Group for Various Machine Foundations Operating Frequencies (Center Micropile)

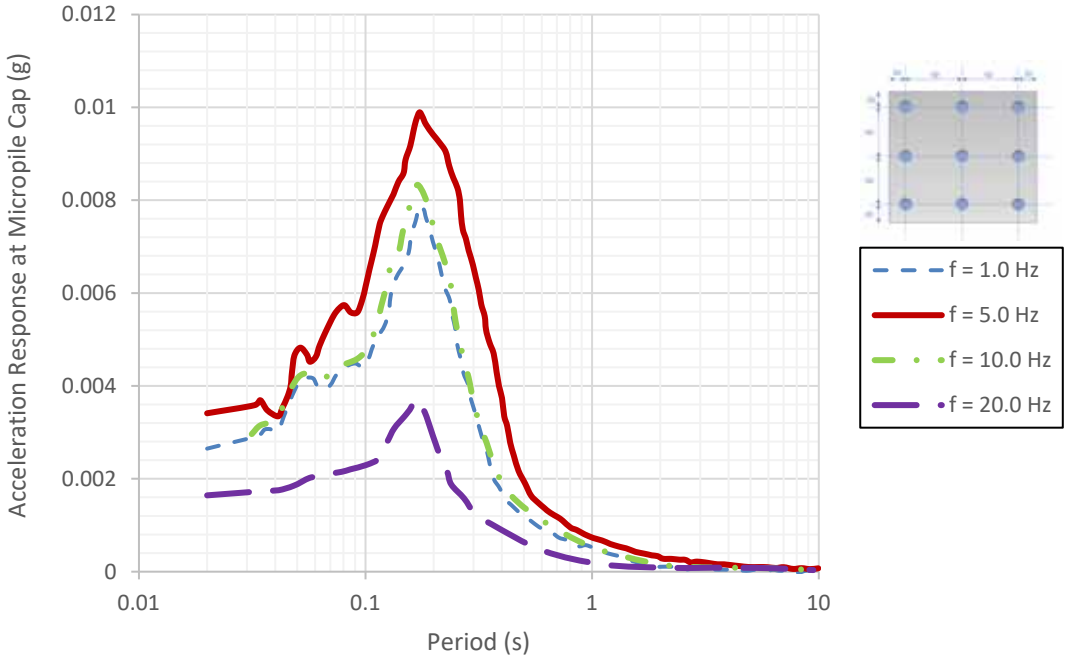

Figure 4-28: Dynamic Acceleration Spectra at Micropile Cap for Various Machine Foundations Operating Frequencies

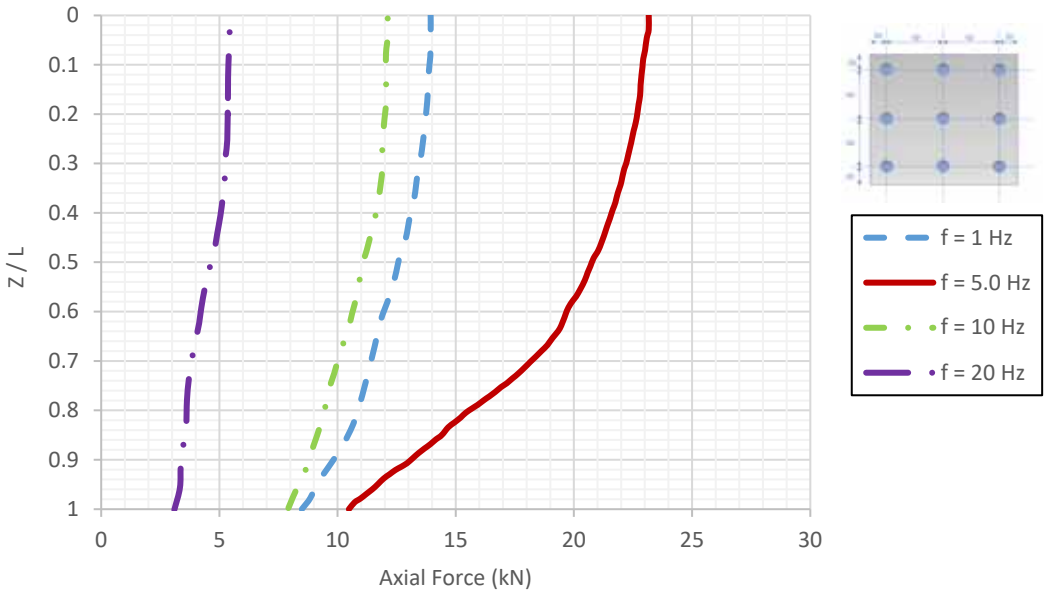

Figure 4-29: Comparison of Axial Force Envelope for Various Machine Foundations Operating Frequencies

4.4.3 Effect of Machine Foundation Mass (*m*) on the Response of Micropile Groups subject to Vertical Dynamic Load of Machine Foundations

The effect of machine foundation mass (m) on the response of micropile groups subject to dynamic harmonic loading was further studied in this section. Three (3) 3-D FEM models representing machine foundations masses of 250 *kN*, 500 *kN* and 1000 *kN* were developed in the FEM software and were subjected to dynamic load of a machine foundation. The soil conditions were assumed to be medium dense, and the gapping effect were also taken into account in the interaction properties of the interface elements. The soil behavior was represented using a nonlinear Modified Drucker-Prager with Cap. Figure 4-30 display the dynamic displacement contours at the location of micropile cap for three different masses of 250 *kN*, 500 *kN* and 1000 *kN* at the resonance. As it can be observed, the maximum displacement occurs at the location of

micropile cap for the group supporting the lowest mass of machine foundation i.e., m = 250 *kN*. The variations of the dynamic displacements along the center micropile profile are compared for various machine foundation masses and is illustrated in Figure 4-31. In addition, dynamic acceleration spectra at micropile cap for various masses of machine foundation are illustrated in Figure 4-32. As the machine foundation mass rises from 250 *kN* to 500 *kN*, the displacement at the micropile head reduced by approximately 32 percent and as the mass rises from 250 *kN* to 1000 *kN*, the displacement at the micropile head reduced by approximately 47 percent.

Figure 4-33 illustrates the dynamic displacement amplitude response as a function of frequency (*Hz*) for various machine foundation masses. As the machine foundation mass rises, the resonant frequency of the system shifts further towards lower frequencies, and the stiffness of the system increases. Additionally, the increase in mass also contributes to an increase in the internal damping of the system. The presence of more mass creates more internal friction and energy dissipation, which leads to an increase in damping. This increased system damping helps to attenuate the vibrations and reduces the amplitude of the response. Therefore, an increase in damping has some implications for reducing the natural frequency of the system, meaning that the system will need to take a longer time to complete its vibrations. As a result, the natural frequency of the system is reduced with the increase in the mass of the machine foundation system. Based on the results of the frequency response analyses for three different foundation masses, it can be concluded that beyond the resonance region (i.e., 19 *Hz*), the increase in mass of the machine foundation may not significantly impact the dynamic displacement amplitudes of the system.

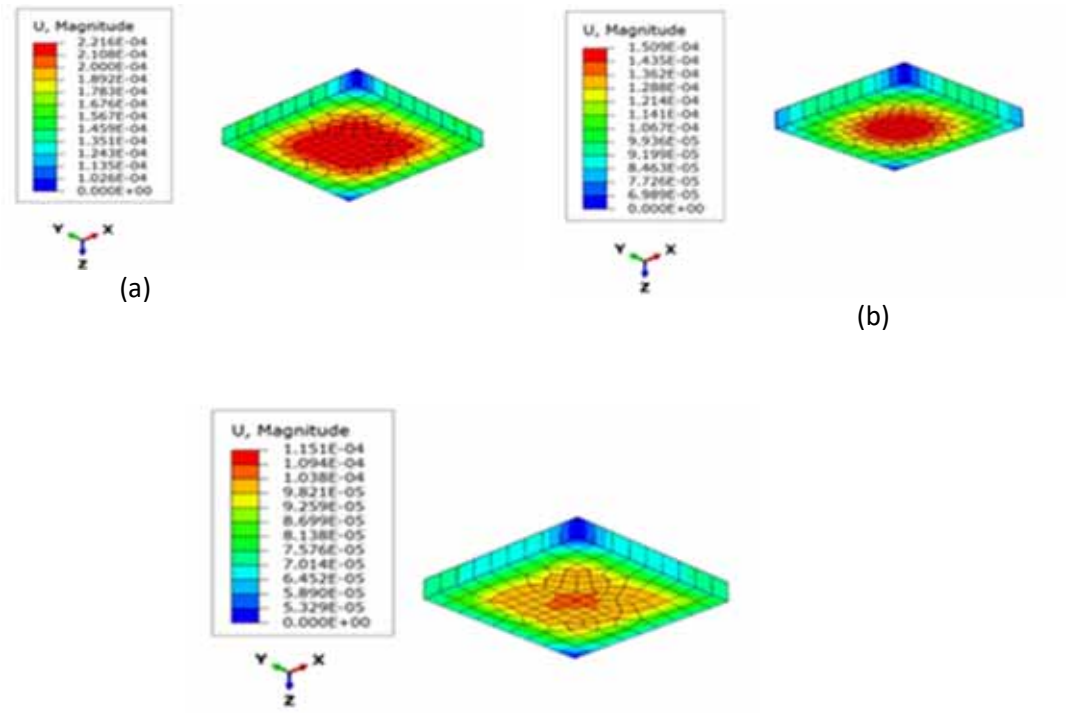

Figure 4-30: Dynamic Displacement Contours at the location of Micropile Cap for Various Machine Foundation Masses a) m = 250 *kN*, b) m = 500 *kN*, c) m = 1000 *kN*

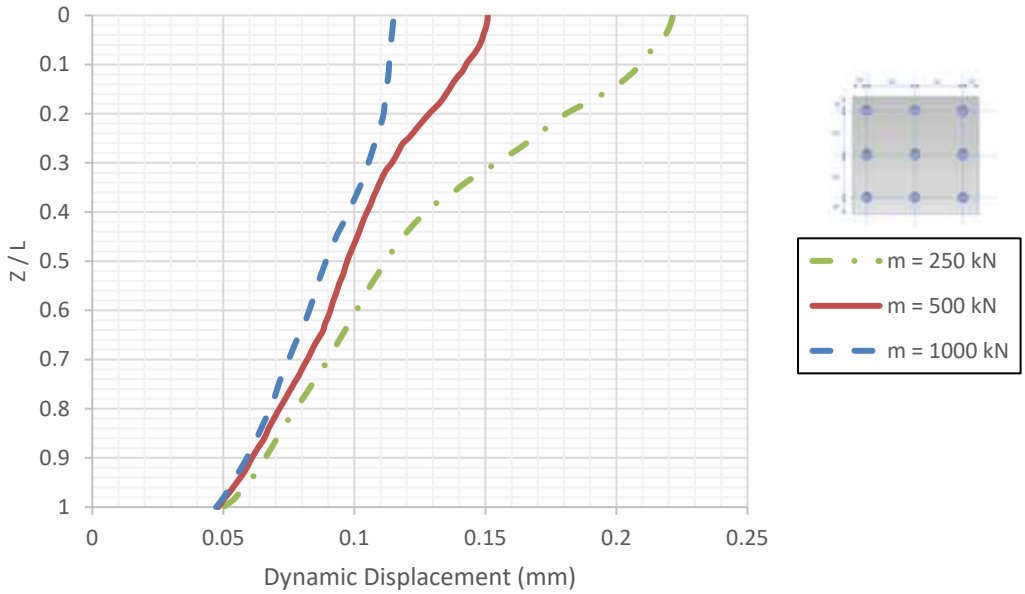

Figure 4-31: Dynamic Displacements along the Micropile Profile in the Micropile Group for Various Machine Foundation Masses at Resonance (Center Micropile)

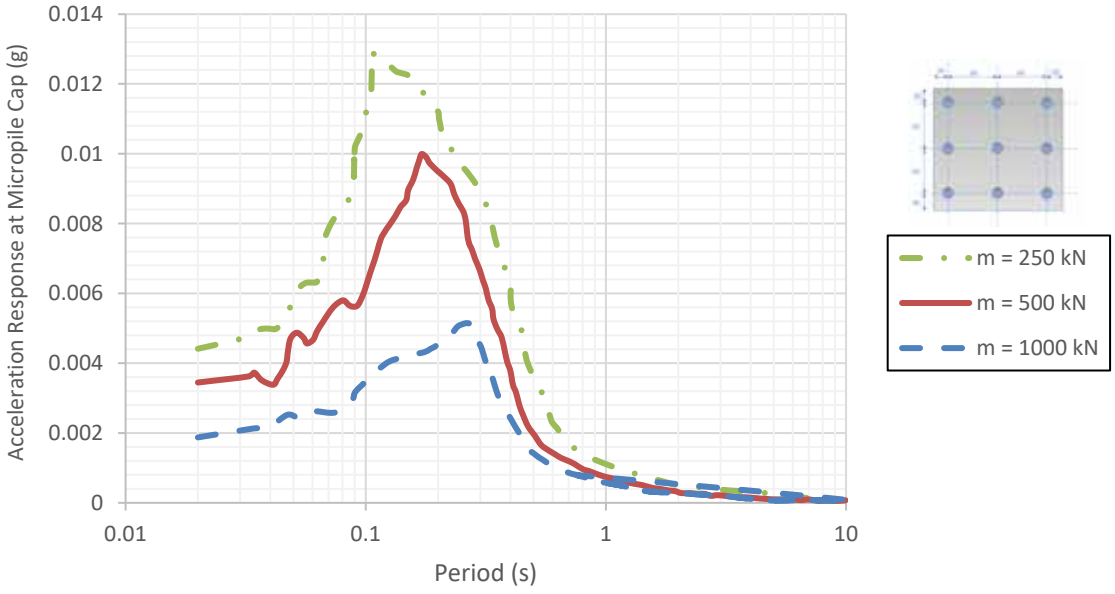

Figure 4-32: Dynamic Acceleration Spectra at Micropile Cap for Various Machine Foundation Masses

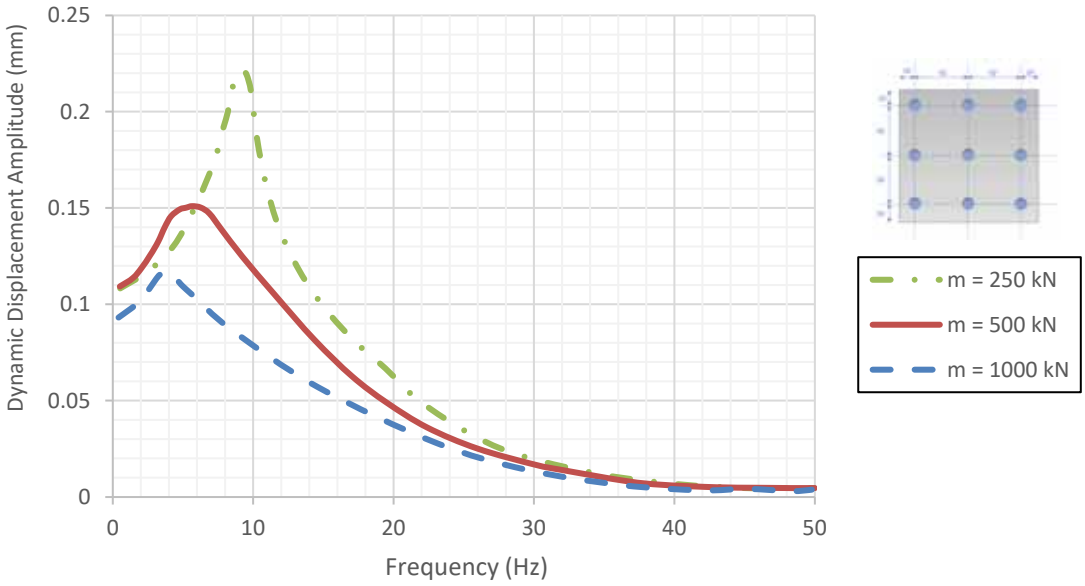

Figure 4-33: Comparison of Dynamic Displacements Amplitude Response for Various Machine Foundation Masses

Figure 4-34 compares the axial forces along the micropile profiles at resonance for three machine foundation masses. As noted, as the mass of the machine foundation increased, less axial forces were mobilized along the micropiles, which can be attributed to the higher stiffness of the system. The higher the mass of the machine foundation, the higher the stiffness of the system, which means that the system is less susceptible to vibrations and less displacements, and forces are mobilized along the micropiles. Per these results, as the mass of the machine foundation increased from 250 *kN* to 500 *kN*, the axial force at resonance was reduced by approximately 17 percent. Similarly, as the mass of the machine was increased from 250 *kN* to 1000 *kN*, the axial force at resonance was reduced by approximately 37 percent. Figure 4-35 shows the axial force response curve for various machine foundation masses. As can be noticed from this figure, the increasing mass of the machine has caused the axial force amplitude to reduce and shift toward lower frequencies.

In conclusion, increasing the mass of the machine foundation can lead to a decrease in the resonant frequency of the system, as well as a decrease in the dynamic displacement and forces along the micropiles. This implies that for a given machine, it may be beneficial to design a heavier foundation to ensure the stability and safety of the entire system, especially if the machine is expected to operate at low frequencies. However, there are many factors to consider, such as damping, mechanical, and dynamic soil properties, for a proper machine design.

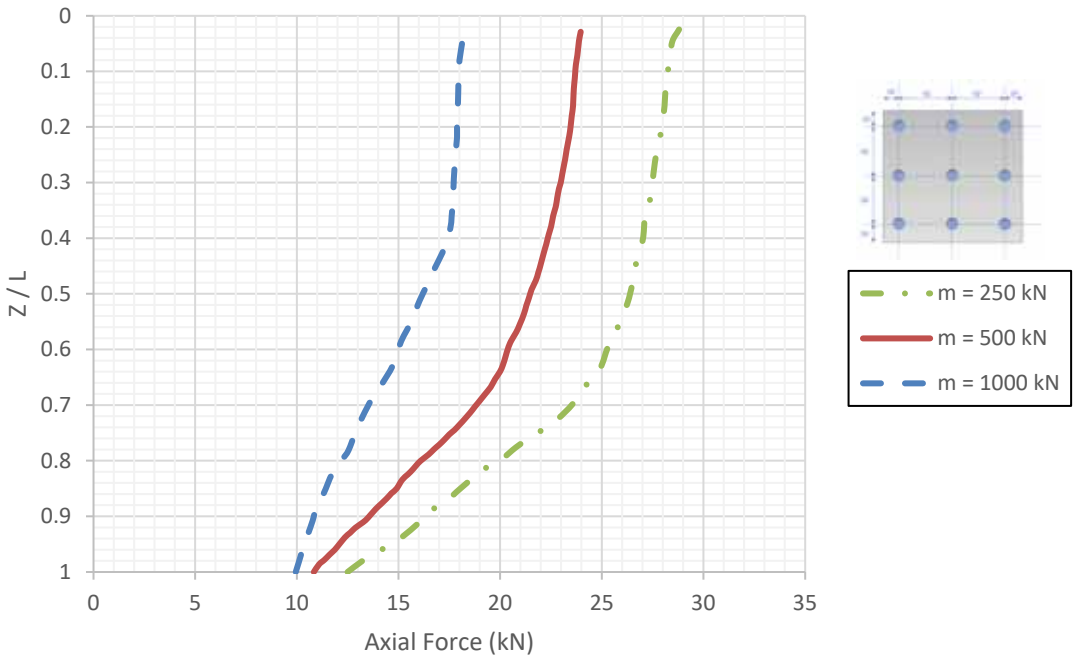

Figure 4-34: Comparison of Axial Force Envelope for Different Machine Foundation Masses at Resonance

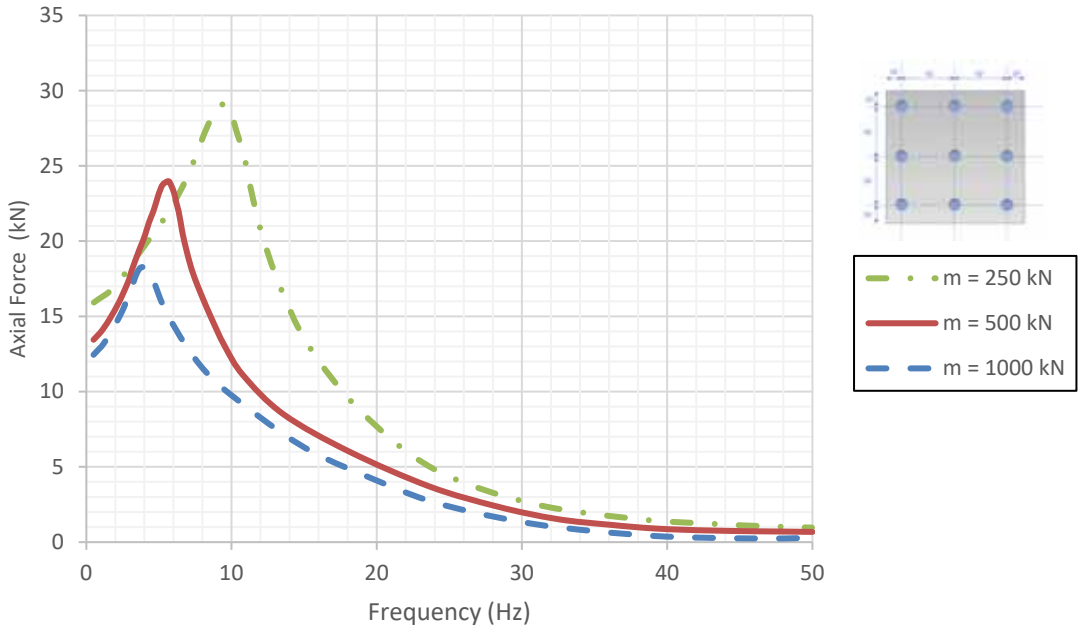

Figure 4-35: Comparison of Axial Force Amplitude Response for Different Machine Foundation Masses

4.4.4 Effect of Soil Shear Modulus/Micropile Stiffness Ratio (*R*) on the Response of Micropile Groups subject to Vertical Dynamic Load of Machine Foundations

In this section, the effect of Soil Shear Modulus (G_{soil}) to Micropile Young Modulus ($E_{micropile}$) ratio (R) on the behavior of Micropile Groups are studied. Three variations of the soil shear modulus to micropile stiffness ratios (R) to represent soft, medium, and stiff soil conditions are assumed in these analyses as summarized in Table 4-4 and a machine dynamic load with amplitude of 100 *kN* is applied at the top of machine foundation. For all the analyses, a nonlinear soil constitutive model of modified Drucker-Prager with cap is assumed for the soil stress-strain behavior, and the parameters for each soil condition are reflected in the soil plastic section properties accordingly in the FEM software. The effect of the gapping is also considered for the contact surfaces of the micropile and the soil elements in the interaction modeling.

Table 4-4 - Different Soil Properties to FEM Analyses for Soil Continuum		
Soft Soil	Medium Soil	Stiff Soil
Young Modulus (E) = 10 MPa	Young Modulus (E) = 100 MPa	Young Modulus (E) = 1000 MPa
Poisson's Ratio (ν) = 0.2	Poisson's Ratio (ν) = 0.2	Poisson's Ratio (ν) = 0.2
Shear Modulus (G) = 4.2 MPa	Shear Modulus (G) = 42 MPa	Shear Modulus (G) = 420 MPa
$R \approx 0.0002$	$R \approx 0.002$	$R \approx 0.02$

Figure 4-36 show the dynamic displacement contours at the location of micropile cap for machine foundations with different soil shear modulus/micropile stiffness ratios of R = 0.0002, 0.002 and 0.02 at resonance. As it can be observed the displacement contours at the location of micropile head show that the micropiles in the group with lowest ratio i.e., R = 0.0002 experience larger displacements than those in the other two groups. This could be justified as the soil stiffness is lower in the case of soft soil, which allows for more deformations and larger displacements around micropile head. In the group with R = 0.02 (stiff soil) smaller displacement was observed due to the higher stiffness of the surrounding soil.

The variations of the dynamic displacements along the center micropile profile are compared for various soil shear modulus/micropile stiffness ratios and is illustrated in Figure 4-37. In addition, dynamic acceleration spectra at micropile cap for various ratios is illustrated in Figure 4-38. As the ratio increased from R = 0.0002 to R = 0.002, the displacement at the micropile head decreased by approximately 38% and similarly, as the ratio increased from R = 0.0002 to R = 0.02, the displacement at the micropile head reduced by approximately 56%.

The results also suggest that as the soil shear modulus/micropile stiffness ratio increases, the dynamic displacement along the micropile profile and the micropile head decreases. As the soil conditions become stronger with respect to micropile stiffness, the micropile group will deform less under the same dynamic load. In a stiffer soil-micropile system, the group can resist deformations more effectively due to the higher stiffness of the system, therefore, resulting in smaller displacements in individual micropiles. On the other hand, a less stiff soil-micropile group will deform more under the same amplitude of load, resulting in larger displacements. It is worth noting that the displacement is highest at the head of the micropile at the location of the cap where the machine load is applied, and as the loads are transmitted down the length of the micropile, the resistance and stiffness of the surrounding soil and micropile cause the displacement to taper towards the tip of the micropile gradually. The damping will further influence this in the system, which will absorb some of the energy from the load and reduce the amplitude of the displacement along the length of the micropile.

Figure 4-39 displays variations of the dynamic displacement amplitude with soil shear modulus/micropile stiffness ratio (R) against various amplitude of the dynamic load. It can be noted that the effect of stiffness ratio on displacement is more pronounced for higher load amplitudes (i.e., 100 *kN*). For instance, at a load amplitude of 100 *kN*, the dynamic displacement decreases from about 0.24 *mm* to 0.11 *mm* as the stiffness ratio increases from 0.0002 to 0.02, a reduction of about 56 percent. However, at a load amplitude of 25 *kN*, the dynamic displacement decreases from about 0.011 *mm* to 0.007 *mm*, a reduction of about 33 percent. These results indicate that increasing the stiffness of the soil-micropile system relative to the applied load can lead to a substantial reduction in dynamic displacement, which it is worth paying attention to

during the design and can help to mitigate the risk of damage or failure of the entire foundation system and the machine.

Figure 4-40 illustrates the dynamic displacement amplitude as a function of frequency (*Hz*) for soil shear modulus/micropile stiffness ratios. As the soil shear/micropile stiffness ratio rise, the resonant frequency shifts towards higher frequencies; This shift occurs because the natural frequency of the soil-micropile system is influenced by the stiffness of the surrounding soil, and as the stiffness increases, the natural frequency also rises.

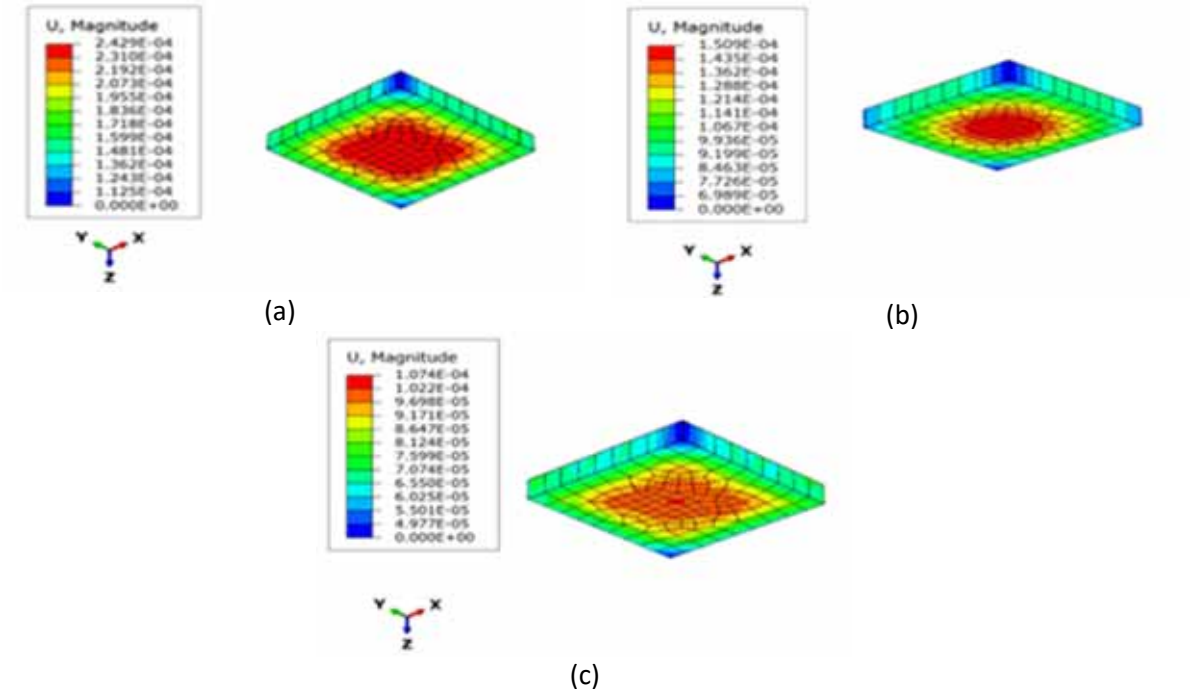

Figure 4-36: Dynamic Displacement Contours at the location of Micropile Cap for Machine Foundations with various Soil Shear Modulus/Micropile Stiffness Ratios of a) R = 0.0 002, b) R = 0.002, c) R = 0.02

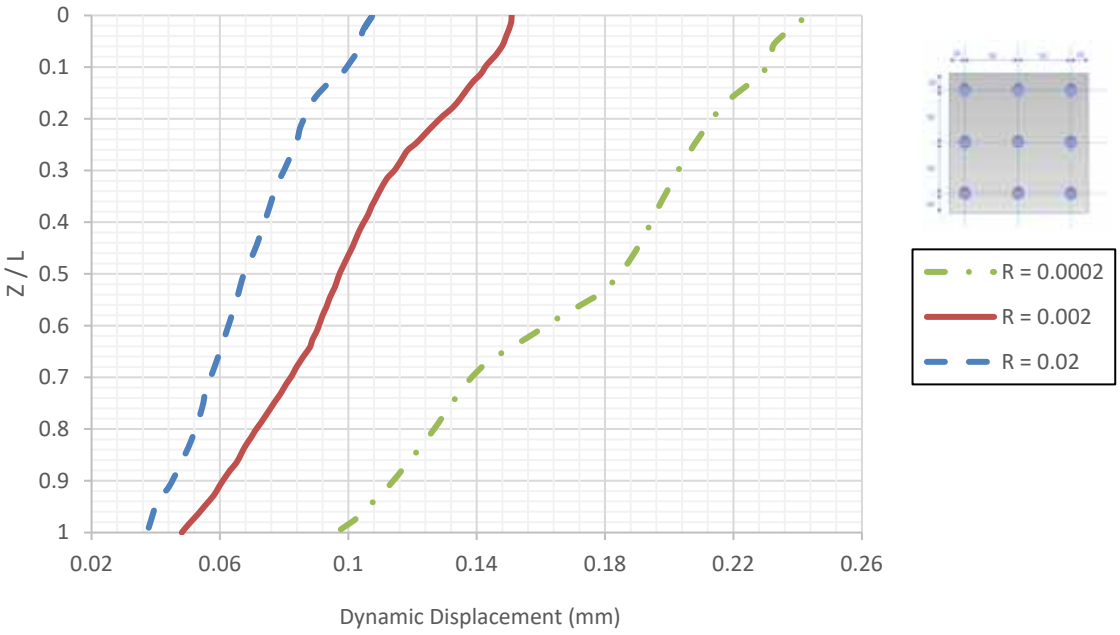

Figure 4-37: Dynamic Displacements along the Micropile Profile in the Micropile Group with various Soil Shear Modulus/Micropile Stiffness Ratios at Resonance - (Center Micropile)

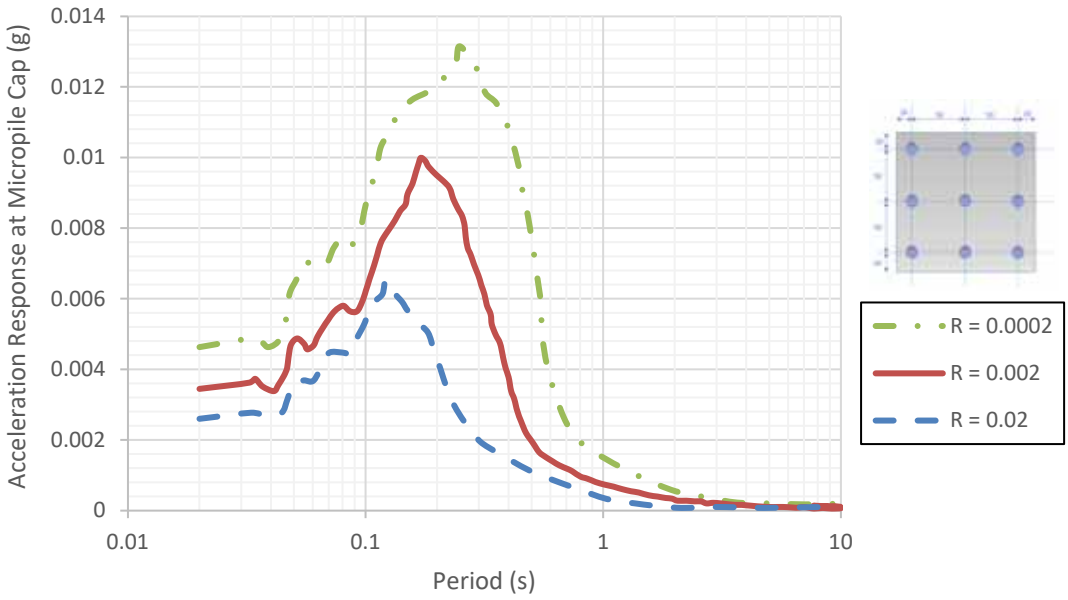

Figure 4-38: Dynamic Acceleration Spectra at Micropile Cap for various Soil Shear Modulus/ Micropile Stiffness Ratios (R)

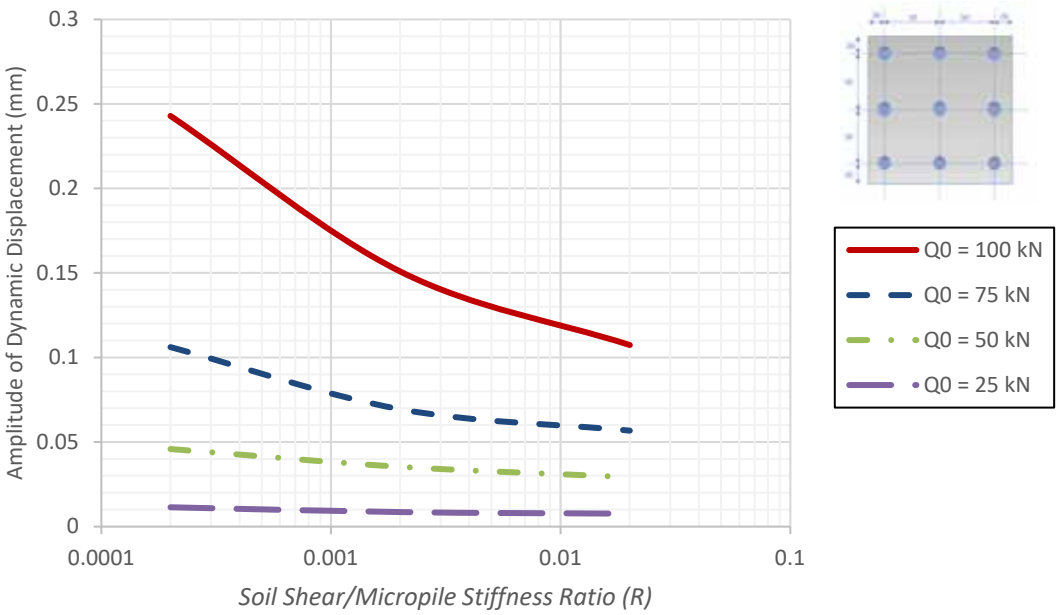

Figure 4-39: Variations of the Dynamic Displacement Amplitude with Soil Shear Modulus/Micropile Stiffness Ratio (R) for various Amplitudes of Dynamic Loads

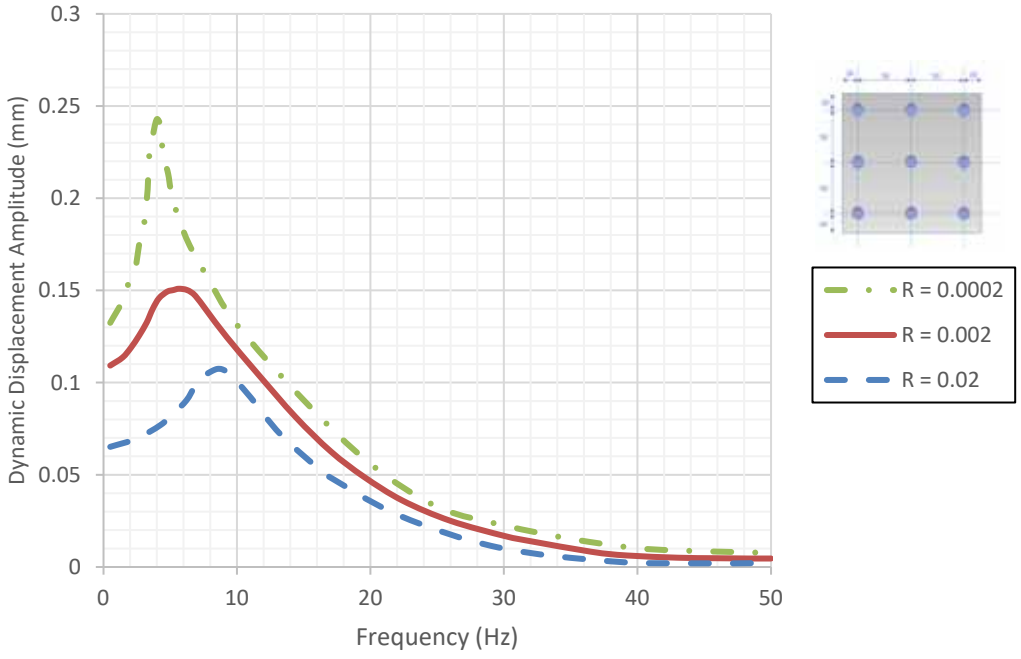

Figure 4-40: Comparison of Dynamic Displacement Amplitude Response for various Soil Shear Modulus/Micropile Stiffness Ratios (R) - (Center Micropile)

In Figure 4-41 the variations of the axial forces along the micropile profile for various soil shear modulus/micropile stiffness ratios is illustrated and as it can observed that the higher the stiffness, the less axial forces are mobilized along the length of the micropiles.

As the ratio increased from R = 0.0002 to R = 0.002, the axial force amplitude reduced by approximately 19 percent and similarly, as the ratio increased from R = 0.0002 to R = 0.02, the axial force amplitude reduced by approximately 43 percent. When the soil is relatively stronger than the micropiles, the micropiles will deflect less and experience lower axial forces. The stiff soil mass around the micropiles contributes to resisting the stresses due to the dynamic load more effectively than soft soils, resulting in less deformation and axial forces along micropiles. Figure 4-42 illustrates the axial force response curve for various soil shear modulus/micropile stiffness ratios. As evident from this figure, as the soil shear/micropile stiffness ratio rises, the resonant frequency shifts towards higher frequencies, and the axial force amplitude reduces.

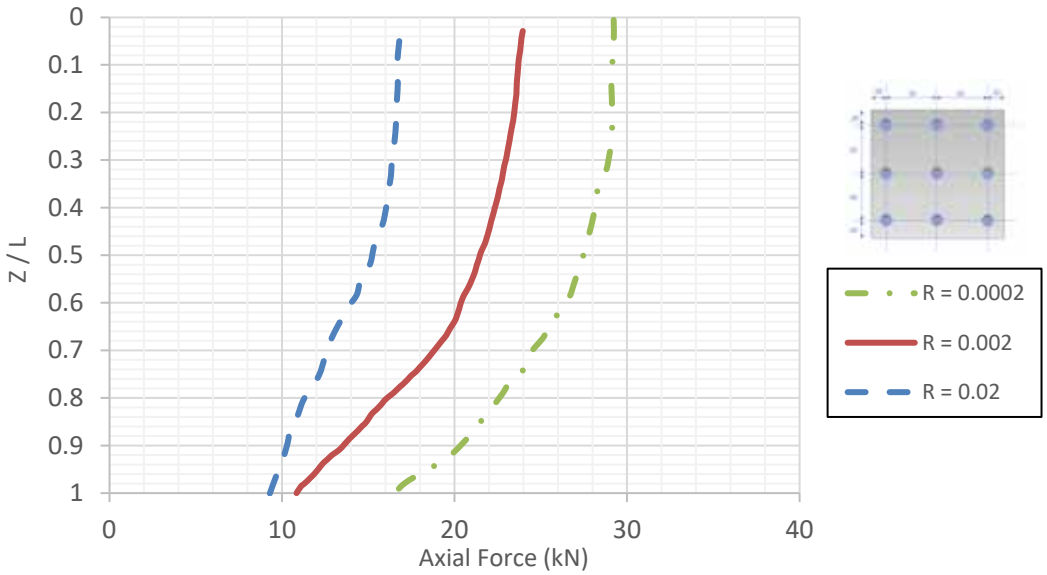

Figure 4-41: Comparison of Axial Force Envelope for various Soil Shear Modulus/Micropile Stiffness Ratios (R) at Resonance

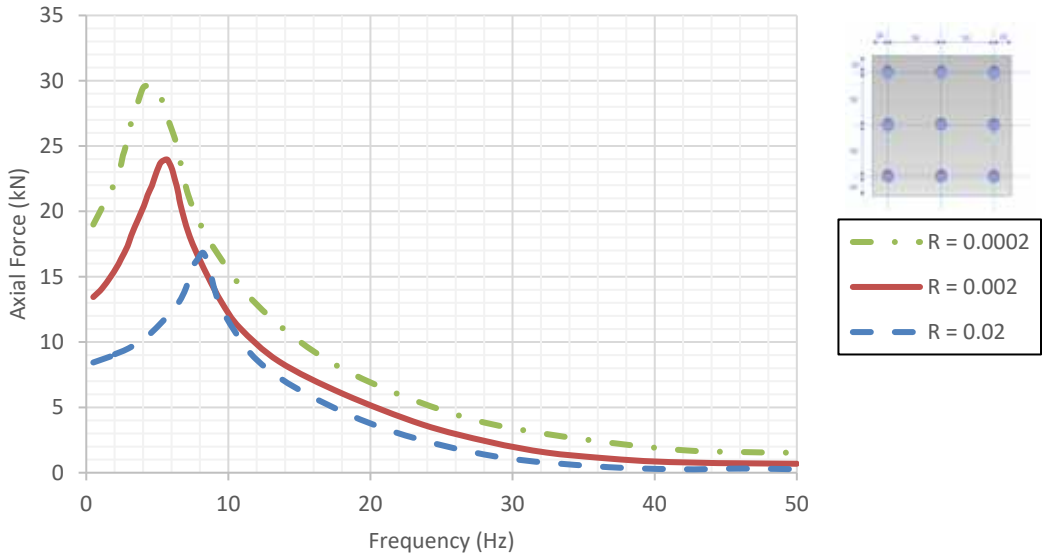

Figure 4-42: Comparison of Axial Force Amplitude Response for Different Soil Shear Modulus/Micropile Stiffness Ratios (R)

4.4.5 Effect of Micropile Inclination Angle (*i*) on the Response of Micropile Groups subject to Vertical Dynamic Load of Machine Foundations

Micropiles are usually installed in large numbers within a group and with different inclination angles to support new foundations, underpin existing ones, or to support other earth-retaining structures. Therefore, micropile inclination angle (*i*) is a key parameter that affects the behavior of micropile groups under both static and dynamic harmonic loading conditions. The inclination angle (*i*) of micropiles plays a significant role in controlling the load transfer mechanism and overall performance of the soil-micropile system. As the inclination angle changes, the stiffness and load-carrying capacity of the micropile group also change. Therefore, it is essential to understand the effect of inclination angle (*i*) on the performance of micropile groups subjected to dynamic load of the machine foundations in order to warrant the safe and efficient design of these foundations. In this section, the effect of micropile inclination angle (*i*) on the response of micropile groups under dynamic harmonic loading is further investigated.

To study the effect micropile inclination angle (*i*) , groups of 3 × 3 micropiles inserted into the ground with varying inclination angles ranging from 0 to 30 degrees from the vertical axis were developed in the FEM software. The soil had a shear modulus/micropile stiffness ratio (R) of 0.002 to represent medium stiff conditions and the micropile groups were subjected to a vertical dynamic load with an amplitude of 100 *kN*. Figure 4-43 illustrates a schematic view of various inclination angles as studied in this research.

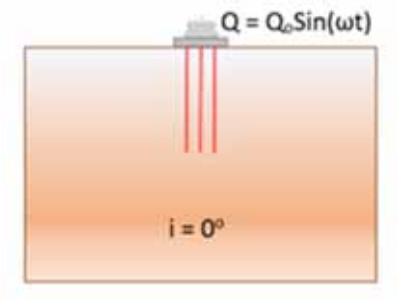

(a)

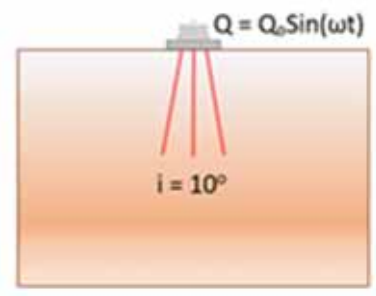

(b)

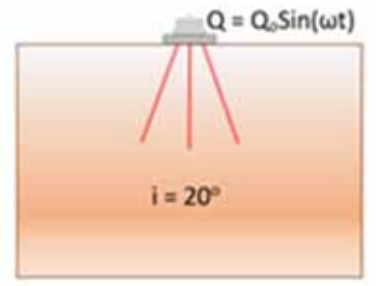

(c)

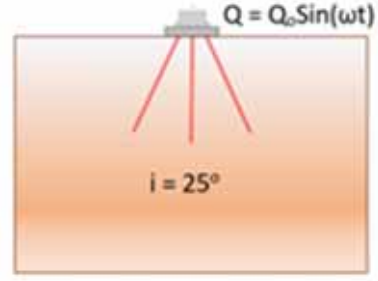

(d)

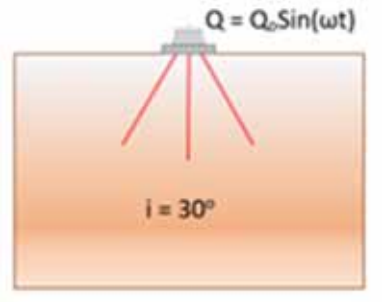

(e)

Figure 4-43: Schematic view of micropile group configurations with different inclination angles (*i*)

Figure 4-44 shows the dynamic displacement contours at the location of the micropile cap for machine foundations supported by vertical micropiles and micropiles with various inclination angles i = 10, 20, 25, and 30 degrees at resonance. The displacement contours at the location of the micropile head show that the micropiles in the group with the inclination angle of 25 degrees experience the least dynamic displacements than those in the vertical and other inclined groups of micropiles.

The variations of the dynamic displacements along the center micropile profile are compared for various inclination angles and illustrated in Figure 4-45. In addition, dynamic acceleration spectra at micropile cap locations for various inclination angles are illustrated in Figure 4-46. Based on the results, it can be observed that the dynamic displacements along the micropile profile and spectral accelerations reduce as the inclination angle increases.

At the resonant frequency, the dynamic displacement for the group of vertical micropiles is around 3.2 times greater than that of inclined micropiles at 25 degrees. The reduction in dynamic displacement observed with increasing inclination angle can be attributed to a higher natural frequency and increased stiffness of the soil-micropile system, which improves the load transfer mechanism. This increased stiffness could be due to the larger wedge-shaped mass of soil that

interacts with the micropile as the inclination angle rises, leading to a greater volume of soil and improved soil-micropile interaction. This increases the stiffness of the soil-micropile system and, as a result, higher natural frequency.

Additionally, as can be observed in the figure, the increase in the inclination angle of the micropile is accompanied by a reduction in the dynamic displacements until the micropile inclination angle of 25 degrees. After that, it was observed that the dynamic displacements slightly rose in the micropile group with inclination angles exceeding 25 degrees. The reduction in displacements can be attributed to a decrease in the system's stiffness, resulting in the load transfer mechanism becoming less effective. After an inclination angle of 25 degrees, the system's stiffness did not improve, which resulted in no significant changes in the displacements. Similar observations are noted for the reduced scale shaking table tests by Panah et al. (2018), where inclining micropiles significantly reduced the accelerations in the micropile cap, but inclining at steeper angles did not reduce the accelerations or improve responses.

Figure 4-47 illustrates the dynamic displacement amplitude as a function of frequency (Hz) for various micropile inclination angles. Increasing the inclination angle of micropiles was found to be effective in reducing dynamic displacements within the resonance region, i.e., frequencies less than 22 Hz. After the resonance region, the dynamic displacement of the micropile in the micropile group with various inclination angles (i.e., 10, 20, 25, and 30) exhibited relatively small differences indicating that the inclination angle may not have a significant effect on the dynamic response of the micropile group beyond the resonance region.

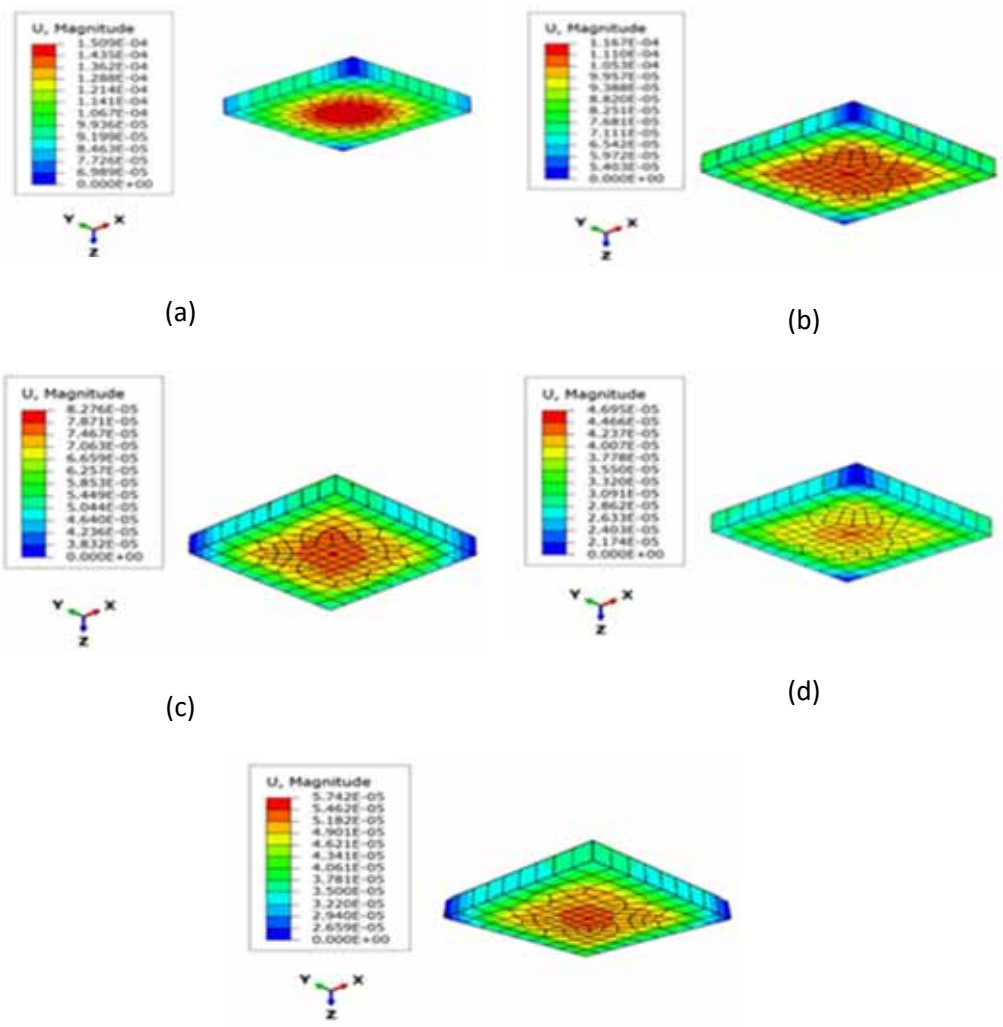

Figure 4-44: Dynamic Displacement Contours at the location of Micropile Cap for Machine Foundations with different inclination angles a) Vertical, b) i=10, c) i=20, d) i=25, e) i=30

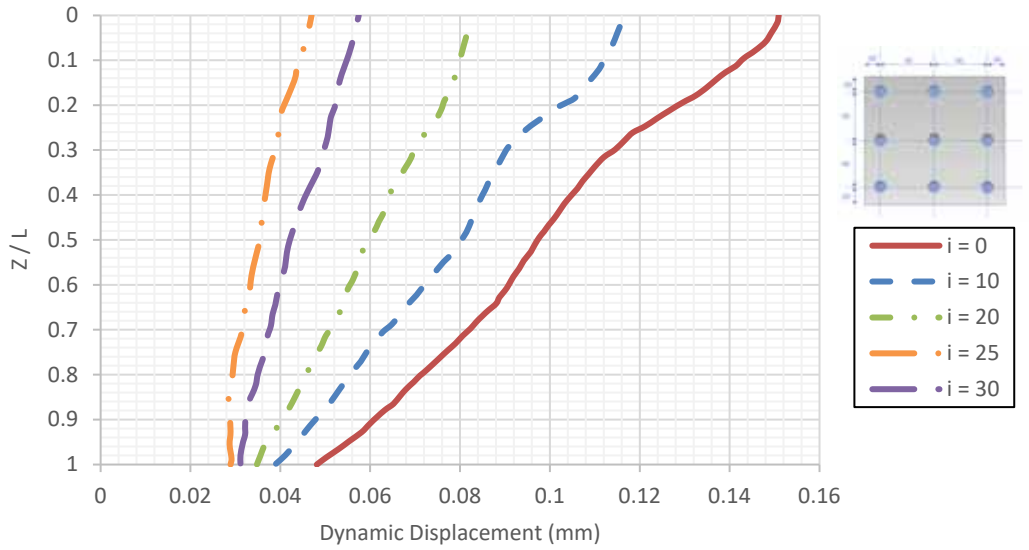

Figure 4-45: Dynamic Displacements along the Micropile Profile in the Micropile Group for different Micropile Inclination Angles (*i*) at Resonance - (Center Micropile)

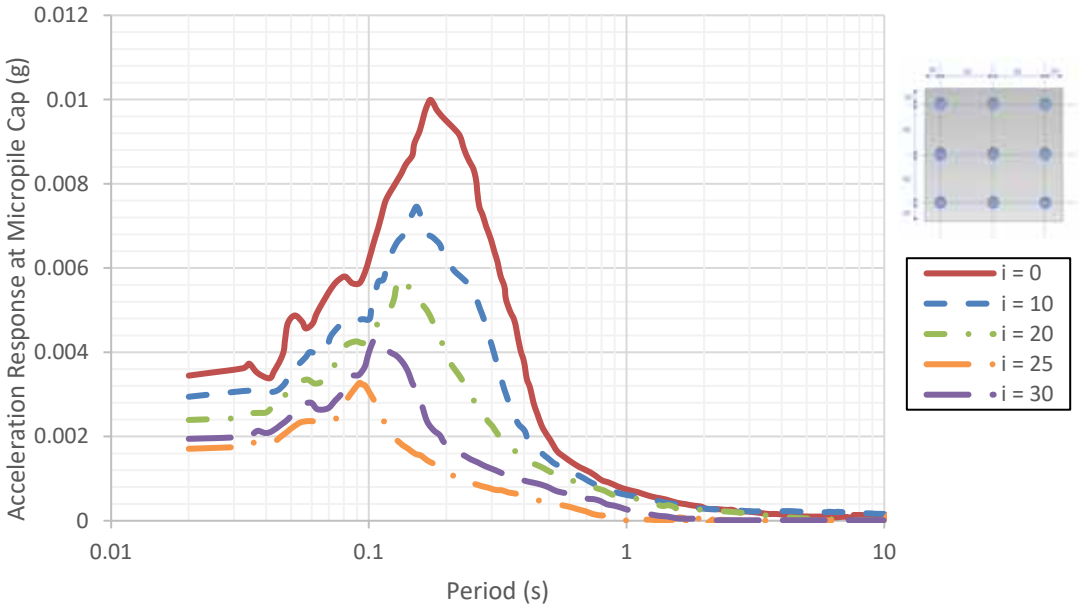

Figure 4-46: Dynamic Acceleration Spectra at Micropile Cap for different Micropile Inclination Angles (*i*)

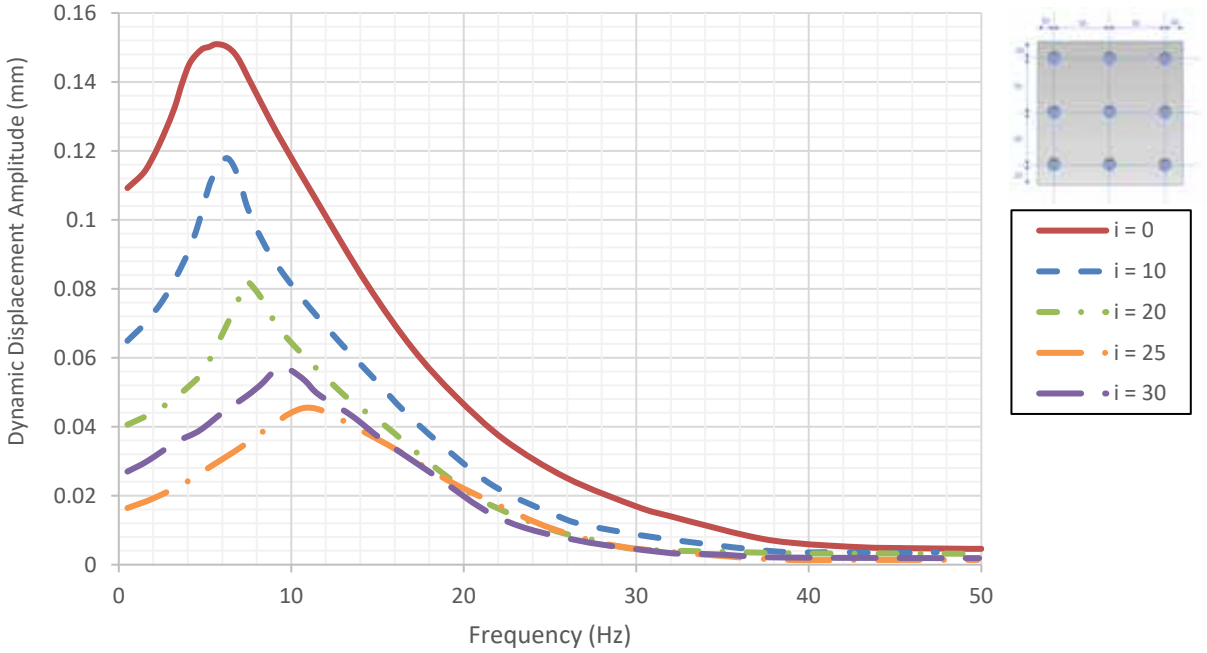

Figure 4-47: Comparison of Dynamic Displacement Amplitude Response for different Micropile Inclination Angles (*i*) - (Center Micropile)

The values of axial forces for various inclination angles are derived and shown in Figure 4-48. As it can be noticed from this figure, it is evident that an increase in the inclination angle (*i*) results in less axial forces to mobilize along the micropiles. The axial force at the resonance at the head of the micropile reduces by approximately 26, 31, 43, and 39 percent when the micropile inclination angle is increased from vertical to 10, 20, 25, and 30 degrees, respectively.

Figure 4-49 illustrates the axial force response curve for various inclination angle configurations. As can be observed from this figure, as the inclination angle increases, the resonant frequency shifts towards higher frequencies, and the axial force amplitudes reduce. This can be attributed to the fact that increasing the micropiles inclination angle results in higher soil-micropile system stiffness, thus furthering the system's natural frequency. In addition, it can be noticed that for frequencies beyond the resonance region (22 *Hz*), the axial force changes in the inclined micropile

group are insignificant. This means that if the machine operates at frequencies beyond the resonance region, the changes in axial force in the micropile become insignificant. Therefore, it can be concluded that the inclination angle of the micropiles is less effective on the further axial force mobilization at frequencies beyond the resonance region. However, for frequencies within the resonance region, the axial force amplitude at the micropile decreases as the inclination angle of the micropile increases. For the group of micropiles inclined at 25 degrees, it was less than 43 percent of the axial forces of the vertical group of micropiles, which is a major reduction in the forces. Therefore, it is best to conduct a frequency response analysis for the micropile group to understand the resonance response of the system. The analysis can provide a more detailed insight into the dynamic response of the system and shed light in making decisions about whether it is beneficial to install micropile at an angle.

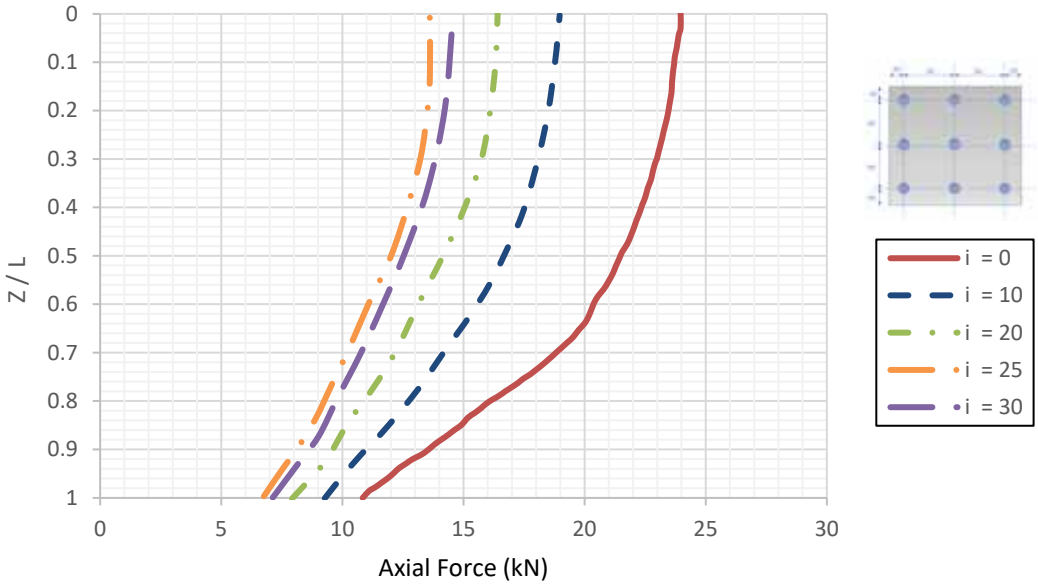

Figure 4-48: Comparison of Axial Force Envelope for different Micropile Inclination Angles (*i*) at Resonance

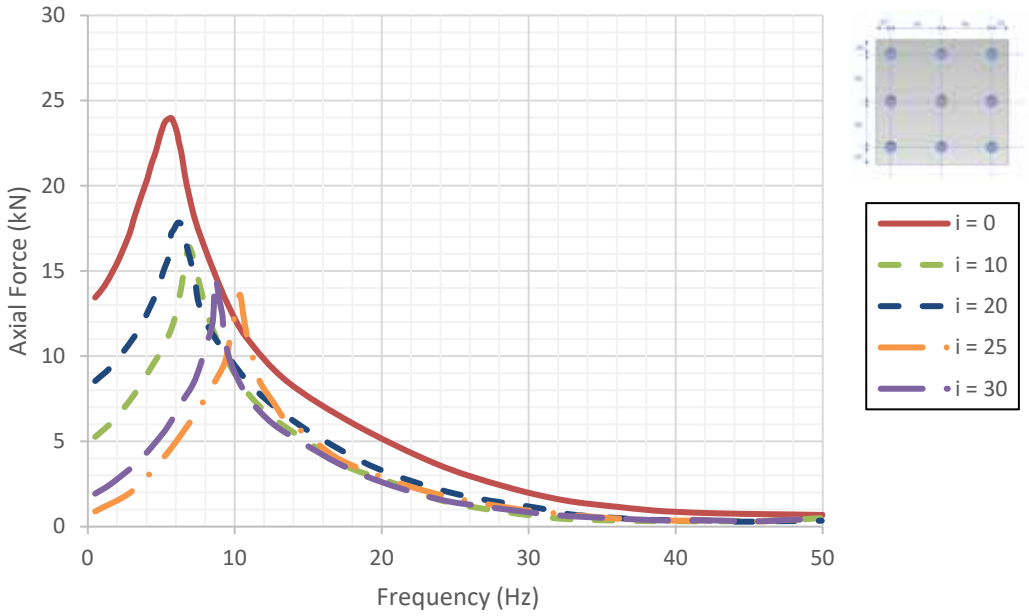

Figure 4-49: Comparison of Axial Force Amplitude for different Micropile Inclination Angles (*i*)

4.4.6 Effect of Micropile Spacing to Micropile Diameter ratio (*s/D*) on the Response of Micropile Groups subject to Vertical Dynamic Load of Machine Foundations

The spacing ratio between micropiles in a group can significantly affect the load-sharing and distribution characteristics of the group. It is therefore important to investigate how varying the spacing ratio can impact the performance of the micropile group under dynamic loading conditions. In this section, the effect of spacing ratio on the response of the micropile group is studied and discussed in detail. To examine the effect of the spacing to micropile diameter ratio on the dynamic response of the micropiles, three (3) groups of 3 × 3 micropiles with varying spacing ratios have been modeled in the FEM software. Specifically, three micropile spacing to diameter ratio (*s/D*) of 3, 5, and 7 were studied. Figure 4-50 illustrates the various micropile group configurations with different spacing ratios.

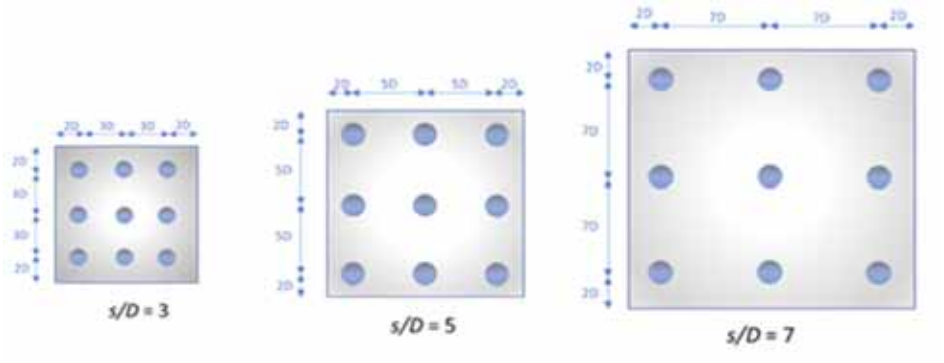

Figure 4-50: : Micropile Group with different Spacing ratios (*s/D*) configurations

Figure 4-51 shows the dynamic displacement contours at the location of the micropile cap for machine foundations with different spacing ratios of *s/D* = 3, 5, and 7 at resonance. The soil is further assumed to have medium stiffness conditions (i.e., R = 0.002). The displacement contours at the location of the micropile cap show that the micropiles in the group with spacing ratio *s/D* = 3 experience larger vertical displacements than those in the other two groups with *s/D* = 5 and *s/D* = 7. This can be attributed to the fact that micropiles with a lower spacing ratio (*s/D* = 3) are closely positioned and, thus, experience more interaction effects, leading to larger displacements. On the other hand, the micropiles in the group with *s/D* = 7 experience the least amount of dynamic displacements, as they are more widely spaced and, therefore, experience less interaction effects. The dynamic response of the micropiles is susceptible to spacing ratio changes with the greater response for closely-spaced micropiles as compared to widely-spaced micropiles, which could be due to the fact that closely-spaced micropiles experience more interaction effects due to the overlapping zones of influence between micropiles. The close presence of grout bond zones can also reduce the relative stiffness of the soil medium between the micropiles compared to the grout itself and can lead to localized zones of reduced stiffness within the soil. On the other hand, widely spaced micropiles experience less interaction and have more isolated zones of influence between

each micropile. This can result in stronger soil surrounding the micropiles, offering more resistance to large deformations and, therefore, a lower amplitude of dynamic displacement. The variations of the dynamic displacements along the center micropile profile at resonance are derived from the FEM analyses and illustrated in Figure 4-52. In addition, dynamic acceleration spectra at micropile cap for various spacing ratios are illustrated in Figure 4-53. Based on these results, it can be observed that the dynamic displacements along the micropile profile reduce as the spacing ratio increases. At the resonant frequency, the dynamic displacement for the spacing ratio of 3 is around 2.5 times larger than that of the spacing ratio of 7. The reduction in the dynamic displacements with increasing spacing ratio can be attributed to the higher natural frequency and increased stiffness of the soil-micropile system. The higher stiffness can be justified by the greater volume of soil surrounding the micropiles as the spacing increases, resulting in improved load sharing between the micropiles and less deformation along micropiles. Ossama (2015) studied behavior of end bearing piles supporting vibration loads and concluded that the effect of the load sharing was reduced when the piles were closely spaced and the interference of the soil shear stress field around the pile reduced of the soil pile system stiffness.

Figure 4-54 illustrates the dynamic displacement amplitude as a function of frequency (*Hz*) for different spacing ratios. The trend in this figure suggests that the effect of spacing ratio on the dynamic vertical displacement amplitude of micropiles is significant only within the resonance region. However, beyond the resonance region, the dynamic displacements tend to converge to nearly similar values. For frequencies after 20 *Hz*, the difference in the dynamic displacements is less than 20 percent, while within the resonance region, the difference in displacements exceeds 50 percent. This response can be attributed to the fact that at higher frequencies, the dynamic

response of the soil-micropile system is predominantly governed by the stiffness and damping properties of the soil rather than the micropile group itself.

Therefore, the influence of micropile spacing, which primarily affects the interaction between adjacent micropiles and hence the soil behavior, becomes less significant as the frequency is higher. These findings highlight that the resonance region is a critical consideration in designing micropiles to mitigate excessive dynamic displacement amplitudes. Therefore, it is best to pick a spacing ratio with consideration to the frequency range of interest that avoids resonance and the corresponding excessive displacement amplitudes.

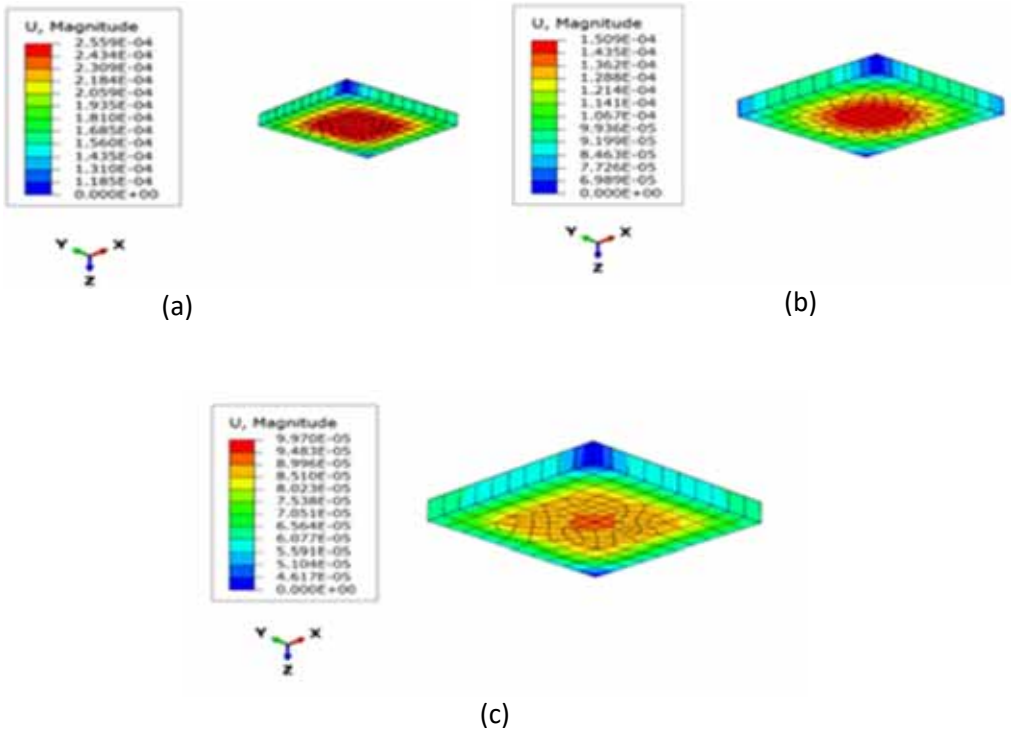

Figure 4-51: Dynamic Displacement Contours at the location of Micropile Cap for Machine Foundations with different Spacing Ratios of a) *s/D* = 3, b) *s/D* = 5, c) *s/D* = 7

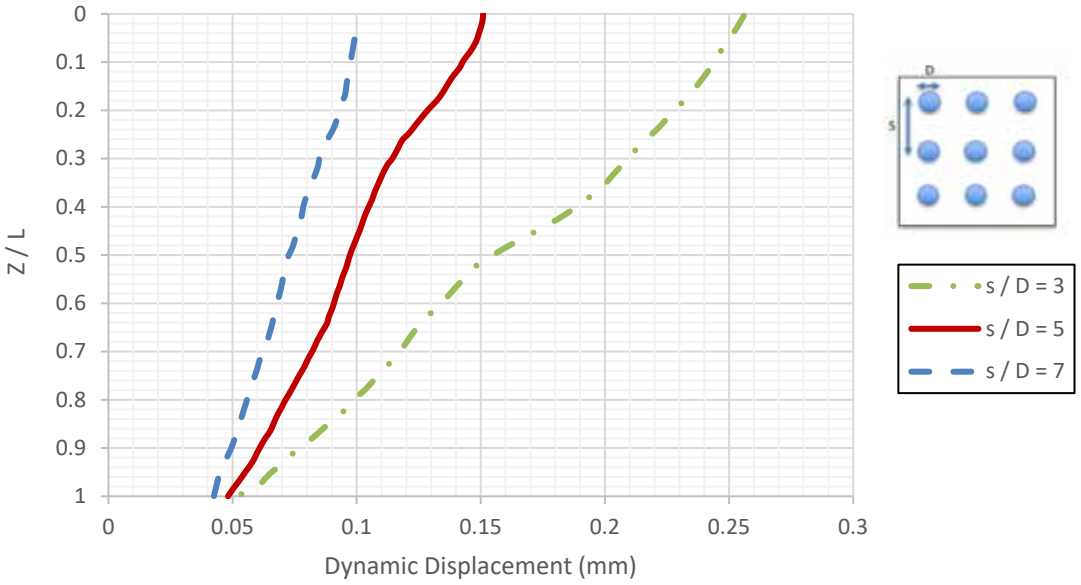

Figure 4-52: Dynamic Displacements along the Micropile Profile in the Micropile Group with different Spacing Ratios (*s/D*) at Resonance - (Center Micropile)

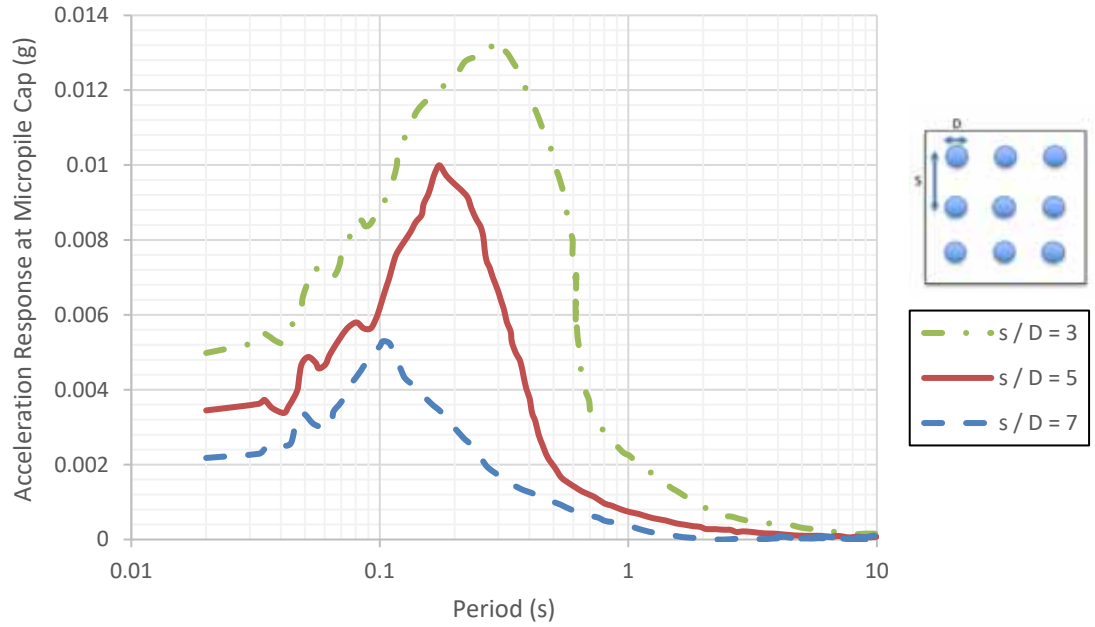

Figure 4-53: Dynamic Acceleration Spectra at Micropile Cap for different Spacing Ratios (*s/D*)

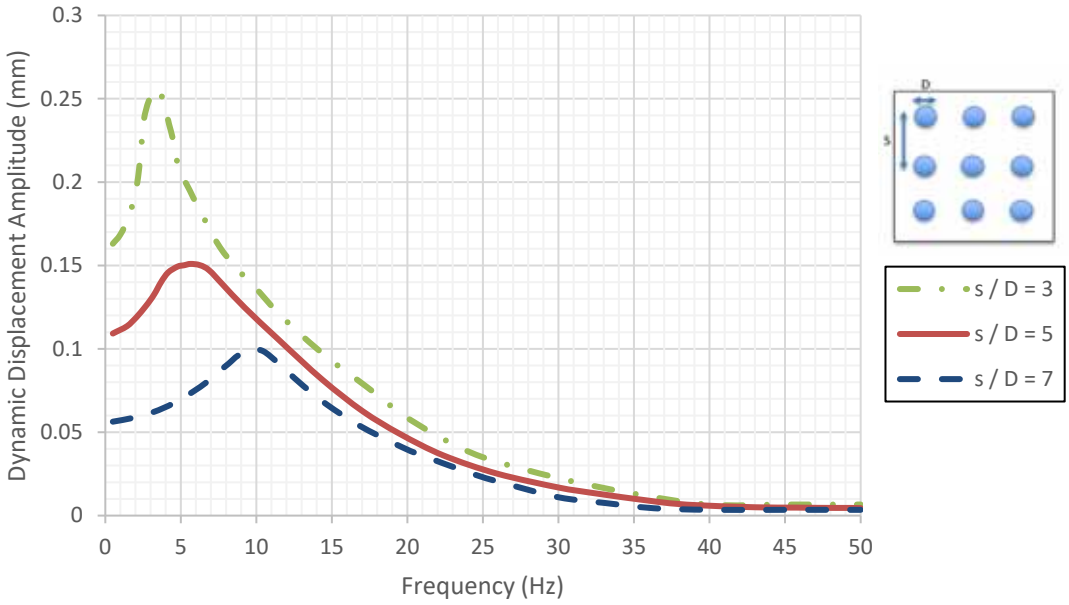

Figure 4-54: Comparison of Dynamic Displacement Amplitude Response for different Spacing Ratios (*s/D*) - (Center Micropile)

The values of axial force for various spacings are derived and shown in Figure 4-55. As it can be noticed, it is evident that an increase in the micropiles spacing ratio (*s/D*) leads to a reduction in the axial forces along the micropiles. The axial force at the resonance at the head of the micropile reduces by approximately 17 percent and 34 percent when the spacing ratio is increased from 3 to 5 and 7, respectively. The reason for this reduction could be that as the spacing ratio increases, the adjacent soil surrounding micropiles provides more contribution to the stresses within the soil. Therefore, the less frictional stresses on the surface of the micropiles are mobilized, and as a result, the axial forces in the micropiles reduce. Another possible explanation for this could be due to the occurrence of gapping between soil and micropile elements as spacings rise, which can cause the micropile load-carrying capacity to reduce. As the spacing increases, the confining effect of micropiles on the surrounding soil reduces, which subsequently results in more deformation within

the soil mass and can cause loss of contact, sliding, and separation to occur between soil and micropile elements. Therefore, it is generally expected that more gapping will occur between the soil and micropiles as the spacing ratio increases. Figure 4-56 illustrates the axial force response curve for various spacing ratios. This graph shows that as the spacing ratio increases, the resonant frequency shifts towards higher frequencies, and the axial force amplitude reduces. This is due to the fact that increasing the spacing ratio increases the stiffness of the soil-micropile system, thus furthering the natural frequency of the system. In addition, it can be concluded that for frequencies beyond the resonance region (20 *Hz*), the changes in the axial forces in the micropiles are insignificant.

The results of the study also indicate that the micropiles contribute significantly to the load-carrying capacity of the machine foundation, particularly at the resonant frequency. As the spacing ratio reduces, the micropiles in the system contribute more force, but the contribution becomes less significant as the spacing ratio increases. It was observed that at the spacing ratio of $s/D = 3$, the total force contribution by micropiles was derived at 259 *kN*, i.e., 260 percent of the amplitude of the applied dynamic load. In contrast, for the group with $s/D = 5$, it was 210 *kN*, i.e., 210 percent of the amplitude of the applied dynamic load, and for the group with $s/D = 7$, it was 168 *kN*, i.e., 168 percent of the amplitude of the applied dynamic load. As the spacing ratio increased from $s/D = 3$ to 5 and 7, the micropile group contribution reduced by 19 and 35 percent, respectively. These results suggest that reducing the spacing ratio between micropiles leads to the micropiles being more effective in the load-carrying capacity of the system. Table 4-5 summarizes the variations of total forces in the group of micropiles for different spacing ratios (s/D).

Table 4-5: Variation of Total Forces in the Group of Micropiles for Different Spacing Ratios (*s/D*)			
Spacing Ratio (*s/D*)	3	5	7
Total Force in the Group of Micropiles	259 *kN*	210 *kN*	168 *kN*
Percentage of the applied load	260%	210%	168%

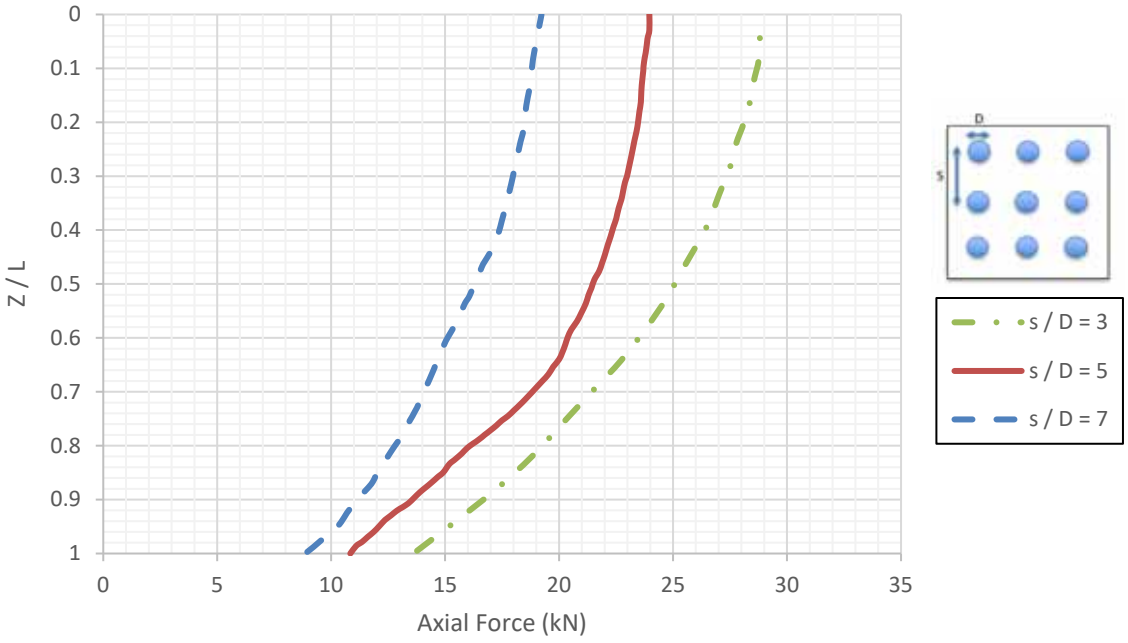

Figure 4-55: Comparison of Axial Force Envelope for different Spacing Ratios (*s/D*) at Resonance

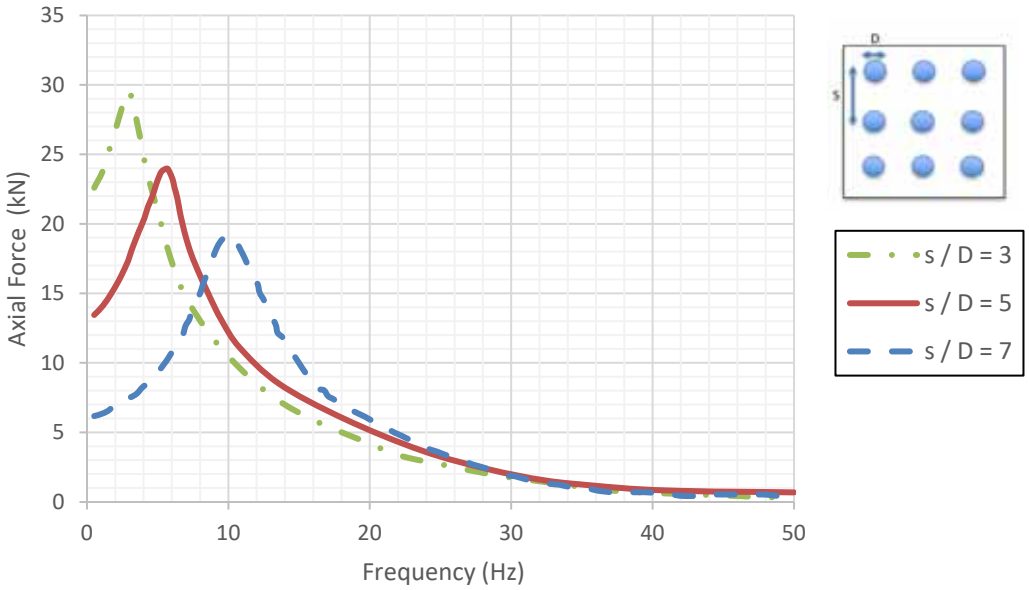

Figure 4-56: Comparison of Axial Force Amplitude Response for different Spacing Ratios (*s/D*)

4.4.7 Effect of Micropile Positioning in the Group on the Response of Micropile Groups subject to Vertical Dynamic Load of Machine Foundations

Micropile foundations are often used to support structures in areas where traditional shallow foundations are not suitable due to soil conditions or space limitations, and they are typically installed in large numbers and different arrangements within the group. Positioning of micropiles in a group can significantly affect their response to different loading conditions. In a micropile group, micropiles are installed in a reasonably close proximity to each other to distribute the load of the superstructure to the ground. In this section, the effect of micropile position in the group and its influence on the overall performance of micropile groups is further examined. The position of the each micropile in the group can impact the load-carrying capacity and stiffness of the soil-micropile system. As discussed in previous chapters, several studies have been conducted to examine the effect of micropile position in the group, including the distance between micropiles

and their arrangement within the group (Shahrour et al., 2001). By understanding the impact of micropile position on the performance of the foundation system, engineers can optimize the design and positioning of micropile groups to achieve the desired performance and ensure the stability of the soil-micropile system. The observation from this study indicates that center micropile experience more displacement than edge and corner micropiles at the micropile head but the displacements along the micropile profiles for all micropiles positions are almost similar and fall within less than approximately 20 percent of each other. This could be due to micropiles group rigid connection to the cap that causes the displacement to be evenly distributed. Figure 4-57 displays the dynamic displacement distributions along the micropile profile for different micropile positions within the group. Additionally, Figure 4-58 illustrates the dynamic displacement amplitude as a function of frequency (*Hz*) for corner, edge and center micropiles in the group.

It is further observed that that most of the axial forces are distributed in the corner micropiles while the center and edge micropile provide slightly less contribution in the mobilized forces, as it is evident in Figure 4-59. Per these results, the axial forces mobilized in the center and edge micropile are about 91 and 96 percent of the forces assumed by corner micropiles. This can be attributed to the effect of load-distribution and better contribution of stress between the surrounding soil and micropile for the edge and center micropiles. The axial force response curves for different micropile positions within the group are presented in Figure 4-60. It can be observed that the corner micropiles exhibit the highest response, while the center micropiles show the slightly lower amplitude of response.

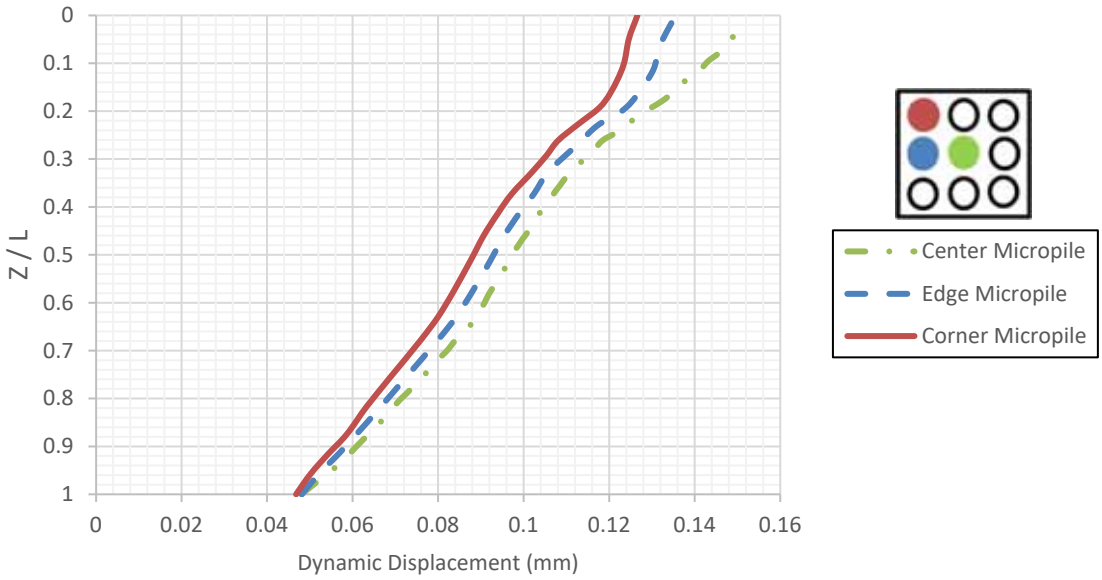

Figure 4-57: Dynamic Displacements along the Micropile Profile in the Micropile Group for Corner, Edge, and Center Micropiles at Resonance

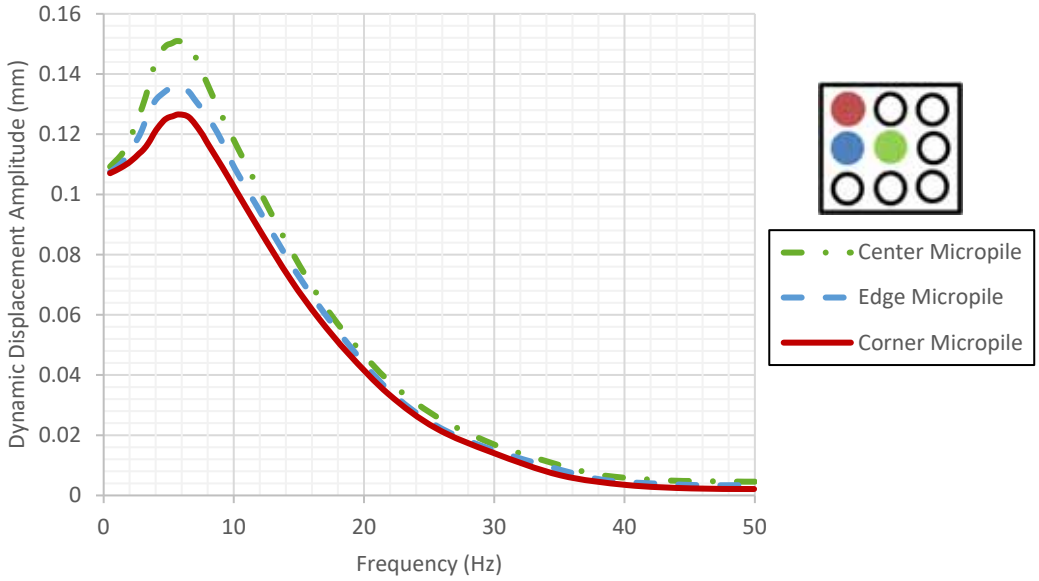

Figure 4-58: Comparison of Dynamic Displacement Amplitude Response for Corner, Edge, and Center Micropiles

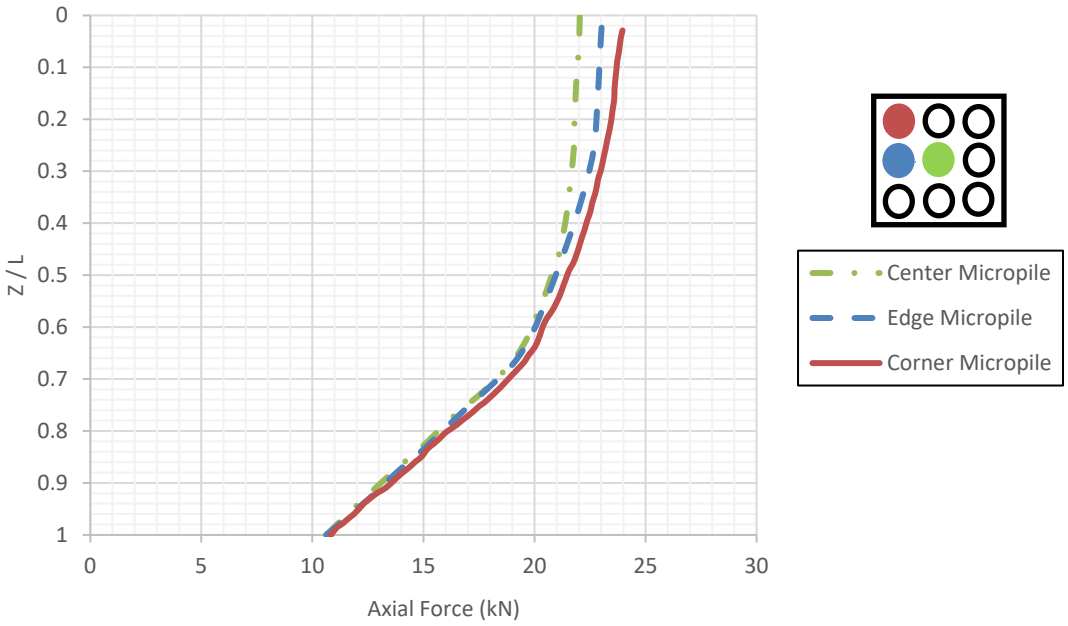

Figure 4-59: Comparison of Axial Force Envelope for Corner, Edge, and Center Micropiles at Resonance

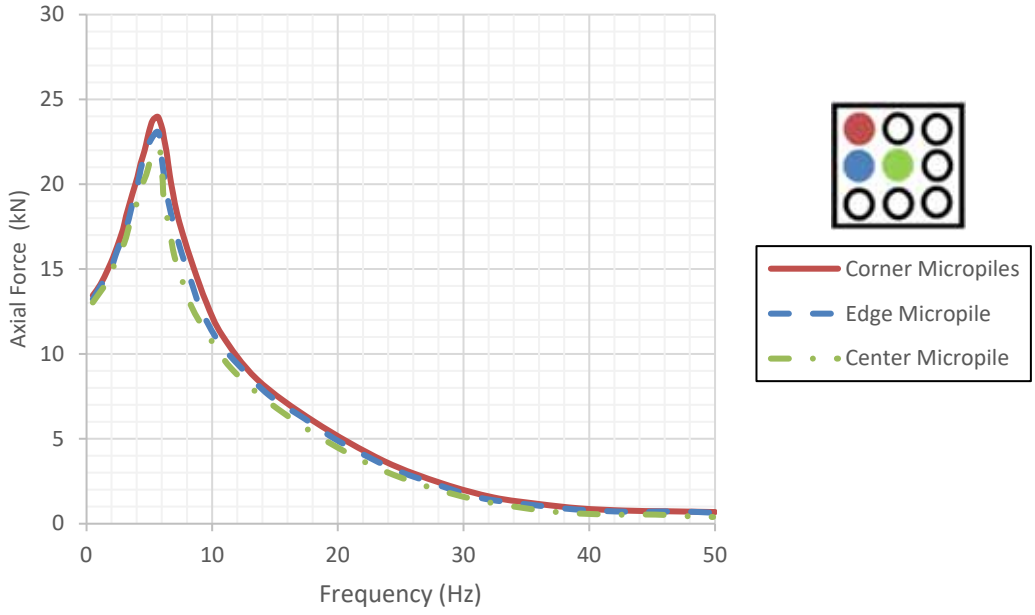

Figure 4-60: Comparison of Axial Force Amplitude Response for Corner, Edge, and Center Micropiles

4.4.8 Design Procedure of Micropile Groups supporting Machine Foundations

The design procedure for a micropile group supporting machine foundation system is a complex process that involves a number of factors, including the dynamic characteristics of the machine, the soil conditions, and the desired response. Below is a summarized overview of the design procedure:

- Analysis/Evaluation: The first step is to conduct a thorough analysis of the dynamic response of the machine and the soil-micropile system to identify the natural frequency of the system with respect to the specific frequency range of interest. This analysis helps determine the expected dominant frequencies and potential resonance regions.
- Design Optimization: Once the dominant frequencies have been identified, the design parameters of the micropile group can be adjusted to achieve the desired response and allowed vibrations. The parameters that are key during the design optimization step are; the number of micropiles, the spacing between micropiles, the inclination angle of the micropiles (if possible and desirable), the stiffness of the micropiles. The goal of the design optimization is to shift the machine operating frequencies away from the dominant frequencies, minimize vibrations, and maintain stability of the machine while running within the frequency range of interest.
- Sensitivity Analysis: Once the design parameters have been optimized, a sensitivity analysis can be done to assess the response of the micropile group to variations in design parameters and soil properties. This can help to identify critical parameters and provides insights into the potential response of the system within different frequency ranges while also ensuring a cost-effective design.
- Mitigation Measures: If the sensitivity analysis identifies any critical parameters or potential areas of concern, proper mitigation measures can be taken into the design. For instance, if the

micropile group falls within the resonance region, measures such as adding damping elements, adjusting stiffness, or altering the mass distribution can help mitigate the amplification effects.

Chapter 5 - Summary, Conclusions and Recommendations

5.1. Introduction

This research aimed to investigate the dynamic response of a group of micropiles under dynamic harmonic loads of a machine foundation, considering the nonlinear soil stress-strain behavior and nonlinear soil-structure interaction (SSI). The soil usually behaves nonlinearly and sustains plastic deformations while undergoing dynamic loads due to the complex interaction between the soil particles, and this can have significant implications on the response of the micropile groups. Therefore, taking into account the nonlinear stress-strain behavior of soil is crucial for designing the micropile system to ensure the safe and efficient operation of a machine foundation. This study uses a nonlinear soil model to conduct a series of parametric studies on a group of micro piles subjected to vertical dynamic loading from a machine foundation. The effects of various parameters, including micropile inclination angle (i), machine foundation mass (m), machine operating frequency (f), micropile spacing (s/D), soil shear modulus/micropile stiffness ratio (R), the position of micro piles in the group are evaluated. The nonlinear soil model used in this study was a Modified Drucker Prager soil model proposed by Drucker (1952), which is commonly used to simulate the behavior of the soil undergoing dynamic loads and can take into account the complex interaction between the soil elements and the micropiles. The Drucker-Prager soil model is a pressure-dependent plasticity model which captures the effects of strain rate and confining pressure on the soil behavior. The study also conducted verification analyses to ensure the model's accuracy under both static and dynamic conditions with available field and experimental data, and it was found that the 3-D FEM model accurately simulates the nonlinear behavior of soil under dynamic loading conditions.

The parametric study results indicated that the natural frequency plays a key role in the dynamic response of the micropiles, with higher displacements and accelerations observed at frequencies at or close to the natural frequency. Below is a summary of the important findings and conclusions from the study, which aimed to investigate the effects of the parameters mentioned above on the dynamic response of a group of micropiles subjected to vertical dynamic loading from a machine foundation:

5.2. Numerical Modeling Verifications

5.2.1 Static Loading Field Tests – French National project (FOREVER) Full-Scale tests at the experimental site (CEBTP site)

The numerical modeling of the micropile groups inserted in the Fontainebleau sand was performed using the finite element technique, and a 3-D FEM mesh, including a 2 × 2 micropile group, was developed in the FEM software. Micropiles were simulated via the structural BEAM elements incorporated by the software, and the soil was represented by the solid elements. 3-D FEM analyses for the 2 × 2 micropile group were conducted using two (2) different soil constitutive models: linear elastic, Modified Drucker Prager. Various vertical load conditions were applied to the model, and the vertical displacement (settlement) at center micro piles for the three models was derived and compared against the field measurements. Results obtained from the 3-D FEM analyses were all within reasonable agreement with the field measurements; however, nonlinear soil models exhibited closer agreement with the field data. The Modified Drucker Prager with Cap model better captured the nonlinearity of the soil response to higher loads. These models resulted in higher displacements than the Elastic model and were closer to

the field measurements. The discrepancy between the field and 3-D FEM results could be attributed to complicated interaction behavior due to the presence of other adjacent isolated micropile or micropile groups in the CEBTP site at the proximity of the 2 × 2 micropiles that was not modeled in this analysis as well as uncertainties from the field measurements to estimate the soil strength properties.

5.2.2 Dynamic Loading Field Tests (Reduced Scale Shaking Table Experiments at Hong Kong Polytechnique University)

A series of dynamic analyses were performed to verify the accuracy of numerical modeling of micropile groups subject to vertical dynamic load using the data from the Hong Kong Polytechnique University shaking table tests. Panah et al. (2018) built a small-scale model of micropile groups, and a number of 1-g shaking table tests were performed to provide insight into how these groups behave under dynamic excitations. The soil and micropile element specifications were chosen based on similitude requirements and scaling laws. Four (4) numerical models were developed using 3-D FEM software to simulate the behavior of micropile groups in these shaking table tests. The 3-D FEM analyses revealed that the nonlinear Modified Drucker Prager model provided more consistent and accurate results for both the vertical and inclined micropiles, and it marginally underestimated the resonant frequency and spectral acceleration. The reduction in acceleration was more significant for the linear elastic model than the nonlinear Modified Drucker Prager model for both vertical and inclined micropiles groups.

5.3. Parametric Studies

A series of parametric studies have been conducted to investigate the behavior of a group of micro piles under vertical dynamic loading from machine foundations. The results of parametric studies will provide more insight into the response of soil-micropile systems in different geotechnical engineering applications such as foundation supports. The effect of parameters such as soil nonlinearity, the machine foundation mass (m), the machine operating frequency (f), soil shear modulus/pile stiffness ratio (R), the inclination angle of the micropile (i), the micropile spacing ratio (s/D), micropile positioning on the dynamic response of the micropile groups has been further studied.

5.3.1 Soil Nonlinear Stress-Strain Behavior

The study investigated the behavior of a micropile group under vertical dynamic machine load using linear elastic and nonlinear Modified Drucker Prager with Cap models. The results showed that the nonlinear model predicted higher displacements than the elastic model for all applied loads due to the soil's nonlinear plastic behavior during dynamic loading. As the magnitude of the applied load increased, the peak dynamic displacement and spectral acceleration also increased for both linear and nonlinear models, with a higher rate of increase for the nonlinear model.

It was observed that at machine loads below 50 *kN*, the soil's response was nearly pseudo-elastic, but beyond that, the soil surpassed its yield strength, resulting in hysteresis behavior, causing significant plastic deformations and larger displacements. Dynamic displacement and spectral

accelerations at the micropile head increased with the amplitude of the load, with a greater rate of change in accelerations at higher amplitudes for the nonlinear soil model. Dynamic Displacements along the micropile profile were more significant for the nonlinear soil model due to the nonlinear stress-strain relationship between soil particles compounded by nonlinear SSI behavior between soil-micropile interface elements. Nonlinear soil stress-strain behavior significantly affected the micropile axial forces at resonance, especially at amplitudes beyond the 50 *kN* limit. The Modified Drucker-Prager model captured the nonlinear behavior of the soil more accurately than linear models, implying that using a nonlinear model for the soil in analyzing the dynamic response of micropile groups can provide more accurate predictions of the system response.

5.3.2 Machine Operating Frequency (*f*)

The dynamic response of the micropile groups was investigated for a range of operating frequencies of the machine foundation. The results show that the dynamic displacement and acceleration magnitudes subside significantly as the operating frequency deviates from the system's natural frequency, which was found to be 5.8 *Hz*. The axial force profile in micro piles for a range of machine foundation operating frequencies indicates that at frequencies beyond the resonance region, the axial forces developed along micro piles are almost more than 60 percent less than axial forces near or at resonance. At the resonance, the natural frequency of the micropile coincides with the frequency of the applied load, resulting in the micropiles absorbing the maximum amount of energy from the machine load vibrations. In contrast, as machine frequency goes beyond the natural frequency of the system, the forces in the micropile gradually reduce, and they become extremely small or negligible as the micropile is not absorbing much of the energy

from the machine vibrations. At high frequencies, the amount of damping required to significantly reduce the amplitude of vibration in the system may be higher, resulting in negligible axial forces along the micropiles.

The micropile group dynamic displacement amplitude response curve is analyzed to determine the resonance region. The natural frequency is typically identified at the peak amplitude, and the resonance region is determined based on the peak width and the amplitudes of surrounding frequencies. The resonance region is a frequency range beyond the natural frequency where displacement amplitudes decrease by 50% or more. The range of the resonance region can vary from 1.2 to 2 times the natural frequency depending on the other system's characteristics. In this study, the resonance region's width was about two times the natural frequency.

5.3.3 Machine Foundation Mass (*m*)

The impact of machine foundation mass on micropile groups' response to dynamic harmonic loading was further studied. Three 3-D FEM models representing machine foundation masses of 250 *kN*, 500 *kN*, and 1000 *kN* were developed and analyzed using 3-D FEM software. The dynamic displacement amplitude and peak spectral acceleration occur at the micropile head/cap connection location for the group supporting the lowest mass of the machine foundation, i.e., 250 *kN*. As the machine foundation mass increases, the resonant frequency of the system shifts towards lower frequencies. Additionally, the stiffness of the system increases with an increase in the mass, but so does the damping of the system, which resists the vibrations of the system and results in wave energy dissipation and a reduction in the natural frequency of the system. It was noted that beyond the resonance region (i.e., frequency of 19 *Hz*), the changes in the mass of the machine foundation

do not have a significant impact on the dynamic displacement amplitudes. As the mass of the machine foundation increases, the axial forces along the micropile profiles decrease; for machine foundations weighed 500 *kN* and 1000 *kN*, the reductions in micropile axial forces were noted at 17 and 37 percent of axial forces in the machines with a mass of 250 *kN* respectively. The higher the mass of the machine foundation, the less the system is susceptible to vibrations, and fewer displacements and forces are mobilized along the micro piles.

In summary, increasing the mass of the machine foundation can lead to a decrease in the resonant frequency of the system, as well as a decrease in the dynamic displacement and forces along the micropiles, which is beneficial for the stability and safety of the entire system, especially if the machine is expected to operate at low frequencies.

5.3.4 Soil Shear Modulus/Micropile Stiffness Ratio (*R*)

The study investigated the effect of soil shear modulus/micropile stiffness ratios on the dynamic response of micropiles under machine foundation loading. The results showed that as the ratio increased, the dynamic displacements and spectral accelerations at the micropile head decreased. The displacement was highest at the head of the micropile where the machine load was applied, and it gradually decreased towards the tip of the micropile.

The results showed that increasing the stiffness of the soil-micropile system relative to the applied load can lead to a reduction in dynamic displacement. However, the effect of stiffness ratio on displacement was found to be more pronounced for higher machine load amplitudes. For instance, at a load amplitude of 100 *kN*, the dynamic displacement decreased from about 0.24 mm to 0.11 mm as the stiffness ratio increased from 0.0002 to 0.02, a reduction of about 56 percent.

However, at a lower amplitude of 25 *kN*, the dynamic displacement decreased from about 0.011 mm to 0.007 mm, a reduction of about 33 percent. This means that when the machine amplitude is higher, increasing the soil shear modulus with respect to the micropile stiffness is a more effective factor in reducing the machine's dynamic displacements and preventing damage or failure.

As the ratio increased from R = 0.0002 to R = 0.002, the axial force at the micropile head decreased by approximately 19 percent, and similarly, as the ratio increased from R = 0.0002 to R = 0.02, the displacement at the micropile head reduced by approximately 43 percent. When the soil is relatively stronger compared to the micropiles, the micropiles will deflect less and hence experience lower axial forces. This is due to the stiff soil mass around the micro piles contributing more effectively to resist the stresses induced by the dynamic load compared to less medium stiff or soft soil conditions.

Also, the resonant frequency shifted towards higher frequencies as the soil shear modulus/micropile stiffness ratio increased. These results highlight the importance of soil shear modulus with respect to micropile stiffness in the design of micropile group foundations to mitigate the risk of any damage or potential failure of the system if the soil conditions are not examined carefully.

5.3.5 Micropile Inclination Angle (*i*)

As discussed thoroughly in Chapter 4, micropiles are mostly inserted at angles; therefore, it is critical to evaluate the impact of inclination angle on the response of the group. This study

analyzed the dynamic displacement of machine foundations supported by vertical micropiles and micropiles with inclination angles of 10, 20, 25, and 30 degrees to the vertical axis at the frequency of resonance. Results showed that micropiles with an inclination angle of 25 degrees experienced the least dynamic displacement at resonance. Increasing the inclination angle of micro piles decreased dynamic displacement along the length of the micro piles due to the increased stiffness of the soil-micropile system, which resulted in an improved load transfer mechanism. However, after a micropile inclination angle of 25 degrees, this improvement is less effective, and displacement slightly rose due to a decrease in the stiffness of the system and a less effective load transfer mechanism. At the resonant frequency, the dynamic displacement for a group of vertical micropiles is around 3.2 times larger than that of a group of inclined micropiles at 25 degrees.

Increasing the inclination angle of micro piles was found to be effective in reducing dynamic displacements and axial forces within the resonance region (frequencies less than 22 *Hz*), and for frequencies higher than this range, it was noted to be less effective. After the resonance region, the dynamic displacement of the micropile in the micropile group with various inclination angles (i.e., 10, 20, 25, and 30) exhibited relatively minor differences.

The axial force values for various inclination angles of micropiles have also been analyzed. The results indicate that an increase in the inclination angle leads to a reduction in axial forces along the micropiles. Specifically at the resonance, the axial force at the micropile head reduces by approximately 26 percent, 31 percent, 43 percent, and 39 percent when the micropile inclination angle increases from vertical to 10, 20, 25, and 30 degrees, respectively. It was also noted that the resonant frequency shifts towards higher frequencies, and the axial force amplitude decreases with a rising micropile inclination angle. For frequencies beyond the resonance region (i.e., frequencies greater than 22 *Hz*), the changes in axial force for the group of inclined micropiles are insignificant.

However, for frequencies within the resonance region, the axial force in the micropile decreases substantially as the inclination angle of the micropile rises due to the higher stiffness of the soil-micropile system. For the group of micropiles inclined at 25 degrees, these forces were less than 43 percent of the axial forces of the vertical group of micropiles, which is a major contribution from the inclination angle and reduction in the forces. Therefore, it is best to conduct a frequency response analysis that can provide detailed insights into the dynamic response of the vertical and inclined micropile group and help in deciding whether it would be beneficial to install micropiles at an angle.

5.3.6 Micropile Spacing to Micropile Diameter ratio (*s/D*)

The micropile spacing ratio was also investigated as part of parametric studies. Three spacing ratios of *s/D* = 3, 5, and 7 assuming medium stiffness conditions (i.e., R = 0.002), were studied to understand this effect. The results showed that the micropiles in the group with a spacing ratio of 3 experienced larger dynamic displacements than those in the other two groups with *s/D* = 5 and *s/D* = 7. The spectral acceleration at the micropile cap also showed a higher amplitude of response for *s/D* = 3 and a lower value for *s/D* = 7. The variations of the dynamic displacement along the profile of the center micropile at resonance were also derived from the numerical analyses, and it was observed that the dynamic displacements reduce as the spacing ratio increases. At the resonant frequency, the dynamic displacement for a spacing ratio of 3 was around 2.5 times larger than that for a spacing ratio of 7. This reduction in the dynamic displacement with increasing spacing ratio can be attributed to the higher natural frequency and increased stiffness of the soil-micropile system. Closely-spaced micropiles experience more interaction effects due to the

overlapping zones of influence, which can lead to a reduction in the stiffness and strength of the soil medium in between the micropiles. As a result, the soil between closely-spaced micropiles may become weaker and less resistant to deformations due to this weakened zone. Widely-spaced micropiles, however, have less interaction and more isolated zones of influence, which can result in a stronger soil condition surrounding the micropiles and provide more resistance to deformations and hence yield a lower dynamic response.

The results also showed that increasing the spacing ratio led to a reduction in axial forces along the micropiles due to less mobilization of frictional stresses on the surface of the micropiles. As the spacing ratio increased from s/D = 3 to 5 and 7, the total micropile contribution reduced by 19 and 35 percent, respectively. These results indicate that reducing the spacing ratio between micropiles in the group leads to the micropiles being more efficient in the load-carrying capacity of the system.

Additionally, micropiles at closer spacings contributed significantly to the load-carrying capacity of the foundation, particularly at the resonant frequency. It was noticed that at the spacing ratio of s/D = 3, the total force contribution by micro piles was at 259 *kN*, i.e., 260 percent of amplitude of the applied dynamic load, whereas for the group with s/D = 5, it was 210 *kN*, i.e., 210 percent of the amplitude of the applied load, and for the group with s/D = 7, it was 168 *kN*, i.e., 168 percent of the amplitude of the applied load. The resonant frequency shifted towards higher frequencies, and the axial force amplitude reduced as the spacing ratio increased. For frequencies beyond the resonance region (20 *Hz*), the changes in axial force in the micropile were noted to be insignificant.

The resonance region is a key consideration in the design of micropiles and their spacings to mitigate excessive dynamic displacements, and it is best to select the spacing ratio based on the

frequency of the operation to avoid resonance and the corresponding excessive displacement amplitudes.

5.3.7 Micropile Positioning in the Group

The center micropile experiences more displacement than the edge and corner micro piles at the micropile head. However, the displacements along the micropile profiles for all cases are almost similar and fall within less than approximately 20 percent of each other. This could be due to the micropile group's rigid connection to the cap, which causes the displacement to be evenly distributed. It was also observed that most of the axial forces are distributed in the corner micropiles while the center and edge micropile provide slightly less contribution in the mobilized forces. The axial forces mobilized in the center and edge micropile is about 91 and 96 percent of the forces assumed by corner micropiles. This is due to high load contribution and better stress redistribution between the surrounding soil and the micropile element for the case of edge and center micro piles.

5.4. Summary

Below is the summary of the important conclusions of this research:

- Natural frequency plays a critical role in the dynamic response of micropile systems; it influences all the parameters studied in the research. Higher displacements and spectral accelerations were observed at or near frequencies close to the natural frequency of the system. The resonance region is crucial in determining the extent of responses, the

dynamic displacements, and axial forces along the micropiles in the group, with a significant decrease occurring at frequencies beyond this region. Thus, understanding the resonance behavior of the micropile-supported machine foundation system is crucial in predicting the system response and designing effective measures to mitigate any potential adverse effects.

- Nonlinear soil models predicted higher displacements and axial forces than linear elastic soil models. Thus, using a nonlinear soil model, in general, will provide more accurate predictions of the soil-micropile system response.
- Under dynamic loading, increasing the mass of the machine foundation leads to the reduction of resonant frequency, hence a reduction in the micropile axial forces.
- Micropile dynamic displacement and acceleration responses decrease with increasing the ratio of the soil shear modulus to the micropile stiffness.
- Inclined Micropiles produce less axial forces in comparison to vertical micropiles. This reduction is a function of the system stiffness and the natural frequency of the system.
- Increasing the ratio of the micropile spacing results in a reduction in the axial forces in the micropile.
- Corner micropile carries most of the force within the group of micro piles, while center and edge micropile carry slightly less force but experience higher displacements.

5.5. Future Work Recommendations

While this study has provided insights into the dynamic response of micropiles under harmonic loads from a machine foundation, there are still opportunities to be pursued for future research in

this field. Based on the findings of this study, the following recommendations can be made for further investigation and improvement of micropile design and performance under dynamic loads:

- Investigate the effects of different soil models: While the Modified Drucker Prager soil model used in this study is widely used to simulate soil behavior under dynamic loading, there are many other soil models that could be employed to see how they affect the behavior of micropiles systems under vertical dynamic loading. For instance, models that account for advanced strain-hardening/softening regime, stress-dilatancy, anisotropic conditions, frequency-dependent and stress-dependent damping, might be worth to be incorporated and conduct analyses. In addition, in some soils the hardening behavior is dependent on not only on the stress state but also on the previous deformation history. A model that accounts for this nonlinear kinematic hardening could provide more accurate predictions of soil behavior under cyclic loading.
- Investigate the effect of different loading types: The study only considered vertical loading from a machine foundation, but future work could investigate the effects of combination of vertical, lateral and earthquake load that in real world situations can act simultaneously on micropiles, potentially leading to complex load transfer mechanisms and affecting the performance and behavior of the micropiles.
- Investigate the long-term performance and durability of the soil-micropile systems: While this study focused on the dynamic response of micropiles under dynamic loads from machine foundation, it is also important to consider their long-term performance and durability. Factors such as corrosion, aging, and environmental conditions can all affect the performance of micropile systems over time.

- Investigate the effect of different micropile designs: The study assumed a specific micropile design, but future work could investigate the effects of different micropile configurations in terms of size, shape, number, length, and reinforcement type, and configuration in the group to support machine foundations. This will provide insight into the optimal micropile design for specific soil and loading conditions, and potentially lead to more efficient and cost-effective designs in practice.

Chapter 6 - Appendix

6.1. Soil Dynamics: An Overview

Soil dynamics is an important aspect to consider in the analysis of the dynamic response of micropile groups. The interaction between the micropiles and the soil can significantly influence the behavior of the system under various loading conditions, such as earthquakes or wind-induced vibrations. This interaction involves complex soil-structure interaction phenomena, which require a good understanding of the soil properties and behavior, as well as appropriate modeling techniques. In this appendix, a brief overview of some of the key concepts and methods in soil dynamics that are relevant to the analysis of micropile group response are provided.[4]

6.2. Single Mass System

Figure 6-1 represents a single degree of freedom system which comprises a rigid mass, an elastic spring for support, and a viscous dashpot damper. When the system is subjected to a dynamic force *F* that varies with time *t*, the effect of mass inertia becomes significant, leading to the application of Newton's second law of motion. As a result, a differential equation emerges, providing a means to describe the system's behavior:

$$m\frac{d^2u}{dt^2} = P(t) \qquad \text{Equation 6.1}$$

[4] The concepts presented in this Appendix on soil dynamics and vibration theory were derived from the Soil dynamics course presented by Professor Arnold Verruijt at Delft University and the 'Principles of Geotechnical Engineering' by Braja M Das.

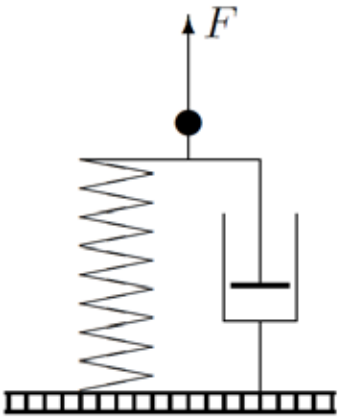

Figure 6-1: Mass supported by spring and damper.

In this equation, *P(t)* is the total force acting upon the mass m, and u is the displacement of the mass.

$$P(t) = F(t) - ku - c\frac{du}{dt} \qquad \text{Equation 6.2}$$

Equation 6.1 can be rewritten to include the spring and damper constants; therefore, we can write:

$$m\frac{d^2u}{dt^2} + c\frac{du}{dt} + ku = F(t) \qquad \text{Equation 6.3}$$

Where *m* is the mass, *u* is the displacement, *c* is the damping coefficient of the dashpot, *k* is the stiffness coefficient of the spring, and *F* is the dynamic force that varies with time t. In this system, the spring responds to the displacement caused by the force, while the damper responds to the velocity. Various methods will be used to analyze the response of the simple system depicted in

Figure 6-1, enabling comparisons with solutions for soil dynamics problems. In many cases, a soil dynamics problem can be simplified to an equivalent single-mass system with equivalent mass, spring constant, and viscosity or damping. Deriving equations for these parameters is a key focus of many studies. As a result, it is crucial to have a comprehensive understanding of the response of a single-mass system to different types of loading. Free and forced vibrations of the system will be studied in detail for this purpose as it is pertinent to the subject of this research.

6.3. Definition of Viscosity

In the previous section, the damper in the system was defined by its viscosity constant i.e., *c*. However, it can also be described by the response time of the spring-damper combination. When a unit step load of magnitude F_0 is applied to a system consisting of a parallel spring and damper, the response can be expressed as:

$$u = \frac{F_0}{k}[1 - \exp(-t/t_r)] \qquad \text{Equation 6.4}$$

where t_r is the response time of the system and it can be written as:

$$t_r = c/k \qquad \text{Equation 6.5}$$

The value of response time (t_r) determines how quickly a system responds to a change in loading. Once the system reaches its final equilibrium state after a time of approximately four times the response time ($4t_r$), the spring becomes the dominant factor in the system's response. If the time t is less than the response time ($t < t_r$), the damper dominates the system's behavior, and it behaves like a stiff system.

6.4. Free vibrations

When the external force applied to the system is zero, i.e., F(t) = 0, the resulting vibrations of the system are referred to as free vibrations. The free vibrations can be described by the homogeneous differential equation.

$$m\frac{d^2u}{dt^2} + c\frac{du}{dt} + ku = 0 \qquad \text{Equation 6.6}$$

The homogeneous equation has a solution of $u = 0$, which implies that the system is at rest. If the system is at rest initially at time $t = 0$, it will remain at rest. However, it is important to study the response of the system when it is disturbed from its equilibrium state by an external influence. It can be expressed it as following:

$$\omega_0 = \sqrt{k/m} \qquad \text{Equation 6.7}$$

And,

$$2\zeta = \omega_0 t_r = \frac{c}{m\omega_0} = \frac{c\omega_0}{k} = \frac{c}{\sqrt{km}} \qquad \text{Equation 6.8}$$

The undamped system's resonance frequency is represented by ω_0, and the damping in the system is indicated by the ζ. By using equations (6.7) and (6.8), the differential equation can be expressed as:

$$\frac{d^2u}{dt^2} + 2\zeta\omega_0 \frac{du}{dt} + \omega_0^2 u = 0 \qquad \text{Equation 6.9}$$

which is the differential equation of the system. Here, ω_0 is the natural or resonance frequency of the undamped system, and ζ is the damping ratio which measures the damping in the system. The differential equation presented has constant coefficients and is a typical example of an ordinary linear differential equation. In the theory of differential equations, the standard approach is to find a solution that can be expressed in a certain form, using the given coefficients and initial conditions; we have:

$$u = Aexp(\alpha t) \qquad \text{Equation 6.10}$$

By assuming that the solution to the differential equation has the form $u = A\ sin(\omega t + \varphi)$, where A is a constant, likely related to the initial displacement u, and ω is an unknown angular frequency, the solution can be substituted into equation (6.9) to obtain a new equation.

$$\alpha^2 + 2\zeta\omega_0\alpha + \omega_0^2 = 0 \qquad \text{Equation 6.11}$$

This is known as the characteristic equation for the problem. If we are able to find a solution for the unknown parameter in equation (6.11), it would be reasonable to assume that the solution takes the form of an exponential function, as depicted in equation (6.10). The roots of the quadratic equation (6.11) determine the values of α, which are typically expressed as below:

$$\alpha_{1,2} = -\zeta\omega_0 \pm \omega_0\sqrt{\zeta^2 - 1} \qquad \text{Equation 6.12}$$

The roots obtained from solving the quadratic equation (6.11) may be either real or complex, depending on the value of ζ^2 - 1. Therefore, the type of response exhibited by the system is influenced by the damping ratio ζ, which determines whether the roots are real or complex.

6.5. Small damping

When the damping ratio is less than 1, ($\zeta < 1$), both roots of the characteristic equation (6.11) are complex and therefore we have:

$$\alpha_{1,2} = -\zeta\omega_0 \pm i\omega_0\sqrt{1-\zeta^2} \qquad \text{Equation 6.13}$$

Here, *i* represents the square root of -1, which is an imaginary unit, the solution can be expressed in the following form:

$$u = A_1 \exp(i\omega_1 t)\exp(-\zeta\omega_0 t) + A_2 \exp(-i\omega_1 t)\exp(-\zeta\omega_0 t) \qquad \text{Equation 6.14}$$

Where;

$$\omega_1 = \omega_0(\sqrt{1-\zeta^2}) \qquad \text{Equation 6.15}$$

The complex exponential function $exp(i\omega_1 t)$ may be written as

$$\exp(i\omega_1 t) = \cos(\omega_1 t) + isin(\omega_1 t) \qquad \text{Equation 6.16}$$

Thus, the solution expressed in equation (6.14) can alternatively be represented using trigonometric functions, which can be more practical in certain situations.

$$u = C_1 \cos(\omega_1 t) \exp(-\zeta \omega_0 t) + C_2 \sin(\omega_1 t) \exp(-\zeta \omega_0 t) \qquad \text{Equation 6.17}$$

The values of the constants C_1 and C_2 are determined by the initial conditions. Specifically, when the initial conditions are such that the displacement at time $t = 0$ is u_0 and the velocity is zero, the final solution can be expressed as...

$$\frac{u}{u_0} = \frac{\cos(\omega_1 t - \psi)}{\cos(\psi)} \exp(-\zeta \omega_0 t) \qquad \text{Equation 6.18}$$

Where ψ is a phase angle and is given by:

$$\tan(\psi) = \frac{\omega_0 \zeta}{\omega_1} = \frac{\zeta}{\sqrt{1 - \zeta^2}} \qquad \text{Equation 6.19}$$

The solution described in equation (6.18) represents a sinusoidal vibration that gradually diminishes in amplitude due to the exponential function $\exp(\zeta\omega_0 t)$. The function $\cos(\omega_1 t - \psi)$ determines the zeroes of the fluctuating solution. Figure 6-2 illustrates the solution for different damping ratio ζ. When damping is small, the frequency of the vibrations is almost the same as that of the undamped system. However, for larger damping ratios, the frequency becomes slightly smaller, and the amplitude of the response is greatly influenced by the frequency. At high frequencies, the amplitude becomes very small. If the damping ratio ζ approaches 1, the solution can even change from a damped fluctuation to the non-fluctuating response of a strongly damped system. These conditions will be examined in more detail below.

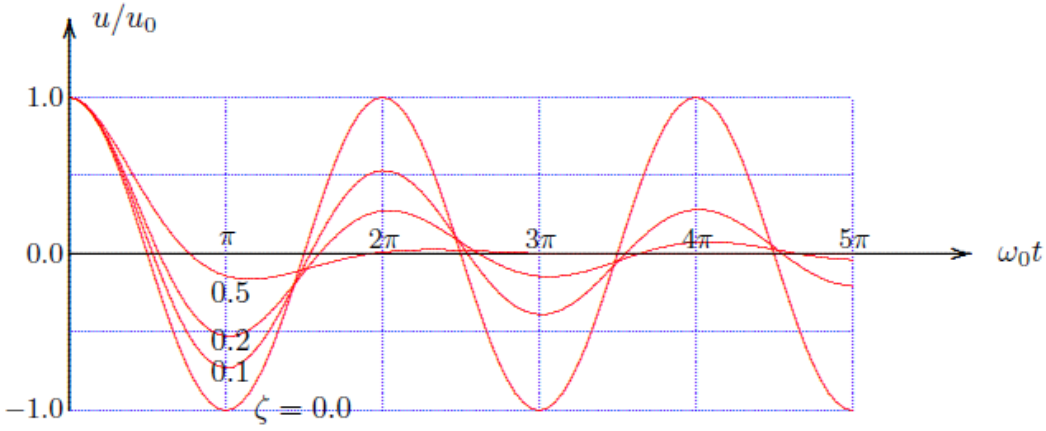

Figure 6-2: Free vibrations of a weakly damped system.

6.6. Critical damping

If the damping ratio is equal to 1, $\zeta = 1$, then the equation (6.11) will yield the following results:

$$\alpha_{1,2} = -\omega_0 \qquad \text{Equation 6.20}$$

When the damping ratio is equal to 1, the damping is known as critical damping, and the solution of the problem can be expressed as:

$$u = (A + Bt)\exp(-\omega_0 t) \qquad \text{Equation 6.21}$$

The values of constants A and B in the critical damping case need to be calculated based on the initial conditions. Assuming the displacement u is u_0 at $t = 0$, and the velocity is zero, the final solution can be expressed using the obtained values of A and B. We have;

$$u = u_0\,(1 + \omega_0 t)\exp(-\omega_0 t) \qquad \text{Equation 6.22}$$

Figure 6-3 illustrates the solution for the case of critical damping, along with some outcomes for high damping ratios.

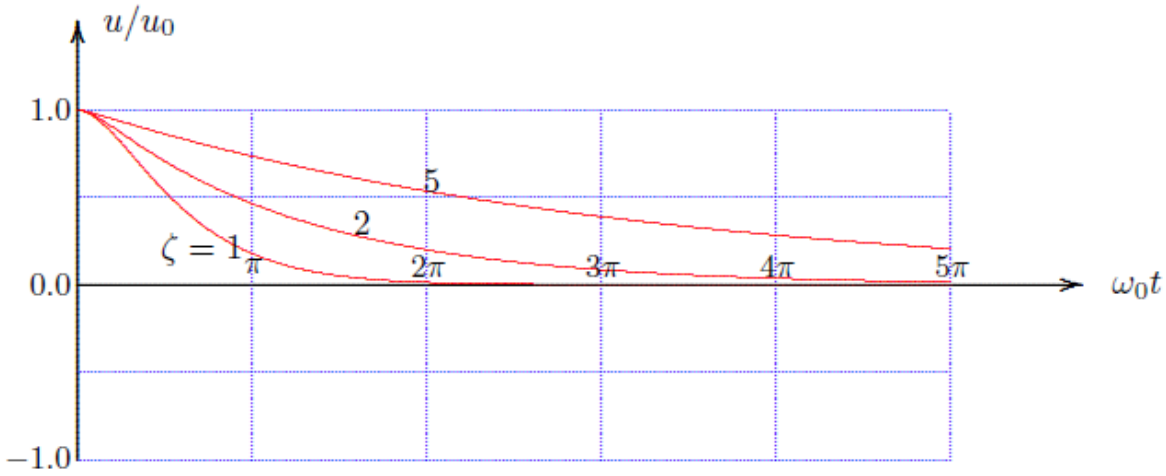

Figure 6-3: Free vibrations of a strongly damped system.

6.7. Large damping

In case of damping ratio greater than 1 ($\zeta > 1$), the equation (6.11) will yield two real roots which can be expressed as follows:

$$\alpha_{1,2} = -\zeta\omega_0 \pm \omega_0\sqrt{\zeta^2 - 1} \qquad \text{Equation 6.23}$$

The solution for the scenario where a mass point has an initial displacement of u_0 and an initial velocity of zero is as follows:

$$\frac{u}{u_0} = \frac{\omega_2}{\omega_2 - \omega_1}\exp(-\omega_1 t) - \frac{\omega_1}{\omega_2 - \omega_1}\exp(-\omega_2 t) \qquad \text{Equation 6.24}$$

Where;

$$\omega_1 = \omega_0(\zeta - \sqrt{\zeta^2 - 1}) \qquad \text{Equation 6.25}$$

And;

$$\omega_2 = \omega_0(\zeta + \sqrt{\zeta^2 - 1}) \qquad \text{Equation 6.26}$$

Figure 6-3 also illustrates the graphical representation of this solution for $\zeta = 2$ and $\zeta = 5$. It can be observed that in these instances, with significant damping, the system will not exhibit oscillatory behavior but will gradually approach the equilibrium state with $u = 0$.

6.8. Forced Vibrations

In this section, the behavior of a system under a forced load is studied, the load could be applied as periodic or otherwise. In this section, the case of periodic loads is focused as it is pertinent to the subject of this research. When a load is periodic, the response of the system depends on the characteristics of the load. The case of forced vibrations due to periodic loads is studied in this section and the next. A periodic load can be represented by a force function F(t), which can be expressed in its simplest form as:

$$F = F_0 Cos(\omega t) \qquad \text{Equation 6.27}$$

To analyze the system's response to a periodic load with a given circular frequency ω, it is best to express the force in the following form:

$$F = Re\{F_0 exp[(i\omega t)\} \quad \text{Equation 6.28}$$

The symbol *Re* denotes the real value of the term within the brackets. Assuming that F_0 is a real quantity, the expressions (6.27) and (6.28) are equivalent. The solution for the displacement *u* can now be expressed in terms of a complex variable:

$$u = Re\{Uexp[(i\omega t)\} \quad \text{Equation 6.29}$$

The displacement *U* appears to be complex. By substituting (6.29) and (6.28) into the differential equation (6.3), we can have:

$$(k + ic\omega - m\omega^2)U = F_0 \quad \text{Equation 6.30}$$

In practice, the real part of the equation is important. Nevertheless, it is best to include the (non-relevant) imaginary part in order to obtain a fully complex equation. However, it is important to emphasize that, after completing all calculations, only the real part should be taken into account, as stated in accordance with equation (6.29). The solution to the equation (6.30) can be determined as below:

$$U = \frac{F_0/k}{1 + 2i\,\zeta\omega/\omega_0 - \omega^2/\omega_0^2} \quad \text{Equation 6.31}$$

Where,

$$\omega_0 = \sqrt{k/m} \quad \text{Equation 6.32}$$

And;

$$2\zeta = \frac{c}{m\omega_0} = \frac{c\omega_0}{k} = \frac{c}{\sqrt{km}} \qquad \text{Equation 6.33}$$

The ω_0 and ζ are the resonance frequency of the undamped system, and the damping in the system.

Using equations (6.29) and (6.31) the displacement u can be written as below:

$$u = u_0 \cos(\omega t - \psi) \qquad \text{Equation 6.34}$$

Where the amplitude u_0 is given by:

$$u_0 = \frac{F_0/k}{\sqrt{(1-\omega^2/\omega_0^2)^2 + (2\zeta\omega/\omega_0)^2}} \qquad \text{Equation 6.35}$$

The phase angle ψ can be defined as:

$$tan\psi = \frac{2\zeta\,\omega/\omega_0}{1-\omega^2/\omega_0^2} \qquad \text{Equation 6.36}$$

And the amplitude can be written as;

$$u_0 = \frac{F_0/k}{\sqrt{(1-m\omega^2/k)^2 + (c\omega/k)^2}} \qquad \text{Equation 6.37}$$

The phase angle ψ is rewritten as;

$$tan\psi = \frac{c\omega/k}{1 - m\omega^2/k}$$ Equation 6.38

In case of a system with zero mass we have:

$$m = 0 : u_0 = \frac{F_0/k}{\sqrt{1 + (c\omega/k)^2}}$$ Equation 6.39

And

$$m = 0 : tan\psi = \frac{c\omega}{k}$$ Equation 6.40

Figure 6-4 illustrates the amplitude of the system, as described by equation (6.35), as a function of frequency for different damping ratios ζ. Notably, the response curve exhibits a distinct maximum for low damping ratios, with the maximum value approaching infinity as ζ approaches zero. This phenomenon is commonly referred to as resonance. In the absence of damping, resonance transpires when the excitation frequency ω equals the natural frequency ω_0 of the undamped system, expressed as $\omega_0 = \sqrt{\mathrm{k/m}}$. The term "eigen frequency" is occasionally used to denote the natural frequency of the system in free vibration. The maximum response occurs when the slope of the curve in Figure 6-4 is horizontal. This is the case when $du_0/d\omega = 0$:

$$\frac{du_0}{d\omega} = 0 : \frac{\omega}{\omega_0} = \sqrt{1 - 2\zeta^2}$$ Equation 6.41

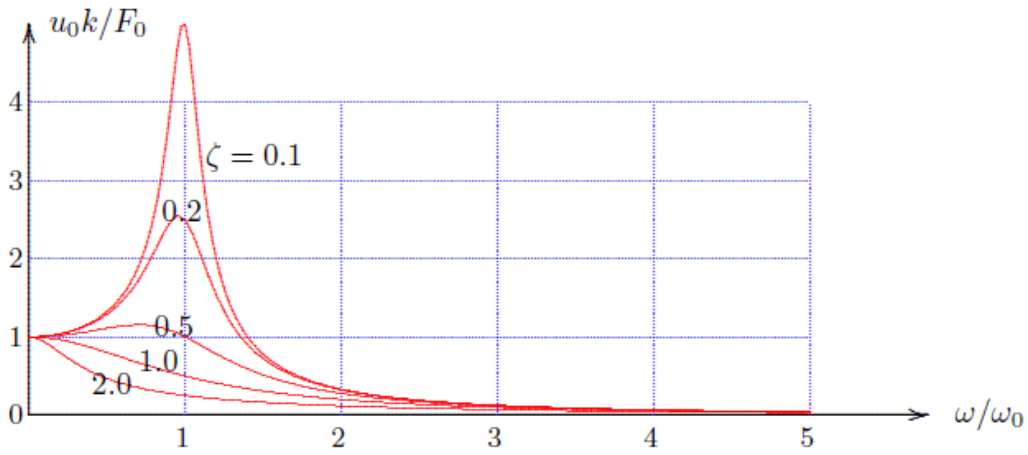

Figure 6-4: Amplitude of Forced Vibration

For low values of the damping ratio ζ, the maximum amplitude occurs when the frequency ω is in close proximity to ω_0, the resonance frequency of the undamped system. As the damping ratio increases, the resonance frequency may slightly decrease, approaching zero when $2\zeta^2$ approaches 1. In the presence of high damping, the system does not exhibit any signs of resonance. The phase angle ψ is depicted in Figure 6-5. At low frequencies, such as during quasi-static loading, the system's amplitude approaches the static response F_0/k, and the phase angle becomes nearly zero. Near the resonance frequency of the undamped system (i.e., when $\omega/\omega_0 \approx 1$), the phase angle is approximately $\pi/2$, indicating that the amplitude is at its maximum when the force is zero, and vice versa. When subjected to rapid fluctuations, the inertia of the system restricts vibrations (as evident from the small amplitude in Figure 6-4), while the system becomes out of phase, as signified by the phase angle approaching π in Figure 6-5.

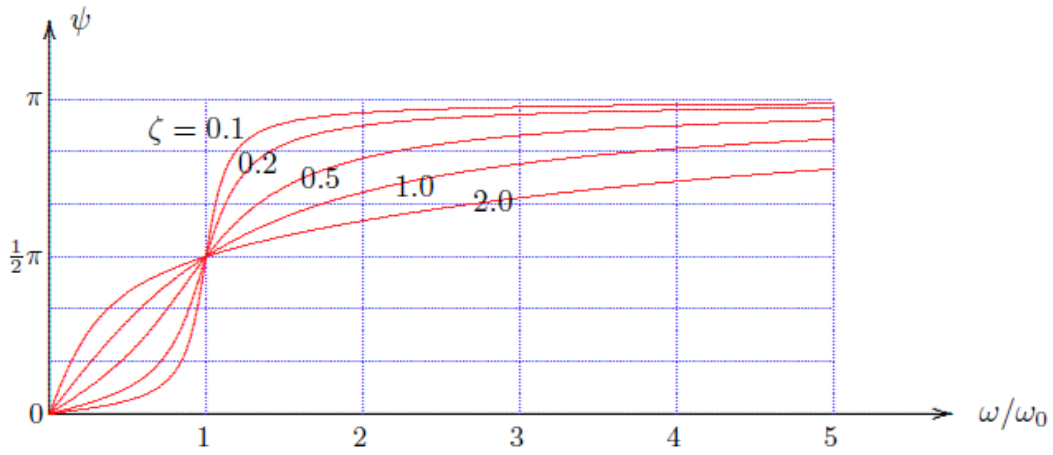

Figure 6-5: Phase Angle of Forced Vibration

6.9. Hysteretic damping

This section presents an alternative form of damping known as hysteretic damping, which offers a more suitable representation of damping in soils. It is important to note that the fundamental equation for a single mass system, as presented in equation (6.3), is rewritten as:

$$m\frac{d^2u}{dt^2} + c\frac{du}{dt} + ku = F(t) \qquad \text{Equation 6.42}$$

Where c is the viscous damping. For forced vibrations, the load is:

$$F(t) = F_0 Cos(\omega t) \qquad \text{Equation 6.43}$$

In this equation, F_0 is a given amplitude, and ω is a given frequency. The response of the system can be written as;

$$u = Re\{Uexp[(i\omega t)\} \quad \text{Equation 6.44}$$

In this equation, *U* may be complex. Substitution of (6.44) and (6.43) into the differential equation (6.42) results the following:

$$(k + ic\omega - m\omega^2)U = F_0 \quad \text{Equation 6.45}$$

Assuming that the viscosity *c* is constant, the damping ratio ζ was defined as:

$$2\zeta = \frac{c}{m\omega_0} = \frac{c\omega_0}{k} = \frac{c}{\sqrt{km}} \quad \text{Equation 6.46}$$

Where;

$$\omega_0 = \sqrt{k/m} \quad \text{Equation 6.47}$$

ω_0 is the resonance frequency (or eigen frequency) of the undamped system. It is important to note that the effect of damping varies with frequency, as illustrated in Figure 6-4. The figure indicates that as the ratio of $\omega/\omega_0 \rightarrow \infty$, the amplitude of the vibrations gradually diminishes and tends towards zero. Hysteretic damping is an alternative form of damping that can be employed to characterize the damping resulting from dry friction in a vibrating system. In this scenario, it is assumed that the ratio of $c\omega_0/k$ remains constant. The damping ratio ζ_h is introduced to describe this type of damping and is defined as follows:

$$2\zeta_h = \omega t_r = \frac{c\omega}{k}$$ Equation 6.48

Hysteretic damping is widely regarded as a more realistic depiction of soil behavior compared to viscous damping. This is primarily due to the fact that the irreversible (plastic) deformations experienced by soils under cyclic loading are not influenced by the loading frequency. This behavior can be effectively captured by using a constant damping ratio ζ_h, as defined earlier. Therefore, Equation (6.45) can be reformulated as follows:

$$k(1 + 2i\zeta_h - \omega^2/\omega_0^2)U = F_0$$ Equation 6.49

And the solution can be written as:

$$U = \frac{F_0/k}{1 + 2i\zeta_h - \omega^2/\omega_0^2}$$ Equation 6.50

The displacement *u* is;

$$u = u_0 Cos(\omega t - \psi_h)$$ Equation 6.51

And the amplitude u_0 is expressed as follows:

$$u_0 = \frac{F_0/k}{\sqrt{(1 - \omega^2/\omega_0^2)^2 + 4\zeta_h^2}}$$ Equation 6.52

And, the phase angle ψ_h is expressed as follows:

$$tan\psi = \frac{2\zeta_h}{1 - \omega^2/\omega_0^2} \quad \text{Equation 6.53}$$

A system of zero mass, the equations are simplified, therefore we can write;

$$m = 0 : u_0 = \frac{F_0/k}{\sqrt{1 + 4\zeta_h^2}} \quad \text{Equation 6.54}$$

And

$$m = 0 : tan\psi_h = 2\zeta_h \quad \text{Equation 6.55}$$

These equations demonstrate that when the mass of the system is negligible, both the amplitude and the phase shift remain constant regardless of the frequency ω. The system's response becomes independent of the speed at which loading and unloading occur. This behavior is commonly observed in materials such as soft soils, particularly granular materials, when subjected to cyclic loading. As a result, hysteretic damping is considered a more realistic form of damping in soils compared to viscous damping (Hardin, 1965; Verruijt, 1999).

The amplitude of the system, as represented by equation (6.52), is presented in Figure 6-7, depicting its variation with frequency for different values of the hysteretic damping ratio ζ_h. The trend closely resembles that of a system with viscous damping, as shown in Figure 6-4, except for low-frequency ranges. However, in this system, the influence of the mass becomes prominent in determining the response, particularly at higher frequencies. The corresponding phase angle is also illustrated in Figure 6-7. The system's behavior differs notably from that of a viscously

damped system, particularly at lower frequencies. At higher frequencies, the impact of the mass becomes more significant, exerting a dominant influence on the system's response.

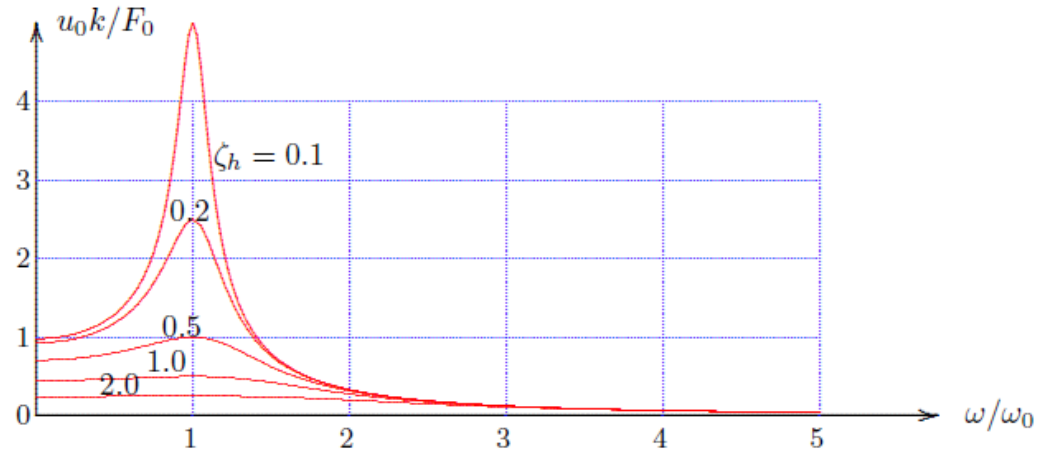

Figure 6-6: Amplitude of forced vibration, hysteretic damping.

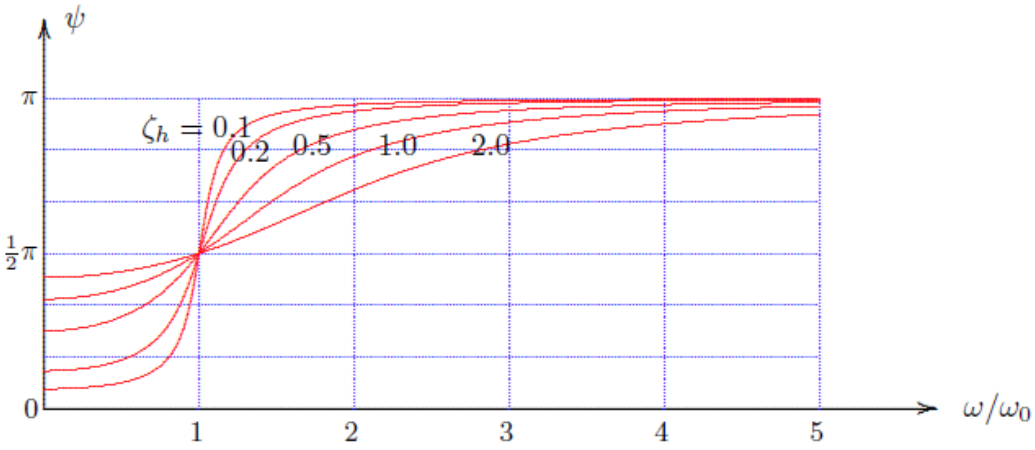

Figure 6-7: Phase angle of forced vibration, hysteretic damping.

It is worth noting that when the system mass is negligible, the response of a system with hysteretic damping differs significantly from that of a system with viscous damping, as noted by the difference between equations (6.39) and (6.54). In a system with viscous damping, the amplitude

diminishes as the frequency increases, as indicated by equation (6.39). However, in a system with hysteretic damping and zero mass, the amplitude remains independent of frequency, as illustrated by equation (6.54).

6.10. Equivalent Spring and Dashpot

The analysis of a system's response to a periodic load often can be expressed as:

$$F = (K + iC\omega)U \qquad \text{Equation 6.56}$$

In this equation, U represents the amplitude of a characteristic displacement, F represents the amplitude of the force, and K and C represent system's properties, stiffness, and damping. Comparing this equation with equation (6.30), it can be concluded that the response function exhibits similar characteristics to a combination of a spring and a dashpot. Therefore, the system can be considered equivalent to a spring-dashpot system with an equivalent stiffness K and equivalent damping C. By employing the properties of a spring-dashpot system, the response of the system can be analyzed. This equivalence will be utilized in Chapter 4 to investigate the response of a vibrating mass, such as a machine foundation supported by micropiles, on an elastoplastic half-plane. Overall, in practice, it is often advantageous and valuable to represent the response of a complex system to a harmonic load using an equivalent spring stiffness K and an equivalent damping C.

Chapter 7 - References

1. American Association of State Highway and Transportation Officials (AASHTO). (1992). Standard Specification for Highway Bridges, revised. Washington D.C.
2. American Association of State Highway and Transportation Officials. (1996). Standard specifications for highway bridges (16th ed.). Washington, D.C.: American Association of State Highway and Transportation Officials.
3. American Association of State Highway and Transportation Officials (AASHTO). (2014). LRFD Bridge Design Specifications (9th Edition). Washington D.C.
4. ABAQUS, Finite Element Program Theory Manual (version 6.5.1), Hibbit, Karlsson & Sorenson Inc., USA, 1993.
5. ABAQUS. (2006, 2008). ABAQUS Documentation - Version 6.6. – 6.8 Dassault Systèmes SIMULIA Corp.
6. ABAQUS Finite Element Program, ABAQUS/Standard User's Manual. Dassault Systèmes.
7. Blaney, G., Kausel, E., and Roesset, J., (1976). Dynamic Stiffness of Piles. Proc. 2nd International Conference on Numerical Methods in Geomechanics, Blacksburg, Vol. 2, pp.1001-1012.
8. British Standards Institution (1989). Ground Anchorages. BSI, Milton Keynes, BS 8081.
9. Brown, D.A., Shie, C.F., and Kumar, M., (1989). P-y curves for laterally loaded piles derived from three-dimensional finite element model. Numerical Models in Geomechanics, NUMOG III, pp. 683-690.
10. Bustamante, M., and Doix, B. (1985). “Une méthode pour le calcul des tirants et des micropieux injectés.” Bulletin de Liaison des Laboratoires des Ponts et Chaussées, LCPC, Paris, pp. 75-92.

11. Butterfield, R., and Banerjee, P.K. (1971). “The elastic analysis of compressible piles and pile groups.” Geotechnique, 21, No. 1, pp. 43-60.
12. Bruce, D.A., and Juran, I. (1997). “Drilled and grouted micropiles: State-of-practice review. Volume II: Design” U.S. Department of Transportation, Federal Highway Administration, Publication No. FHWA-RD-96-017.
13. Capatti, M. C., Dezi, F., Carbonari, S., & Gara, F. (2020). Dynamic performance of a full-scale micropile group: Relevance of nonlinear behavior of the soil adjacent to micropiles. Journal of Soil Dynamics and Earthquake Engineering, 120, 104138.
14. Caltrans – California Department of Transportation (1994). Highway Design Metric. Office of Geotechnical Engineering, Foundation Testing and Instrumentation Branch.
15. CCTG (1993). Technical Rules for the Design and Calculation of the Foundations of the Civil Engineering Works, Fascicule 62, Titre V. CCTG.
16. Chow, Y.K. (1986). “Analysis of vertically loaded pile groups.” International Journal of Numerical and Analytical Methods in Geomechanics, 10, pp. 59-72.
17. Das, B.M. and Ramana, G.V. (2011). Principals of Soil Dynamics, 2nd edition. CENGAGE Learning.
18. Drucker, D.C. and Prager, W. (1952). Soil mechanics and plastic analysis or limit design, Quarterly of Applied Mathematics, Vol. 10, pp. 157-165.
19. El Naggar, M.H., Abdrabbo, M.A., Haque, A., and Basma, A.A. (2010). Effect of Drill Bit Diameter and Micropile Spacing on Group Performance. Journal of Geotechnical and Geoenvironmental Engineering, ASCE, Vol. 136, No. 7, pp. 981-991.

20. Elsawwaf A, Nazir A, Azzam W. (2022). The effect of combined loading on the behavior of micropiled rafts installed with inclined condition. Environmental Science and Pollution Research, 29(29), 81321-81336.
21. Estephan, R. (2003). Contributions aux méthodes de calcul des groupes et des réseaux de micropieux. Dar Al Handasah.
22. Federal Highway Administration (FHWA) (2005). Micropile design and construction. (FHWA NHI-05-039). Washington, D.C.: U.S. Department of Transportation.
23. Federal Highway Administration (FHWA) (1997), Drilled and Grouted Micropiles, State-of-Practice Review. Federal Highway Administration Publication, Report No. FHWA-RD-96-016/019, July 1997, Four Volumes.
24. Fleming, W.G.K., Weltman, A.J., Randolph, M.F., and Elson, W.K. (1985). Piling Engineering, Wiley.
25. Frank R., Schlosser F. (2012). Some lessons learnt from the "Forever" Research Project on micropiles. Proc. of the Int. Conf. on Ground Improvement and Ground Control.
26. Frank, R., Schlosser, F. (2008). FOREVER Synthesis of the Results and Recommendations of the French National Research Project on Micropiles. ADSC, Dallas, Texas.
27. Hardin, B.O. (1965), The nature of damping in soils, J. Soil Mech. and Found. Div., Proc. ASCE, 91, No. SM1, 63-97
28. Helwany, S. (2007). Applied Soil Mechanics with ABAQUS Applications. John Wiley & Sons.
29. Hokmabadi, A. S., B. Fatahi, and B. Samali. (2014). "Assessment of soil–pile–structure interaction influencing seismic response of mid-rise buildings sitting on floating pile foundations." Comput. Geotech. 55: 172–186.

30. Hokmabadi, A. S., B. Fatahi, and B. Samali. (2015). “Physical modeling of seismic soil-pile-structure interaction for buildings on soft soils.” Int. J. Geomech. 15 (2): 04014046.
31. Idriss, I.M., Seed, H.B. (1968). Seismic response of horizontal soil layers. J. Soil Mech. Found. Div., ASCE, 94, pp. 1003-1029.
32. Iai, S. (1989). “Similitude for shaking table tests on soil-structure-fluid model in 1g gravitational field.” Soils Found. 29 (1): 105–118.
33. Iai, S., T. Tobita, T. Nakahara. (2005). “Generalized scaling relations for dynamic centrifuge tests.” Geotech. 55 (5): 355–362.
34. Juran, I., Benslimane, A., Hanna, S. (2001). Engineering analysis of the dynamic behavior of micropile systems. Transportation Research Record, No. 01-2936, pp. 91–106.
35. Juran, I., Bruce, D.A., DiMillio, A., Benslimane, A. (1999). Micropiles: the state of practice. Part II: design of single micropiles and groups and networks of micropiles. Ground Improvement, 3(3), July.
36. Kishishita, T., Saito, E., Miura, F. (2000). Dynamic-response characteristics of structures with micropile foundation system. 12th World Conference on Earthquake Engineering, Auckland, New Zealand.
37. Kuhlmeyer, R. (1979). Static and Dynamic Laterally Loaded Floating Piles. Journal of Geotechnical Engineering, ASCE, 105(2), pp. 289-304.
38. Littlejohn, G.S., and Bruce, D.A. (1977). Rock Anchors – State of the Art. Foundation Publication Ltd, Brentwood.
39. Lysmer, J., Kuhlemeyer, R.L. (1969). Finite dynamic model for infinite media. Journal of the Engineering Mechanics Division, ASCE, 95(EM4), pp. 859-877.

40. Maheshwari, B.K., Truman, K.Z., Naggar, M.H.EI., Gould, P.L. (2005). Three-Dimensional Nonlinear Seismic Analysis of Single Piles Using Finite Element Model: Effects of Plasticity of Soil. International Journal of Geomechanics, ASCE, 5(1), pp. 35-44.
41. Maleki, F. and Frank, R. (1994). “Groupes de Pieux Charges Axialement.” Project National FOREVER, Programme 1993, CERMES, 1994.
42. Manna, B. and Baidya, D. (2009). ”Vertical Vibration of Full-Scale Pile Analytical and Experimental Study.” J. of Geotech. and Geoenvironmental. Eng., ASCE, 135(10), 1452–1461.
43. Margasson, E. (1977). Pile Bending Duration Earthquake, Design, Construction, and Performance of Deep Foundation Seminar, ASCE, Berkeley, CA.
44. Martin, P.P. and Seed, H.B. (1982). One-dimensional dynamic ground response analyses. J. Geotech. Engineering. Div., ASCE, 108(7), pp. 935-953.
45. Meyerhof G.G. (1976). “Bearing capacity and settlement of pile foundations.” Journal of Geotechnical Engineering, ASCE, 102, No. GT3, pp. 195-228.
46. Micropile Design and Construction Guidelines; Implementation Manual (2000). Federal Highway Administration.
47. Mindlin, R.D. (1936). Foundation and Earth Structures. Naval Facilities Engineering Command, Alexandria, VA.
48. Miura, K., Tsukada, Y., Tsubokawa, Y., Ishito, M., Nishimura, N., Ohtani, Y. and You, G L. (2000). Bearing capacity during earthquake of the spread footing reinforced with micropiles. 12th World Conference on Earthquake Engineering, Auckland, New Zealand.

49. Ossama S.A.A. (2015), Vertical Dynamic Soil-Pile Interaction for Machine Foundations, Dept. of Civil and Environmental Engineering, University of Maryland – College Park, A PhD Dissertation.
50. O'Neill, M.N., Ghazzaly, O.I., and Ha, H.B. (1977). "Analysis of three-dimensional pile groups with nonlinear soil response and pile-soil-pile interaction." Proceedings of the 9th Annual OTC, pp. 245-256.
51. Ousta R, Shahrour I. (2001). Three-dimensional analysis of the seismic behavior of micropiles used in the reinforcement of saturated soil. International Journal for Numerical and Analytical Methods in Geomechanics, No. 25, pp. 183-196.
52. Poulos, H.G., and Davies, E.H. (1980). Pile Foundation Analysis and Design, Wiley, New York.
53. Rajkumar, K., Ayothiraman, R., & Matsagar, V. A. (2020). Effects of Soil–Structure Interaction on Dynamic Response of Framed Machine Foundation Resting on Raft and Piles. Practice Periodical on Structural Design and Construction, 20(2), 04014030
54. Randolph, M.F., and Wroth, C.P. (1979). "An analysis of the vertical deformation of pile groups." Geotechnical Engineering, ASCE, 104, No. GT12, pp. 1466-1488.
55. Rodriguez-Marek A., Balasingam Muhunthan (2005), Seismic behavior of micropiles, FHWA Supported Structures Research, Washington State University, Research Report, Agreement T2696, Task 02 Micropiles, WA-RD 604.1.
56. Sadek, M. and Shahrour, I. (2006). Influence of the head and tip connection on the seismic performance of micropiles. Soil Dynamics and Earthquake Engineering, No. 26, pp. 461-468.

57. Sadek, M. and Shahrour, I. (2004). Three-dimensional finite element analysis of the seismic behavior of inclined micropiles. Soil Dynamics and Earthquake Engineering, No. 24, pp. 473-48.

58. Schlosser, F., Plumelle, C., Frank, R., Puech, A., Gonin, H., Rocher-Lacoste, F., Simon, B. (2013). Micropile installation in dense alluvial deposits in the Geneva basin. Proceedings of the 18th International Conference on Soil Mechanics and Geotechnical Engineering, Paris, Volume 6.

59. Schofield, A. N., and Wroth, C. P. (1968). "Critical State Soil Mechanics." McGraw-Hill, London.

60. Seed R.B., Riemer F., M. Pestana J.M., Maymand F.J., and Lok T.M. (1999). Seismic Response of Pile Research Project. Department of Civil and Environment Engineering, University of California at Berkeley, CA.

61. Shahrour I, Juran I. (2004). Seismic behavior of micropile systems. Ground Improvement, No. 3, pp. 109-120.

62. Sharma, B., Zaheer, S., Hussain, Z. (2014). Experimental Model for Studying the Performance of Vertical and Batter Micropiles. Geo-Congress 2014 Technical Papers, February 2014.

63. Sharma, B., & Hussain, Z. (2019). Behavior of Batter Micropiles Subjected to Vertical and ateral Loading Conditions. Journal of Geoscience and Environment Protection, 7(2), 47-57.

64. Shu, S. (2005). Sand State and Performance Analysis of Micropiles. Ph.D. dissertation, Washington State University, Washington.

65. Skempton, A.W. (1935). “Discussion: Piles and pile foundations, settlement of pile foundations.” Proceedings of the 3rd International Conference on Soil Mechanics and Foundation Engineering, 3, 172 p.

66. Teerawut, Juirnarongrit (2002). Effect of diameter on the behavior of laterally loaded piles in weakly cemented sand. Ph.D. Dissertation, University of California, San Diego.
67. Terzaghi, K., and Peck, R.B. (1948). Soil Mechanics in Engineering Practice, 1st edition, Wiley, New York.
68. Terzaghi, K. (1943). Theoretical Soil Mechanics, Wiley, New York
69. Turan, A., El Naggar, M. H., Hinchberger, S. (2008), Lateral behavior of micro-pile groups under static and dynamic loads, Proceedings of the 4th Canadian Conference on Geohazards: From Causes to Management, Presse de l'Université Laval, Québec.
70. Vesic, A.S. (1969). "Experiment with instrumented pile groups in sand." ASTM Special Technical Publication, No. 444, pp. 172-222.
71. Verruijt, Arnold (1999). Dynamics of soils with hysteretic damping, Proc. 12th Eur. Conf. Soil Mech. and Geotechnical Engineering, vol. 1, (F.B.J. Barends et al., editors), Balkema, Rotterdam, 3-14.
72. Verruijt, Arnold (2008). Soil Dynamics. Delft University of Technology,
73. Wu, G., Finn, D.L.W. (1997). Dynamic nonlinear analysis of pile foundations using finite element method in the time domain. Canadian Geotechnical Journal, v 34, No 1, pp. 44-52.
74. Yamane, T., Nakata, Y., and Otani, Y. (2000). Efficiency of micropile for seismic retrofit of foundation system. 12th World Conference on Earthquake Engineering, Auckland, New Zealand.
75. Yamashita, K., Tomono, M., and Kakurai, M. (1987). "A method for estimating immediate settlement of piles and pile groups." Soils and Foundations, 27, No. 1, pp. 61-76.
76. Yang, J., Mcmanus, K., and Berrill, J. (2000). Kinematic soil-micropile interaction. 12th World Conference on Earthquake Engineering, Auckland, New Zealand.